INVESTIGATION OF THE MECHANISMS OF RECEPTOR-MEDIATED IMMUNOGLOBULIN TRANSPORT IN MAMMALS AND BIRDS

Thesis by

Devin Brent Tesar

In Partial Fulfillment of the Requirements

for the Degree of

Doctor of Philosophy

CALIFORNIA INSTITUTE OF TECHNOLOGY

Pasadena, California

2009

(Defended September 12th, 2008)

© 2009

Devin Tesar

All Rights Reserved

ACKNOWLEDGEMENTS

Writing the acknowledgements section for an endeavor such as the Ph.D.—which has spread out over so many years—is a very satisfying and, in some ways, a somewhat uncomfortable proposition. It is satisfying because one wants to be able to graciously thank all those who have helped him/her during the long process without regard for the fear of sounding sentimental or cheesy. It is uncomfortable because (at least for me) one doesn't want to get so caught up in the catharsis that they lose their heads completely and let slip a line so absurd or melodramatic that it is recited behind their back by their closest friends for years to come (I could cite references here, but I won't).

I have been very fortunate during my graduate career in that I have had ample opportunity to read the acknowledgements sections from theses written by friends and associates that have gone before me. In doing so I developed a list of rules that I hope can prevent one's acknowledgement section from being embarrassing in retrospect.

1) Don't try to be funny too many times. Three attempts is a good maximum, zero is even better.

2) Do not make pop culture references for any reason. They serve only to date you and also display to the whole world which terrible FX or WB programs you watch when no one is looking (again, I could cite references).

3) Absolutely no inside jokes between you and the reader. Inside jokes are an admission that you are unable to be funny for a general audience and must therefore target people that are socially obligated to laugh at your reference because they were present with you when some—in all likelihood not-so-funny-anyhow—event took place three years ago at a Denny's in downtown after a Carly Simon concert (just for example).

4) Don't try to use words that are bigger than those you use in your everyday conversation. People who are going to read this know how you talk and will spot it in a heartbeat. Then they will think that you are pretentious and will impersonate you with a high-pitched British accent when you're not around (could cite one specific reference).

First and foremost I wish to thank Pamela Bjorkman for being such a wonderful advisor. She has a remarkable talent for science—both for the intellectual and non-intellectual components of the profession—and had led through example more than I think most mentors ever do. I appreciate all she has done to prepare me for a career in science, such as involving me in the process of paper reviews and grant submissions, as well as helping me to understand the less exciting (often bureaucratic) nuances of the profession that graduate students do not normally get to see or understand until years later when they are setting up their own lab and learning them the hard way. Above all, however, I want to thank her for being a good-hearted and understanding person, for having a great sense of humor, and for being someone that I today think of as being both a mentor and a friend.

Technical assistance in the lab has come from many sources while I've been here. Of particular importance, Shelley Diamond of the cell sorting facility, whose technical expertise and kind friendship were always refreshing, and Peter Snow, Inder Nangiana, Chris Foglesong, and Jost Vielmetter of the Caltech Protein Expression Facility, who offered help on countless projects in the lab. Special thanks goes to my undergraduate assistant Evelyn Cheung for a great year of hard work.

Life in the lab has been made more enjoyable by the presence of several individuals, past and present. Adrian Rice and his wife Sharla (not a lab member but a great gal nonetheless), Tony Giannetti, Alexander Hamilton Farley, and Rachel Galimidi are a few of these. Also thanks to Rich Olson, Josh Klein, and Anthony West for being great and helpful co-workers. Special thanks to Noreen Tiangco, Beth Huey-Tubman, and Priyanthi Peiris for being such a tremendous help over all of the years and for doing it all with a smile and relentlessly good attitude.

Outside of the lab I have been lucky to have a lot of great friends during my time at Caltech that have made life here far more enjoyable than it otherwise would have been. In my graduate class Amber Southwell and her husband Jason Hovel (also not a Caltech person, but a great gal nonetheless), Jordan Benjamin, Mark Zarnegar, Julien Muffat, and Meghan Adams have served as great sources of memories and good times. Other graduate student friends from Caltech who are neither from my year nor from my lab have included Steve Smith, Alice Robie, Holly Beale, Dan Gold, Mary Devlin, Sarina Mohanty, Johnson Ngo, Phil Romero, and Dan Pragel. Finally, thanks to my friends outside of Caltech that were

instrumental in giving me the chance every now and then to forget that graduate school even existed; Dave Seal, Graeme Fordyce, and Eric Wilson.

Special thanks go out to my two favorite Caltech undergrads of all time; Dann Dempsey and Damien Soghoian.

More special thanks to my friends back home in Kansas City who I've kept in close contact with; Scott L. Cox, Mark Hill, Sarah Jones, Cyndi Price, and Shelley McLendon.

Thanks to my family members, immediate and extended, particularly my siblings, Brandon and Megan.

Most importantly, thank to my parents Larry and Holly Tesar, whose love, support, and collective sense of humor were vital in getting me where I am today. It is to them that I dedicate this work.

ABSTRACT

The neonatal Fc receptor (FcRn) mediates the passive acquisition of humoral immunity in early pre- or post-natal mammals by transferring maternal IgG to the fetus or suckling newborn. In addition, FcRn serves to extend the serum half-life of IgG in adult mammals by protecting it from a default degradative pathway in vascular endothelial cells. For both of these functions, FcRn binds the Fc domain of IgG with high affinity at the acidic pH (≤6.5) of the intestinal lumen and acidic endosomes, and releases the IgG at the slightly basic pH (~7.4) of blood. While the ability of FcRn to transcytose IgG bidirectionally in polarized cell models has been well documented, the specific mechanism(s) by which endocytosed IgG is sorted from other vesicular cargo and directed through a progression of endosomal compartments ultimately leading to the apical or basolateral membrane are poorly understood.

We wished to develop an *in vitro* system with which to study the trafficking behavior of rat FcRn in polarized epithelia. I developed such a model system using Madin-Darby Canine Kidney cells stably-transfected with the rat FcRn. The cells bind, endocytose, recycle and bidirectionally transcytose FcRn ligands, faithfully recapitulating the function of FcRn in the neonatal rodent gut. We used these cells to test whether or not the presence of two FcRn binding sites on an Fc ligand are required for transport. The results demonstrated that ligand bivalency is not strictly required for transport but does increase the transcytosis efficiency of the system, an interesting result in light of the fact that FcRn binds and transports a naturally monovalent ligand – serum albumin.

We have used the FcRn-MDCK cells to study trafficking of the receptor in living cells using spinning disk confocal microscopy. For these studies I developed a recombinant Fc ligand containing a tandem dimer of fluorescent proteins on each chain and demonstrated that this ligand is brighter and more photostable than conventional chemically-labeled Fc molecules used in other confocal studies. Our FcRn-MDCK cells have also been used to examine trafficking events at the plasma membrane leading up to exocytosis though use of total internal reflection microscopy (TIRFM).

I also created a model system to study an avian Fc receptor present in yolk sac (FcRY). FcRY has been shown to bind IgY (the avian counterpart of IgG) with the same pH-dependence that FcRn exhibits for IgG. Transcytosis and recycling experiments using polarized rat inner medullary collecting duct (IMCD) cells stably transfected with the FcRY gene demonstrated that this receptor is a true functional equivalent of FcRn despite being structurally distinct from FcRn. This presents a striking example of convergent evolution and demonstrates that certain versatile protein folds can play key roles in more than one functional context within a complex organism.

TABLE OF CONTENTS

Acknowledgments……..iii

Abstract……..……vii

Table of Contents...……...……..ix

Chapter 1:
Introduction……...…….. 1

Chapter 2:
Ligand Valency Affects Transcytosis, Recycling, and Intracellular Trafficking
Mediated by the Neonatal Fc Receptor……...……..…….…42

Chapter 3:
Immunoglobulin Transcytosis and Recycling by an Avian Functional
Equivalent of FcRn……..…….....…….59

Chapter 4:
A Freeze Substitution Fixation-Based Gold Enlarging Technique for EM Studies
of Endocytosed Nanogold-Labeled Molecules……..……..…....67

Chapter 5:
Investigation of FcRn Exocytosis by Total Internal Reflection Fluorescence
Microscopy……...…….79

Appendix I:
Generation of a Recombinant Fluorescent Ligand for Live-Cell Imaging of FcRn
Trafficking……...105

Appendix II:
Attempts to Detect FcRn Homodimers Using Förster Resonance Energy
Transfer and Bimolecular Fluorescence Complementation……....117

Chapter 1:

Introduction

Introduction

The evolution of complex organisms requires the successful integration of multiple themes. One of the simplest and yet most pervasive and vital of these is the theme of compartmentalization—the sequestration of specific biological components into distinct regions within a cell or organism. This theme is so prevalent that it applies from the cellular level—where the molecular components required for cellular structure and function are maintained within the confines of the plasma membrane and many of these so-contained components are further sequestered into the various organelles that permit cellular function—all the way up to the level of the whole organism—where different cell types and tissues associate with one another to produce organs and organ systems that are spatially and functionally separated from each other, and, more importantly, from the external world. The protein and cellular components that create and maintain these separations, whether at the level of the cell or of the whole organism, do so by regulating physical or chemical barriers in such a way that maintains the integrity of the internal environment while allowing for regulated alteration of these barriers in response to conditional influences from the external environment.

Polarized epithelia

Higher animals must reconcile the requirement of maintaining a controlled internal environment with the need to participate in selective exchange with the external environment. Epithelial cell barriers serve as a means for complex organisms to distinguish, both spatially and functionally, between the external environment and the underlying tissue.

A vital characteristic of such cellular barriers is their ability to selectively allow the passage of materials—such as ions, small molecules, peptides, lipids, and proteins—either by passive or active (receptor-mediated) transport mechanisms. Polarized epithelial cells are joined to one another by a structured, oligomeric transmembrane protein complex known as the tight-junction (TJ) (Simons and Wandinger-Ness, 1990). Although many of the precise details of the TJ's structure and composition remain to be elucidated, to date more than 50 proteins are known to be associated with the TJ (Gonzalez-Mariscal et al., 2003; Miyoshi and Takai, 2005; Schneeberger and Lynch, 2004). Tight junctions serve three purposes: 1) they hold adjacent cells together and provide structure to the monolayer; 2) they prevent the free diffusion of materials between the cells in the monolayer, thus requiring that materials enter the cells through diffusion or active transport in order to cross the tissue layer; and 3) they prevent the contents of the membranes above and below the TJ from mixing, thus allowing these respective membrane domains to maintain distinct protein and lipid compositions. The two membrane faces created as a result of this physical separation are referred to as the apical (Ap) surface, which faces the external surface of the mucosae or the lumen of an organ, and the basolateral (BL) surface, which faces the serosal surface or bloodstream (Simons and Wandinger-Ness, 1990) (Figure 1).

Transcytosis and cellular trafficking

The apical and basolateral surfaces of polarized cells are connected to one another via a multivesicular transport pathway called transcytosis (Tuma and Hubbard, 2003). Transcytosis is mediated by transmembrane receptors that originate on either the apical or

basolateral cell surface. This process requires that receptor-bound cargo be internalized into the endosomal membrane system and trafficked to its target destination as determined by motifs within the cytoplasmic tail of the receptor itself. During the first step of receptor-mediated transport—endocytosis—the cytoplasmic tail plays a central role by harboring the amino acid sequences necessary for the interaction of the receptor with cytosolic mediators such as AP-2, a tetrameric complex that serves as an adaptor between transmembrane receptors and components of the endocytic machinery. Of central importance is the ability of AP-2 to provide a direct link between the receptor and the clathrin coat (Tuma and Hubbard, 2003; Ungewickell and Hinrichsen, 2007), although clathrin-independent mechanisms of internalization do exist (Mayor and Pagano, 2007). Subsequent to internalization via clathrin-coated pits, clathrin-coated vesicles (CCVs) are uncoated in an ATP-dependant manner by the uncoating enzyme Hsc70 (Eisenberg and Greene, 2007) allowing the now-exposed membrane to be primed for fusion into the endosomal membrane network (Ungewickell and Hinrichsen, 2007).

The endosomes of a cell are membrane-bound compartments that serve as the staging ground for intracellular trafficking and protein sorting (Sachse et al., 2002) (Figure 1). The vast number of endosomes within the cell are classified into different subpopulations that maintain their identities based on unique combinations of traffic-regulating membrane proteins associated with them (Perret et al., 2005; Piper and Luzio, 2001; van Ijzendoorn, 2006). One of the larger classes of such proteins is the Rab family of small GTPases. These small (~ 25 kDa) proteins exist in either the inactive GDP-bound or the active GTP-bound state (Deneka et al., 2003). Rab proteins are soluble cytoplasmic proteins that are prenylated

in a regulated fashion by the enzyme Rab geranylgeranyl transferase (RabGG transferase), which in turn allows them to be inserted into endosomal membranes (Pereira-Leal et al., 2001). RabGG transferase adds two geranylgeranyl groups to cysteines at the C-terminus of Rab proteins (Pereira-Leal et al., 2001). Because Rab proteins do not a bear the canonical CAAX box used for recognition for the two other principle prenylating enzymes in the cell (farnesyltransferase and geranylgeranyl transferase I), they must first be bound by the Rab escort protein (REP) at more conserved sites within the Rab protein for subsequent presentation to RabGG transferase (Leung et al., 2006; Pfeffer and Aivazian, 2004). Prenylation allows their insertion into endosomal membranes where they in turn carry out trafficking-related effector functions (Fukuda, 2007; Seabra et al., 2002; Smythe, 2002). Only after receptors and their bound cargo have entered endosomes can the processes of receptor sorting and trafficking be performed through a series of interactions between the receptor and the various membrane proteins, adaptor proteins, and cytoskeletal components that comprise the intracellular trafficking machinery (Tuma and Hubbard, 2003). It is this step-wise progression through the intracellular trafficking itinerary that allows for transport to be precisely regulated by the cell.

The regulated transport of proteins within and across both polarized and non-polarized cells makes an essential contribution to the function of the immune system. Because epithelial linings are vulnerable to infectious agents within the environment, the transport of antibodies into mucosal secretions plays a key role in first-line defense immunity (Lamm et al., 1992). Additionally, the transport of antibodies within non-polarized vascular endothelial cells is essential for maintaining their high levels in the circulation (Junghans and Anderson, 1996).

A detailed understanding of the receptors responsible for these trafficking roles and their properties has implications both for gaining a better understanding of immune function in general and for developing effective strategies to treat diseases resulting from their dysfunction.

Immunoglobulin structure and function

Immunoglobulins (Igs or antibodies) are the fundamental protein players of both innate and acquired immunity. They are produced and secreted by a special class of lymphocytes called B-cells in response to the detection of a foreign agent (antigen) in their environment. Immunoglobulins are tetramers consisting of two light chains (LCs, ~ 25 kDa each) and two heavy chains (HCs, ~ 55 kDa each) arranged in a shape that resembles the letter "Y". The LCs contain an N-terminal variable domain and a C-terminal constant domain, while the heavy chains consist of a variable N-terminal domain and three to four C-terminal constant domains. The Fab (Fragment antigen binding) domain is composed of the LC and the first two N-terminal domains of the HC. The association of the LC and HC variable domains create an N-terminal combining site that confers the specificity of the antibody by virtue of the interaction of amino acids within the hypervariable regions of each variable domain with an antigen. The Fc (Fragment crystalline) region is a dimer of the two or more C-terminal domains of the HC that are not part of the Fab. Whereas the Fab is responsible for antigen recognition and binding, the Fc regulates the biological functions of the antibody by binding to Fc receptors and eliciting immune effector functions. Binding to Fc receptors can also

mediate transport of antibodies within cells or protect them from proteolytic degradation (Kindt et al., 2007).

Immunoglobulin isotypes

Mature, naïve B-cells express a single clonal variant of IgD and IgM on their surface. After being stimulated by antigen these cells differentiate into plasma cells and begin secreting IgM or undergo "class switching" to secrete IgA, IgE, or IgG (Figure 2). These isotypes differ from one another by amino acid sequences in their constant regions that confer class-specific structural and functional characteristics upon the molecule. Secreted IgM is a pentamer in which five monomeric IgM molecules are assembled together by disulfide bonds between each of their two C-terminal heavy chain domains. The pentamer also contains J chain (joining chain), which is disulfide bonded to a terminal cysteine residue in two of the monomers and is required for assembly of the pentamer (Kindt et al., 2007).

IgA is the most abundant Ig in external secretions such as mucus, tears, saliva, and breast milk. While a small amount of monomeric IgA is present in serum (only 10%–15% of total serum Ig), IgA in secretions (secretory IgA) is a dimer or tetramer containing J chain (Lamm et al., 1992; Lycke, 2005). Both IgM and IgA are delivered into mucosal secretions by the polymeric Ig receptor (pIgR) and provide a first line of defense against pathogens by inhibiting infection by viruses and colonization by bacteria. The secreted Ig oligomers are bound by a 70 kDa protein called secretory component (SC), which is proteolytically released from pIgR upon delivery of the Ig to the lumen of the relevant organ. SC consists of

five Ig-like domains and binds to the Fc region of IgA or IgM, with domain five forming a disulfide bond with the Fc of IgA. SC masks protease-sensitive sites in the Fc and allows secretory IgA and IgM to persist longer in the protease-rich environment of the mucosae (Brandtzaeg and Johansen, 2001; Rojas and Apodaca, 2002).

Another Ig isotype, IgE, is responsible for mediating reaction to allergens, causing the symptoms of allergies. IgE is present in serum at low concentrations (0.3 μg/mL) but is expressed on the surface of basophils and mast cells. When multiple IgE molecules on the surface of these cells are cross-linked by antigen the cells are stimulated to release stored granules containing histamine and other compounds that promote the allergic reaction (Kindt et al., 2007).

In mammals, IgG is the most abundant Ig in serum (~ 80% of total serum Ig) and is the principle Ig that participates in the adaptive immune response. There are four human IgG subclasses (IgG_1, IgG_2, IgG_3, and IgG_4) that are distinguished from one another by differences in the constant region of the heavy chain. These sequence differences affect the length of the hinge region as well as the position and number of disulfide bonds between the two heavy chains of the IgG molecule (Kindt et al., 2007). Additionally, different IgG subclasses bind to different Fc receptors with varying affinities. Thus, IgGs of one subclass may be more or less efficient at eliciting certain effector functions than IgGs of another subclass. For example, IgG_3 is the most effective subclass at activating complement, followed by IgG_1 and IgG_2, whereas IgG_4 cannot activate complement (Chatron and Pontet,

1992; Kindt et al., 2007; Smith, 1992). Circulating IgG participates in adaptive immunity by binding to antigens in the circulation. Antigens are then cleared through the subsequent activation of the complement cascade and/or other effector functions such as opsonization (phagocytosis of antigen/pathogen by macrophages and neutrophils) and antibody-dependent cell-mediated cytotoxicity (ADCC) (Kindt et al., 2007).

Passive immunization of newborn and gestating mammals by the mother via receptor-mediated transfer of IgG

Adult mammals have the capacity to generate antibodies against environmental antigens that are encountered during their lifetime. An animal that has generated an antibody response to an antigen is said to be actively immune to that antigen. There is, however, a certain lag time after initial exposure to the antigen before antibodies appear in the blood. This lag time appears to be about one week in mammals, during which the animal is vulnerable to the infectious agent (Kindt et al., 2007). Alternatively, pre-formed antibodies from one individual can be transferred to another and confer immediate immunity to the antigen. Because the immune-rendered individual does not produce the antibodies themselves, this is refereed to as passive immunity.

Passive acquistion of antibodies is particularly important in the case of rodents and several other mammals (see Table 1) whose young are unable to produce their own IgG for up to two weeks post-natally (Brambell, 1970), despite being exposed to the external environment during this time. To compensate, these animals acquire passive immunity during early life

via IgG transferred from the mother. IgG-rich colostrum is ingested and passes through the intestine where it is transferred across the polarized epithelial cell lining into the bloodstream. This transfer is mediated by the class I major histocompatability complex (MHC)-related neonatal Fc receptor (FcRn). FcRn is a heterodimeric type I transmembrane glycoprotein consisting of a heavy chain that is non-covalently associated with a light chain, β_2-microglobulin (β_2m), that also binds to class I MHC heavy chains (Rodewald and Kraehenbuhl, 1984; Simister and Rees, 1985). High-resolution crystal structures of human and rat FcRn, as well as a complex structure of rat FcRn in complex with Fc have been obtained (Burmeister et al., 1994a; Burmeister et al., 1994b; Martin et al., 2001; West and Bjorkman, 2000). FcRn is structurally similar to class I MHC molecules, although the counterpart of the MHC peptide-binding groove is narrowed and non-functional in FcRn.

FcRn binds to the Fc region of IgG with nanomolar affinity at pH ≤ 6.0, but exhibits no binding at the basic pH of blood (pH 7.4) (Simister and Mostov, 1989). This pH-dependent binding helps to promote the efficient unidirectional transfer of IgG from the acidic environment of the intestinal lumen to the blood stream of the neonate (Figure 3). Unlike rodents, humans and non-human primates are born with the capacity to produce serum IgG, thus post-natal transfer of maternal IgG does not occur (Brambell, 1970; Oxelius and Svenningsen, 1984). During gestation when the fetus is vulnerable, however, maternal IgG is transferred to the fetus via FcRn-mediated transcytosis across placental syncitiotrophoblast cells to provide the fetus with immunity to antigens encountered by the mother (Figure 4). The discovery that FcRn is expressed in the human fetal small intestine (Shah et al., 2003) suggests that maternal IgG in ingested amniotic fluid could also be delivered to the fetal

circulation by transport across intestinal epithelial cells, consistent with a common mechanism for passive immunization of human and rodent offspring.

Unlike the case of post-natal intestinal transfer in rodents, trans-placental IgG transfer in humans occurs in the absence of a net pH gradient. In this process, rather than being taken up actively after binding to FcRn at the cell surface, IgG is taken up passively via fluid-phase endocytosis by syncitiotrophoblast cells. Once within the acidic environment of endosomes, the IgG is bound by FcRn and transcytosed into the fetal circulation (Kristoffersen, 1996; Leach et al., 1996; Simister et al., 1996). Thus, although acidic pH greatly facilitates the uptake of IgG by FcRn by allowing the receptor to bind ligand at the cell surface prior to internalization, acidity is not an absolute requirement for efficient IgG uptake provided that the cell internalizes a sufficient amount of fluid-phase material to allow binding and transfer of physiologically relevant quantities of IgG by FcRn.

FcRn-mediated recycling of IgG and serum persistence

FcRn also plays an integral role in maintaining high serum levels of IgG. It has long been known that IgG has a long half-life relative to other serum proteins. It was also established by Brambell that the extended half-life of IgG was inversely proportional to the serum concentration of IgG (that is, the effect was saturable), leading him to postulate the existence of a protection receptor (which came to be called the Brambell protection receptor or FcRB)

(Brambell et al., 1964). Subsequent work demonstrated that FcRB and FcRn were, in fact, the same protein and that FcRn serves as a protection receptor by rescuing IgG that has been passively internalized via pinocytosis by vascular endothelial cells from a default catabolic pathway (Ghetie et al., 1996; Israel et al., 1996; Junghans and Anderson, 1996). Similar to the mechanism of materno-fetal transfer during primate gestation, FcRn binds to pinocytosed IgG in the acidic environment of the endosomes (Figure 5). However in this setting FcRn then recycles the IgG back to the cell surface where the IgG can dissociate and re-enter the circulation. Mouse knockouts in which either the FcRn heavy chain or the β_2-microglobulin light chain is deleted exhibit a greatly reduced serum IgG half-life (Ghetie et al., 1996; Junghans and Anderson, 1996). As a result, many studies over the past several years have sought to improve the serum half-lives of therapeutic antibodies by modulating the FcRn-Fc interaction (Dall'Acqua et al., 2006; Ferl et al., 2005; Petkova et al., 2006). An IgG that is capable of binding to FcRn with higher affinity at pH 6.0 but still dissociates readily at pH 7.4 should persist longer in the circulation, thus requiring fewer administrations of less antibody to achieve the desired therapeutic effect. Conversely, the use of peptide inhibitors against FcRn to block its IgG salvage capacity has shown promise as an alternative to conventional auto-immune disease therapies that involve intravenous administration of saturating doses of human IgG (IVIg) to promote the clearance of harmful endogenous host IgGs (Getman and Balthasar, 2005; Mezo et al., 2008).

FcRn expression in the adult gut suggests a role in the adaptive immune response

The pattern and time course of FcRn expression differs greatly between rodents and humans. Rodents express FcRn on intestinal epithelia at high levels at birth and these levels dissipate after weaning. By contrast, humans express the receptor in intestinal cells of both the fetus and adult (Israel et al., 1997; Roopenian and Akilesh, 2007). Cultured adult intestinal carcinoma cells have been used as a model for hFcRn transcytosis (Dickinson et al., 1999). Interestingly, it was recently shown that human FcRn transgenically expressed in the adult mouse gut is capable of transcytosing IgG in the basolateral to apical direction for deposition into luminal secretions where it can bind to antigen. Antigen-IgG complexes were then re-internalized and transcytosed back to the lamina propria where they could interact with dendritic cells (DCs), which in turn were able to prime an antigen-specific T-cell response (Yoshida et al., 2004; Yoshida et al., 2006a; Yoshida et al., 2006b). These results implicate FcRn as an important player in initial stages of the adaptive immune response. Interestingly, the lack of FcRn expression in the normal adult rodent gut suggests that this function of FcRn is not characteristic in all species and may even be unique to humans and perhaps non-human primates.

The role of FcRn in serum albumin salvage

One of the more unexpected discoveries concerning FcRn function in recent years has been the observation that hFcRn is capable of binding to human serum albumin (HSA) in biochemical assays (Chaudhury et al., 2003). The interaction exhibits the same pH-dependence as the FcRn-IgG interaction, suggesting a possible role for FcRn in the intracellular transport of albumin. This led researchers to investigate the effects of FcRn

heavy chain knockout mice on serum albumin levels. FcRn-deficient mice exhibit both a shortened serum albumin half-life and an increased rate of albumin biosynthesis (likely due to feedback mechanisms that compensate for the lowered plasma oncotic pressure caused by low albumin levels) (Anderson et al., 2006; Chaudhury et al., 2006; Chaudhury et al., 2003). Consistent with these data, at least one case of familial hypoalbuminemia in humans has been shown to result from a single nucleotide transversion that disrupts the signal sequence of β_2m (Wani et al., 2006). Biochemical and biophysical studies have suggested that albumin and IgG bind to FcRn at distinct, non-cooperative sites (Chaudhury et al., 2006). Interestingly, the FcRn-albumin interaction is inhibited by low concentration of the detergent Octyl-β-D-Glucopyranoside, whereas the FcRn-IgG interaction is not (Chaudhury et al., 2003). While the involvement of FcRn in the serum maintenance of albumin has been experimentally demonstrated in mice, Chapter 2 describes that *in vitro* experiments using rat FcRn expressed in polarized MDCK cells failed to demonstrated specific binding, transcytosis, or recycling of rat albumin by rFcRn. Thus whether or not the FcRn-albumin interaction is a universal feature of all species of FcRn is not yet clear.

A structure-based hypothesis for FcRn trafficking

An interesting feature of the FcRn-IgG interaction is that each IgG ligand contains two FcRn binding sites, one in the constant region of each heavy chain at the interface between the Cγ2 and Cγ3 domains, allowing for the formation of FcRn:Fc complexes with a 2:1 stoichiometry in solution (Huber et al., 1993; Martin and Bjorkman, 1999). This is not characteristic of all Fc receptors, many of which have only a single binding site and thus form 1:1 receptor:Fc

complexes (Sondermann and Oosthuizen, 2002a, b). While the benefit of a bivalent ligand seems apparent—two binding sites should yield a higher macroscopic dissociation constant (K_D) due to avidity effects—it is interesting to note that another natural FcRn ligand, albumin, is a monovalent ligand.

This raises the interesting question as to whether or not two sites are strictly required for transport of IgG for FcRn. This question was made even more intriguing by the co-crystal structure of rat FcRn in complex with a recombinant Fc molecule from rat IgG_{2a} (Burmeister et al., 1994b). The structure showed an oligomeric array of FcRn dimers bridged to one another through homodimeric Fc (referred to as an "oligomeric ribbon") yielding an overall 2n:1n FcRn:Fc stoichiometry (Figure 6). The natural question to ask was whether or not this oligomeric structure formed within trafficking vesicles and served as a signal to guide FcRn-IgG complexes to their target destinations. Two aspects of the structure made this possibility particularly appealing. First, the formation of this structure would require the opposing membrane faces to be held in close (~ 200 Å) proximity to one another. Indeed, long tubular vesicles are more prominently involved in transport and trafficking functions, whereas large spherical vesicles are generally associated more with degradative functions (Marsh et al., 1986). Second, formation of the oligomeric ribbon structure would induce a linearly ordered arrangement of FcRn cytoplasmic tails. The cytosolic trafficking machinery might utilize one or both of these features as an indicator that the compartment bearing them is to be transcytosed or recycled rather than catabolized.

Formation of the ribbon structure requires the simultaneous occurrence of two separate phenomena: 1) FcRn dimerization, and 2) bridging of opposing membrane faces through the ligand molecules. Conclusive evidence that both events occur at the same time in cells would constitute strong evidence for the existence of the oligomeric ribbon. Conversely, successful demonstration that one phenomenon or the other is not required for FcRn mediated transport would not completely rule out the possibility of ribbon formation, but would show that it is not required for proper transport of FcRn-IgG complexes. When I began my studies, one of the primary goals was to determine whether structural features of the FcRn-IgG interaction, such as the 2:1 FcRn:Fc stoichiometry, oligomeric ribbon formation, or receptor dimerization, were required for proper trafficking of these complexes. For example, it is possible that complex formation results in the emergence of unique structural features that are essential for proper recognition and movement of FcRn-IgG complexes by the intracellular trafficking machinery. Conversely, it is possible that all information required to properly traffic FcRn-IgG complexes is constitutively presented by the receptor regardless of whether or not ligand is present.

To address this question in a system that was amenable to experimental manipulations and perturbations, I generated an *in vitro* system based on stably transfected Madin-Darby canine kidney (MDCK) cells expressing rat FcRn. These epithelial cells form well-polarized monolayers at confluence and have long served as an established model system for the study of protein trafficking in polarized cells (Rojas and Apodaca, 2002; Simmons, 1982). Chapter 2 describes the generation and characterization of this cell line. Using recombinantly - expressed rat Fc molecules containing two, one, or zero FcRn binding sites, I addressed the

question of whether 2:1 complex formation and/or ribbon formation are required for proper transport of FcRn-Fc complexes using *in vitro* transcytosis and recycling assays. My results show that the presence of two FcRn-binding sites on a ligand molecule are not a strict requirement for FcRn-mediated trafficking, but that the resulting avidity effect makes transport of a bivalent ligand more efficient. Appendix I describes attempts to determine if FcRn dimerizes on the cell membrane using fluorescence resonance energy transfer (FRET) and bimolecular fluorescence complementation (BiFC).

Investigation of FcRn trafficking pathways in neonatal rat gut by electron tomography

Electron tomography (ET) is an electron microscopy (EM) technique used to obtain three-dimensional data from an EM sample (Donohoe et al., 2006; Frey et al., 2006; Subramaniam, 2005). The technique involves collecting a series of two-dimensional images from a thinly sectioned sample while tilting the specimen. This series of 2D images is then used to computationally reconstruct the specimen in 3D. A variety of factors limit the maximum quality of reconstruction that can be obtained by ET, but a resolution of ~ 4 nm is generally attainable (Donohoe et al., 2006; Frey et al., 2006; Subramaniam, 2005). Chapter 3 describes my early work in the generation of 1.4 nm gold cluster-labeled Fc molecules (Au-Fc) for use as an electron-dense marker for FcRn trafficking in ET studies. The preparation of this reagent served as a basis for later work in the lab. In experiments performed by Wanzhong He, a postdoctoral scholar in the laboratory, Au-Fc was fed to neonatal rats to allow FcRn-mediated uptake of the labeled ligand in the intestine, mimicking the transfer of maternal IgG across the intestine of the newborn. Electron tomography performed on harvested intestinal

samples revealed many Au-Fc-containing endosomes possessing distinct morphologies in different regions of the cell.

One of the more surprising observations from the electron tomography studies was the presence of clathrin-coated vesicles containing Au-Fc that appeared to be fusing with the lateral plasma membrane (He, et al. 2008). While clathrin is classically believed to be involved in only endocytosis via coated pits and some intracellular trafficking functions, its involvement in exocytosis was previously not considered a possibility because it has long been believed that the clathrin coats on trafficking vesicles are shed prior to membrane fusion (Altstiel and Branton, 1983; Brodsky et al., 2001; Conner and Schmid, 2003). However, two lines of evidence suggested that these clathrin-coated structures could not be endocytosing Au-Fc. First, the pH in the lateral intracellular space (LIS) should not be permissive for FcRn binding, as this space is contiguous with the circulation (pH 7.4). Second, the concentration of Au-Fc in the blood of the rat should not be high enough to permit binding to FcRn and should furthermore be competed away by the high concentration of unlabeled, endogenous IgG in the circulation. For these reasons we hypothesized that clathrin-coated vesicles containing FcRn-ligand complexes can partially uncoat and fuse with the target membrane. Subsequently, the vesicle may fully uncoat, releasing the FcRn molecules into the target membrane and allowing for its bound cargo to dissociate into the extracellular space. Alternatively, the partially clathrin-coated vesicle may remain at the membrane, allowing diffusion of ligand through the opening of the partially fused vesicle in a process akin to so-called “kiss-and-run” (Fesce et al., 1994) or “prolonged release” (Ober et al., 2004) before pinching back off and transporting the free receptor back to the apical surface to

acquire more ligand. The later model has the advantage of conserving the energy that would be required to fully uncoat the vesicle (and ATP-dependent process) and to reassemble the endocytic machinery required to return ligand-free FcRn back to the apical surface for subsequent round of transcytosis. Chapter 4 describes collaborative work I performed in the laboratory of Professor Sandy Simon at The Rockefeller University using total internal reflection fluorescence microscopy (TIRFM) to examine the dynamics of FcRn and clathrin during exocytosis at the plasma membrane of living MDCK cells.

An avian functional homologue of FcRn

While all classes of vertebrates have the capacity to mount an immune response, a majority of what is known about the complexities of these processes is limited to mammals and birds. Birds have long been known to possess highly developed cellular and serological immunity (Brambell, 1970). It is perhaps not surprising, therefore, that the transfer of passive immunity from mother to young is not a phenomenon unique to mammals. Indeed, the transfer of passive immunity to tetanus toxin in birds was first described by Klemperer in 1893, just one year after the same phenomenon was described in mammals by Ehlrich (Brambell, 1970). During avian development the gestating fetus has all of its nutritional requirements met by the yolk, which also contains a significant store of IgY (the avian and reptilian equivalent to IgG) from the mother. Transport of IgY from the yolk to the chick occurs across the yolk sac membranes and confers passive immunity to antigens encountered by the mother, despite the fetus having no direct contact with the mother (Kowalczyk et al., 1985). Persistence of maternal antibodies in fish (carp, *Cyprinus carpi*) and reptile (the

desert tortoise, *Gopherus agassizii*) hatchlings has also been described (Grindstaff et al., 2003).

Whereas the MHC in mammals is organized within a single locus, in birds the class I and class II MHC are arranged in at least two gene clusters that contain both MHC class I and class II *B* genes (Wittzell et al., 1998). In light of these differences in MHC organization, it is of clear interest to know if the receptor responsible for the transfer of IgY from the yolk to the fetus (and possibly responsible for transporting IgY from the mother into the ovum that eventually gives rise to the yolk) is truly a functional equivalent of FcRn and if it shares structural similarities with its mammalian homologue. The first step towards answering this question came when a protein fraction was isolated from chicken egg yolk sacs that bound to IgY in a pH-dependent fashion (West et al., 2004). Because of its expression in yolk sac and its pH-dependent binding properties reminiscent of the FcRn-IgG interaction, the receptor was believed to be the avian functional equivalent of FcRn and was named FcRY.

Surprisingly, FcRY shares no homology with class I MHC molecules or FcRn, but is instead a homolog of the mammalian phospholipase A_2 receptor (PLA_2R), a member of the mannose receptor (MR) family (East and Isacke, 2002) (Figure 7). The four members of the mammalian MR family mediate a variety of functions, including roles in the innate and adaptive immune systems (MR), internalization of soluble PLA_2 enzymes (PLA_2R), presentation of antigens to T cells (DEC-205), and remodeling of the extracellular matrix (Endo180). FcRY shares structural features with other MR family members, which consist of

an N-terminal cysteine-rich domain, a single fibronectin type II (FNII) domain, eight to ten tandem C-type lectin-like domains (CTLDs), a single-pass transmembrane region, and a short cytoplasmic tail (East and Isacke, 2002). The presence of tandem lectin-like domains does not necessarily imply carbohydrate-binding lectin activity, since only the MR and Endo180 bind to monosaccharide. Indeed the CTLDs in PLA_2R mediate a protein-protein interaction independently of carbohydrate (East and Isacke, 2002) and FcRY is thought to recognize IgY through a protein-protein interaction (West et al., 2004).

While other members of the MR family can mediate trafficking functions such as endocytosis, recycling, and delivery of internalized contents to lysosomes for antigen processing and presentation, no experimental evaluation of the trafficking behavior of FcRY had been performed since it was first isolated. Chapter 3 describes the demonstration of true functional equivalence between FcRn and FcRY using stably transfected rat inner medullary collecting duct (IMCD) cells as a model for polarized epithelia. These cells have been used previously to investigate the trafficking of FcRn (McCarthy et al., 2001; McCarthy et al., 2000; Wu and Simister, 2001), making them a useful model for comparison of the function of these two receptors in a similar cellular context. My results show that FcRY is able to endocytose, recycle, and transcytose FcY and IgY in polarized cells. Faithfully recapitulating the behavior of mammalian FcRn in the same cellular context.

References

Altstiel, L., and Branton, D. (1983). Fusion of coated vesicles with lysosomes: measurement with a fluorescence assay. Cell *32*, 921-929.

Anderson, C.L., Chaudhury, C., Kim, J., Bronson, C.L., Wani, M.A., and Mohanty, S. (2006). Perspective-- FcRn transports albumin: relevance to immunology and medicine. Trends in immunology *27*, 343-348.

Brambell, F.W., Hemmings, W.A., and Morris, I.G. (1964). A Theoretical Model of Gamma-Globulin Catabolism. Nature *203*, 1352-1354.

Brambell, F.W.R. (1970). The transmission of passive immunity from mother to young (Amsterdam,
New York,, North-Holland Pub. Co.;
American Elsevier).

Brandtzaeg, P., and Johansen, F.E. (2001). Confusion about the polymeric Ig receptor. Trends in immunology *22*, 545-546.

Brodsky, F.M., Chen, C.Y., Knuehl, C., Towler, M.C., and Wakeham, D.E. (2001). Biological basket weaving: formation and function of clathrin-coated vesicles. Annual review of cell and developmental biology *17*, 517-568.

Burmeister, W.P., Gastinel, L.N., Simister, N.E., Blum, M.L., and Bjorkman, P.J. (1994a). Crystal structure at 2.2 A resolution of the MHC-related neonatal Fc receptor. Nature *372*, 336-343.

Burmeister, W.P., Huber, A.H., and Bjorkman, P.J. (1994b). Crystal structure of the complex of rat neonatal Fc receptor with Fc. Nature *372*, 379-383.

Chatron, P., and Pontet, F. (1992). [Structure an functions of IgG subclasses]. Annales de biologie clinique *50*, 565-575.

Chaudhury, C., Brooks, C.L., Carter, D.C., Robinson, J.M., and Anderson, C.L. (2006). Albumin binding to FcRn: distinct from the FcRn-IgG interaction. Biochemistry *45*, 4983-4990.

Chaudhury, C., Mehnaz, S., Robinson, J.M., Hayton, W.L., Pearl, D.K., Roopenian, D.C., and Anderson, C.L. (2003). The major histocompatibility complex-related Fc receptor for IgG (FcRn) binds albumin and prolongs its lifespan. The Journal of experimental medicine *197*, 315-322.

Conner, S.D., and Schmid, S.L. (2003). Regulated portals of entry into the cell. Nature *422*, 37-44.

Dall'Acqua, W.F., Kiener, P.A., and Wu, H. (2006). Properties of human IgG1s engineered for enhanced binding to the neonatal Fc receptor (FcRn). The Journal of biological chemistry *281*, 23514-23524.

Deneka, M., Neeft, M., and van der Sluijs, P. (2003). Regulation of membrane transport by rab GTPases. Critical reviews in biochemistry and molecular biology *38*, 121-142.

Dickinson, B.L., Badizadegan, K., Wu, Z., Ahouse, J.C., Zhu, X., Simister, N.E., Blumberg, R.S., and Lencer, W.I. (1999). Bidirectional FcRn-dependent IgG transport in a polarized human intestinal epithelial cell line. J Clin Invest *104*, 903-911.

Donohoe, B.S., Mogelsvang, S., and Staehelin, L.A. (2006). Electron tomography of ER, Golgi and related membrane systems. Methods (San Diego, Calif *39*, 154-162.

East, L., and Isacke, C.M. (2002). The mannose receptor family. Biochim Biophys Acta *1572*, 364-386.

Eisenberg, E., and Greene, L.E. (2007). Multiple roles of auxilin and hsc70 in clathrin-mediated endocytosis. Traffic (Copenhagen, Denmark) *8*, 640-646.

Ferl, G.Z., Wu, A.M., and DiStefano, J.J., 3rd (2005). A predictive model of therapeutic monoclonal antibody dynamics and regulation by the neonatal Fc receptor (FcRn). Annals of biomedical engineering *33*, 1640-1652.

Fesce, R., Grohovaz, F., Valtorta, F., and Meldolesi, J. (1994). Neurotransmitter release: fusion or 'kiss-and-run'? Trends in cell biology *4*, 1-4.

Frey, T.G., Perkins, G.A., and Ellisman, M.H. (2006). Electron tomography of membrane-bound cellular organelles. Annual review of biophysics and biomolecular structure *35*, 199-224.

Fukuda, M. (2007). [Specificity and diversity of Rab family GTPases in membrane traffic]. Seikagaku *79*, 1046-1051.

Getman, K.E., and Balthasar, J.P. (2005). Pharmacokinetic effects of 4C9, an anti-FcRn antibody, in rats: implications for the use of FcRn inhibitors for the treatment of humoral autoimmune and alloimmune conditions. Journal of pharmaceutical sciences *94*, 718-729.

Ghetie, V., Hubbard, J.G., Kim, J.K., Tsen, M.F., Lee, Y., and Ward, E.S. (1996). Abnormally short serum half-lives of IgG in beta 2-microglobulin-deficient mice. Eur J Immunol *26*, 690-696.

Gonzalez-Mariscal, L., Betanzos, A., Nava, P., and Jaramillo, B.E. (2003). Tight junction proteins. Prog Biophys Mol Biol *81*, 1-44.

Grindstaff, J.L., Brodie, E.D., 3rd, and Ketterson, E.D. (2003). Immune function across generations: integrating mechanism and evolutionary process in maternal antibody transmission. Proceedings *270*, 2309-2319.

Huber, A.H., Kelley, R.F., Gastinel, L.N., and Bjorkman, P.J. (1993). Crystallization and stoichiometry of binding of a complex between a rat intestinal Fc receptor and Fc. J Mol Biol *230*, 1077-1083.

Israel, E.J., Taylor, S., Wu, Z., Mizoguchi, E., Blumberg, R.S., Bhan, A., and Simister, N.E. (1997). Expression of the neonatal Fc receptor, FcRn, on human intestinal epithelial cells. Immunology *92*, 69-74.

Israel, E.J., Wilsker, D.F., Hayes, K.C., Schoenfeld, D., and Simister, N.E. (1996). Increased clearance of IgG in mice that lack beta 2-microglobulin: possible protective role of FcRn. Immunology *89*, 573-578.

Junghans, R.P., and Anderson, C.L. (1996). The protection receptor for IgG catabolism is the beta2-microglobulin-containing neonatal intestinal transport receptor. Proc Natl Acad Sci U S A *93*, 5512-5516.

Kindt, T.J., Goldsby, R.A., Osborne, B.A., and Kuby, J. (2007). Immunology, 6th edn (New York, W.H. Freeman).

Kowalczyk, K., Daiss, J., Halpern, J., and Roth, T.F. (1985). Quantitation of maternal-fetal IgG transport in the chicken. Immunology *54*, 755-762.

Kristoffersen, E.K. (1996). Human placental Fc gamma-binding proteins in the maternofetal transfer of IgG. APMIS Suppl *64*, 5-36.

Lamm, M.E., Robinson, J.K., and Kaetzel, C.S. (1992). Transport of IgA immune complexes across epithelial membranes: new concepts in mucosal immunity. Advances in experimental medicine and biology *327*, 91-94.

Leach, J.L., Sedmak, D.D., Osborne, J.M., Rahill, B., Lairmore, M.D., and Anderson, C.L. (1996). Isolation from human placenta of the IgG transporter, FcRn, and localization to the syncytiotrophoblast: implications for maternal-fetal antibody transport. J Immunol *157*, 3317-3322.

Leung, K.F., Baron, R., and Seabra, M.C. (2006). Thematic review series: lipid posttranslational modifications. geranylgeranylation of Rab GTPases. Journal of lipid research *47*, 467-475.

Lycke, N. (2005). From toxin to adjuvant: basic mechanisms for the control of mucosal IgA immunity and tolerance. Immunology letters *97*, 193-198.

Marsh, M., Griffiths, G., Dean, G.E., Mellman, I., and Helenius, A. (1986). Three-dimensional structure of endosomes in BHK-21 cells. Proceedings of the National Academy of Sciences of the United States of America *83*, 2899-2903.

Martin, W.L., and Bjorkman, P.J. (1999). Characterization of the 2:1 complex between the class I MHC-related Fc receptor and its Fc ligand in solution. Biochemistry *38*, 12639-12647.

Martin, W.L., West, A.P., Jr., Gan, L., and Bjorkman, P.J. (2001). Crystal structure at 2.8 A of an FcRn/heterodimeric Fc complex: mechanism of pH-dependent binding. Mol Cell *7*, 867-877.

Mayor, S., and Pagano, R.E. (2007). Pathways of clathrin-independent endocytosis. Nature reviews *8*, 603-612.

McCarthy, K.M., Lam, M., Subramanian, L., Shakya, R., Wu, Z., Newton, E.E., and Simister, N.E. (2001). Effects of mutations in potential phosphorylation sites on transcytosis of FcRn. J Cell Sci *114*, 1591-1598.

McCarthy, K.M., Yoong, Y., and Simister, N.E. (2000). Bidirectional transcytosis of IgG by the rat neonatal Fc receptor expressed in a rat kidney cell line: a system to study protein transport across epithelia. J Cell Sci *113 (Pt 7)*, 1277-1285.

Mezo, A.R., McDonnell, K.A., Castro, A., and Fraley, C. (2008). Structure-activity relationships of a peptide inhibitor of the human FcRn:human IgG interaction. Bioorganic & medicinal chemistry *16*, 6394-6405.

Miyoshi, J., and Takai, Y. (2005). Molecular perspective on tight-junction assembly and epithelial polarity. Adv Drug Deliv Rev *57*, 815-855.

Ober, R.J., Martinez, C., Lai, X., Zhou, J., and Ward, E.S. (2004). Exocytosis of IgG as mediated by the receptor, FcRn: an analysis at the single-molecule level. Proceedings of the National Academy of Sciences of the United States of America *101*, 11076-11081.

Oxelius, V.A., and Svenningsen, N.W. (1984). IgG subclass concentrations in preterm neonates. Acta paediatrica Scandinavica *73*, 626-630.

Pereira-Leal, J.B., Hume, A.N., and Seabra, M.C. (2001). Prenylation of Rab GTPases: molecular mechanisms and involvement in genetic disease. FEBS letters *498*, 197-200.

Perret, E., Lakkaraju, A., Deborde, S., Schreiner, R., and Rodriguez-Boulan, E. (2005). Evolving endosomes: how many varieties and why? Current opinion in cell biology *17*, 423-434.

Petkova, S.B., Akilesh, S., Sproule, T.J., Christianson, G.J., Al Khabbaz, H., Brown, A.C., Presta, L.G., Meng, Y.G., and Roopenian, D.C. (2006). Enhanced half-life of genetically engineered human IgG1 antibodies in a humanized FcRn mouse model: potential application in humorally mediated autoimmune disease. International immunology *18*, 1759-1769.

Pfeffer, S., and Aivazian, D. (2004). Targeting Rab GTPases to distinct membrane compartments. Nature reviews *5*, 886-896.

Piper, R.C., and Luzio, J.P. (2001). Late endosomes: sorting and partitioning in multivesicular bodies. Traffic (Copenhagen, Denmark) *2*, 612-621.

Rodewald, R., and Kraehenbuhl, J.P. (1984). Receptor-mediated transport of IgG. The Journal of cell biology *99*, 159s-164s.

Rojas, R., and Apodaca, G. (2002). Immunoglobulin transport across polarized epithelial cells. Nature reviews *3*, 944-955.

Roopenian, D.C., and Akilesh, S. (2007). FcRn: the neonatal Fc receptor comes of age. Nat Rev Immunol *7*, 715-725.

Sachse, M., Ramm, G., Strous, G., and Klumperman, J. (2002). Endosomes: multipurpose designs for integrating housekeeping and specialized tasks. Histochemistry and cell biology *117*, 91-104.

Schneeberger, E.E., and Lynch, R.D. (2004). The tight junction: a multifunctional complex. Am J Physiol Cell Physiol *286*, C1213-1228.

Seabra, M.C., Mules, E.H., and Hume, A.N. (2002). Rab GTPases, intracellular traffic and disease. Trends in molecular medicine *8*, 23-30.

Shah, U., Dickinson, B.L., Blumberg, R.S., Simister, N.E., Lencer, W.I., and Walker, W.A. (2003). Distribution of the IgG Fc receptor, FcRn, in the human fetal intestine. Pediatr Res *53*, 295-301.

Simister, N.E., and Mostov, K.E. (1989). An Fc receptor structurally related to MHC class I antigens. Nature *337*, 184-187.

Simister, N.E., and Rees, A.R. (1985). Isolation and characterization of an Fc receptor from neonatal rat small intestine. Eur J Immunol *15*, 733-738.

Simister, N.E., Story, C.M., Chen, H.L., and Hunt, J.S. (1996). An IgG-transporting Fc receptor expressed in the syncytiotrophoblast of human placenta. Eur J Immunol *26*, 1527-1531.

Simmons, N.L. (1982). Cultured monolayers of MDCK cells: a novel model system for the study of epithelial development and function. General pharmacology *13*, 287-291.

Simons, K., and Wandinger-Ness, A. (1990). Polarized sorting in epithelia. Cell *62*, 207-210.

Smith, T.F. (1992). IgG subclasses. Advances in pediatrics *39*, 101-126.

Smythe, E. (2002). Direct interactions between rab GTPases and cargo. Molecular cell *9*, 205-206.

Sondermann, P., and Oosthuizen, V. (2002a). The structure of Fc receptor/Ig complexes: considerations on stoichiometry and potential inhibitors. Immunology letters *82*, 51-56.

Sondermann, P., and Oosthuizen, V. (2002b). X-ray crystallographic studies of IgG-Fc gamma receptor interactions. Biochemical Society transactions *30*, 481-486.

Subramaniam, S. (2005). Bridging the imaging gap: visualizing subcellular architecture with electron tomography. Current opinion in microbiology *8*, 316-322.

Tuma, P.L., and Hubbard, A.L. (2003). Transcytosis: crossing cellular barriers. Physiological reviews *83*, 871-932.

Ungewickell, E.J., and Hinrichsen, L. (2007). Endocytosis: clathrin-mediated membrane budding. Current opinion in cell biology *19*, 417-425.

van Ijzendoorn, S.C. (2006). Recycling endosomes. Journal of cell science *119*, 1679-1681.

Wani, M.A., Haynes, L.D., Kim, J., Bronson, C.L., Chaudhury, C., Mohanty, S., Waldmann, T.A., Robinson, J.M., and Anderson, C.L. (2006). Familial hypercatabolic hypoproteinemia caused by deficiency of the neonatal Fc receptor, FcRn, due to a mutant beta2-microglobulin gene. Proceedings of the National Academy of Sciences of the United States of America *103*, 5084-5089.

West, A.P., Jr., and Bjorkman, P.J. (2000). Crystal structure and immunoglobulin G binding properties of the human major histocompatibility complex-related Fc receptor(,). Biochemistry *39*, 9698-9708.

West, A.P., Jr., Herr, A.B., and Bjorkman, P.J. (2004). The chicken yolk sac IgY receptor, a functional equivalent of the mammalian MHC-related Fc receptor, is a phospholipase A2 receptor homolog. Immunity *20*, 601-610.

Wittzell, H., Madsen, T., Westerdahl, H., Shine, R., and von Schantz, T. (1998). MHC variation in birds and reptiles. Genetica *104*, 301-309.

Wu, Z., and Simister, N.E. (2001). Tryptophan- and dileucine-based endocytosis signals in the neonatal Fc receptor. J Biol Chem *276*, 5240-5247.

Yoshida, M., Claypool, S.M., Wagner, J.S., Mizoguchi, E., Mizoguchi, A., Roopenian, D.C., Lencer, W.I., and Blumberg, R.S. (2004). Human neonatal Fc receptor mediates transport of IgG into luminal secretions for delivery of antigens to mucosal dendritic cells. Immunity *20*, 769-783.

Yoshida, M., Kobayashi, K., Kuo, T.T., Bry, L., Glickman, J.N., Claypool, S.M., Kaser, A., Nagaishi, T., Higgins, D.E., Mizoguchi, E.*, et al.* (2006a). Neonatal Fc receptor for IgG regulates mucosal immune responses to luminal bacteria. The Journal of clinical investigation *116*, 2142-2151.

Yoshida, M., Masuda, A., Kuo, T.T., Kobayashi, K., Claypool, S.M., Takagawa, T., Kutsumi, H., Azuma, T., Lencer, W.I., and Blumberg, R.S. (2006b). IgG transport across mucosal barriers by neonatal Fc receptor for IgG and mucosal immunity. Springer seminars in immunopathology *28*, 397-403.

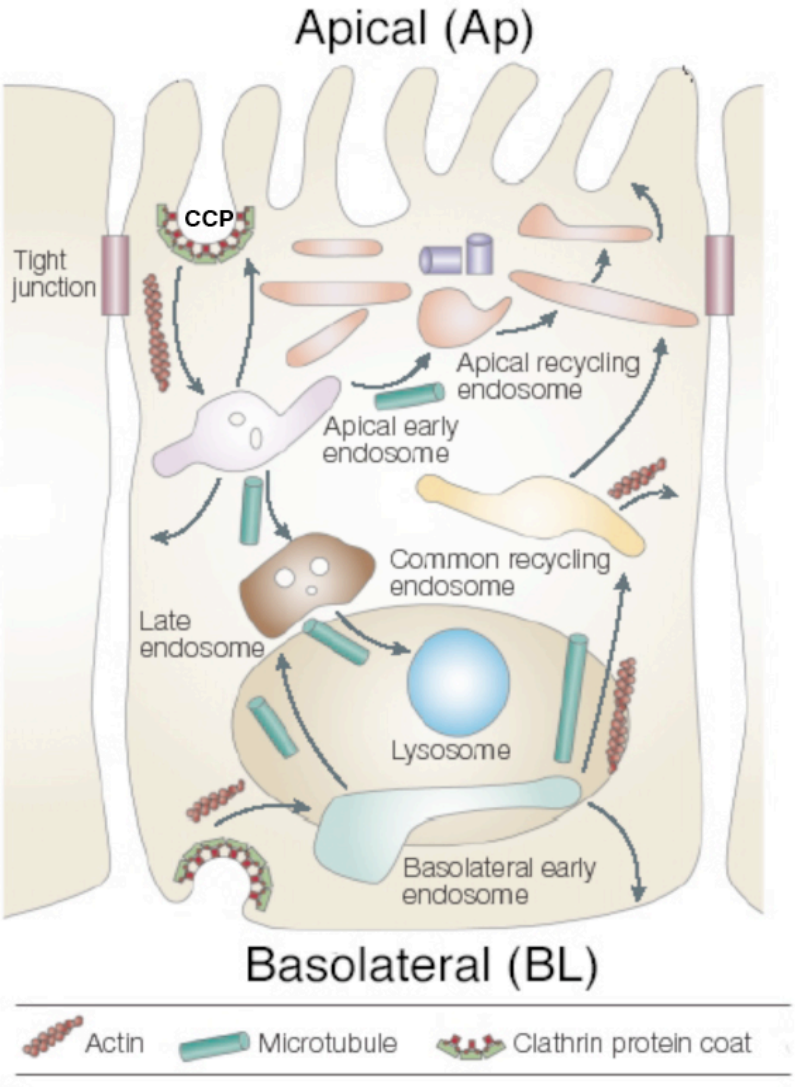

Figure 1. Schematic representation of endosomal trafficking pathways in a polarized epithelia cell. The apical and basolateral surfaces of epithelia are separated by tight junctions (TJs) which allow these domains to maintain distinct protein and lipid compositions. Transfer of materials across epithelia occur through diffusion for small materials such as ions, or through receptor-mediated transcytosis processes for large molecules such as proteins. For receptor-mediated transcytosis, ligands are bound by their cognate receptors and internalized through clathrin-coated pits (CCPs). Motifs in the receptor cytoplasmic tail communicate with the cellular trafficking machinery which regulates the navigation of receptor-ligand complexes through the various subpopulations of membrane-bound compartments that constitute the endosomal network. (Adapted from Rojas and Apodaca, 2002)

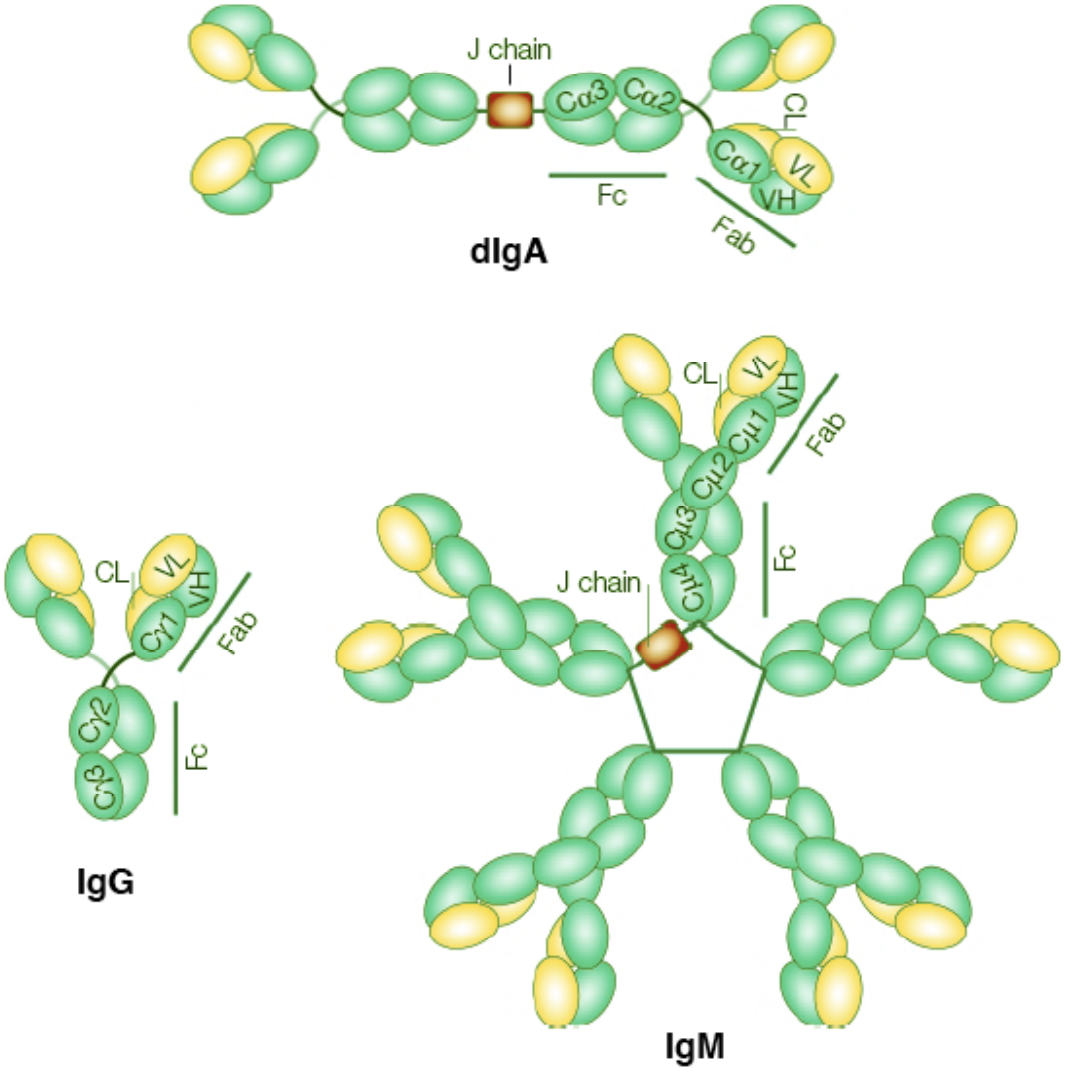

Figure 2. Immunoglobulin isotypes. IgD and monomeric IgM are displayed on the surface of naïve B-cells. After exposure to antigen and activation by helper T-cells the B-cell will begin secreting pentameric IgM or undergo class switching, after which the cell will secrete IgA, IgE, or IgG. IgA exists as both a monomer in serum and as a dimer (dIgA) in mucosal secretions in which two IgA monomers are attached by J chain. IgE attaches to the surface of mast cells where it mediates the allergic response. IgG is the most abundant immunoglobulin in serum and plays the most prominent role in the adaptive immune response. Both IgE and IgG exist only as monomers. (Adapted from Rojas and Apodaca, 2002)

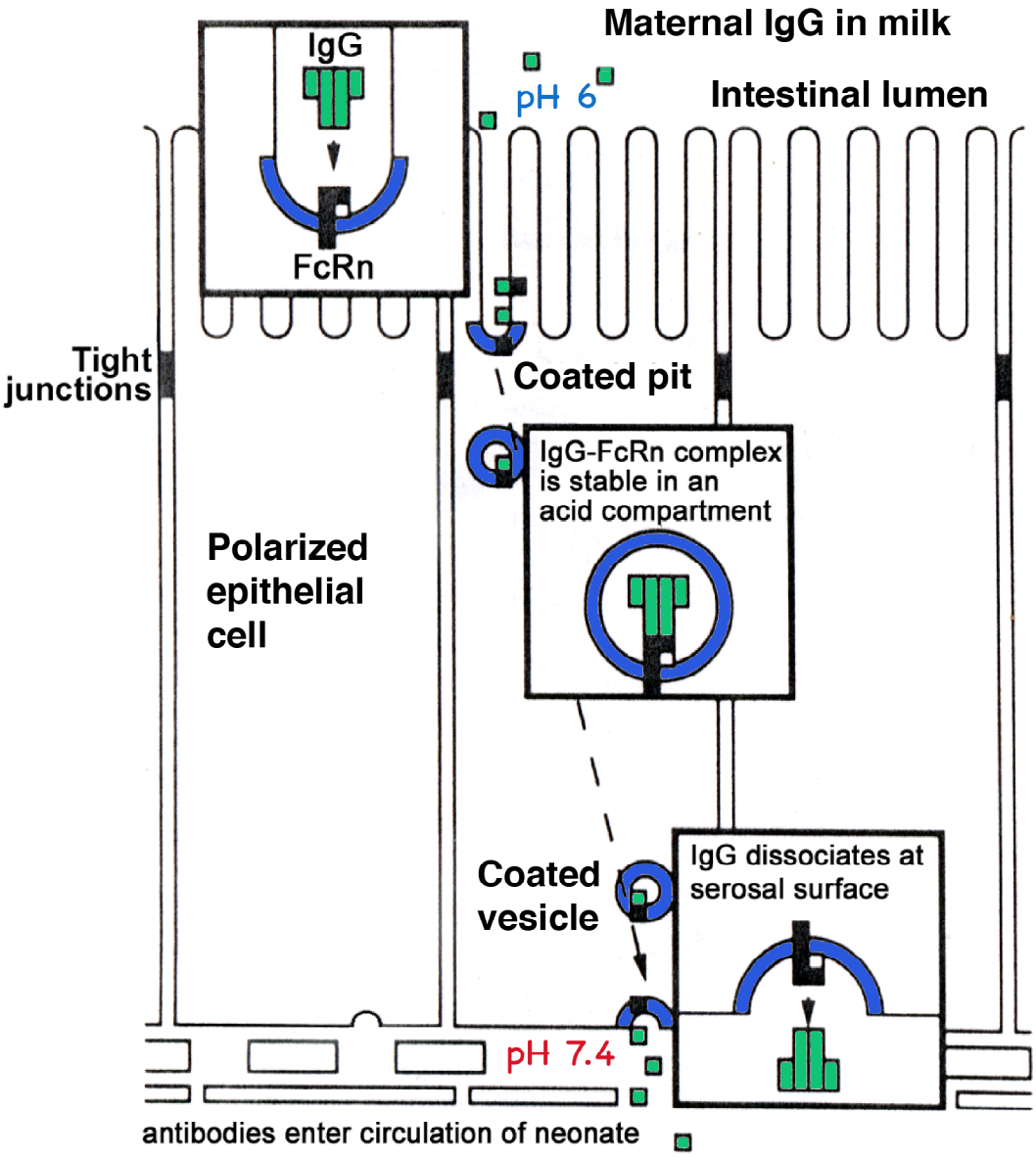

Figure 3. Schematic representation of FcRn function in the neonatal rodent gut. IgG present in maternal milk passing through the acidic environment of the intestinal lumen is bound by FcRn at the apical surface of polarized intestinal epithelial cells. Subsequent internalization and transcytosis of the IgG allows it to dissociate from FcRn upon exposure to the slightly basic pH of the newborn blood, thus entering the circulation. This process confers passive immunity to antigens encountered by the mother. (Adapted from Simister, et al., 1997)

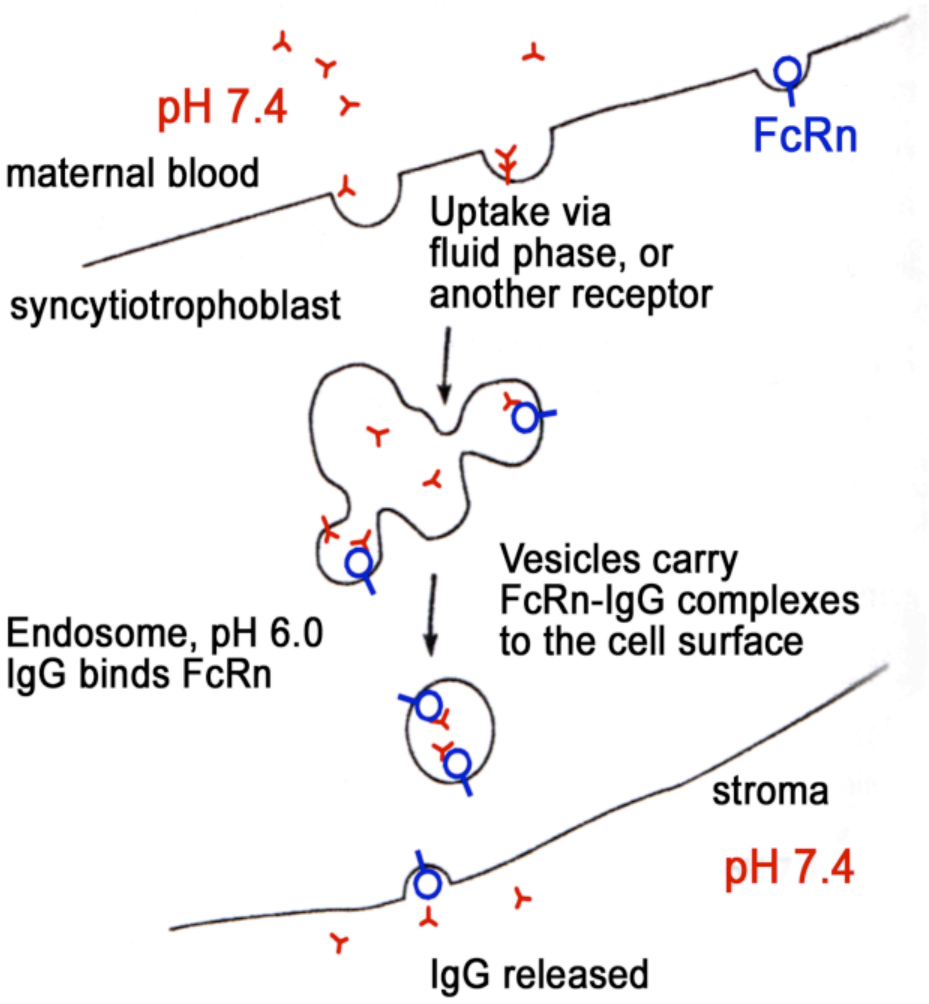

Figure 4. Placental transfer of IgG in the gestating primate**.** FcRn present in placental syncitiotrophoblast cells binds to fluid-phase internalized IgG in acidic endosomes. FcRn-IgG complexes are transcytosed across the placental tissue layer into the fetal circulation. The route of transfer is seen in both humans and non-human primates. (Adapted from Biochem. Soc. Trans. 25:481-487)

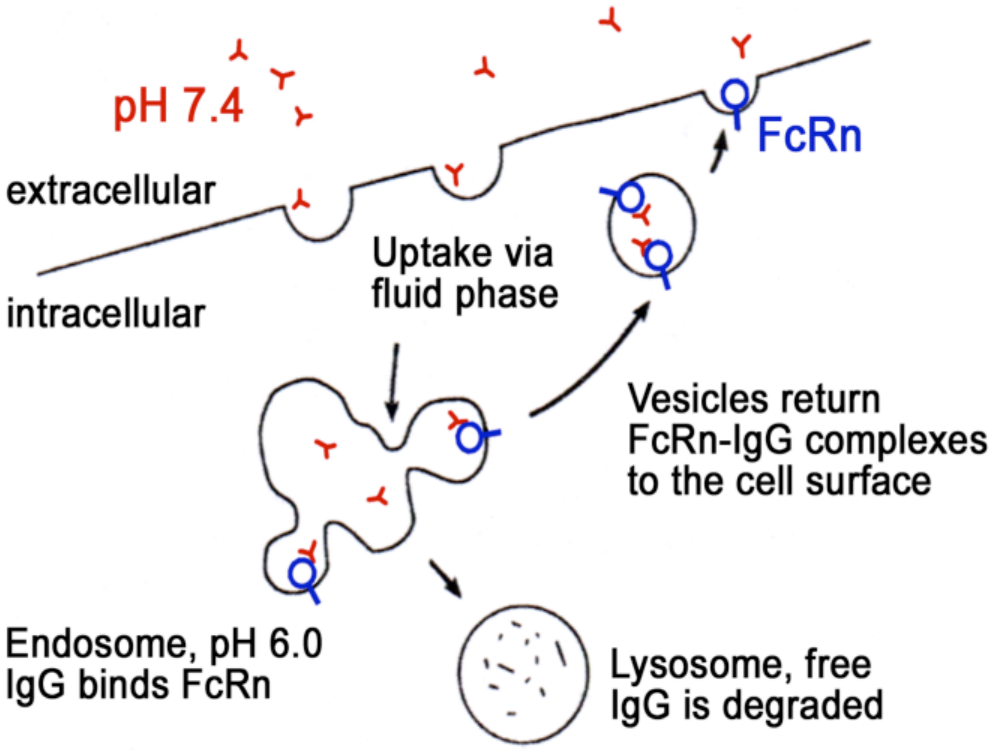

Figure 5. FcRn-mediated recycling of IgG. Circulating IgG is internalized via the fluid-phase by vascular endothelial cells. Fluid-phase material is targeted for destruction by a default catabolic pathway. FcRn present in acidic endosomes binds to IgG and transports it back to the cell surface where it can re-enter the circulation. This process confers a long serum half-life upon IgG relative to other serum proteins. A similar process has been proposed for FcRn-mediated salvage of albumin. (Adapted from Biochem. Soc. Trans. 25: 481-487)

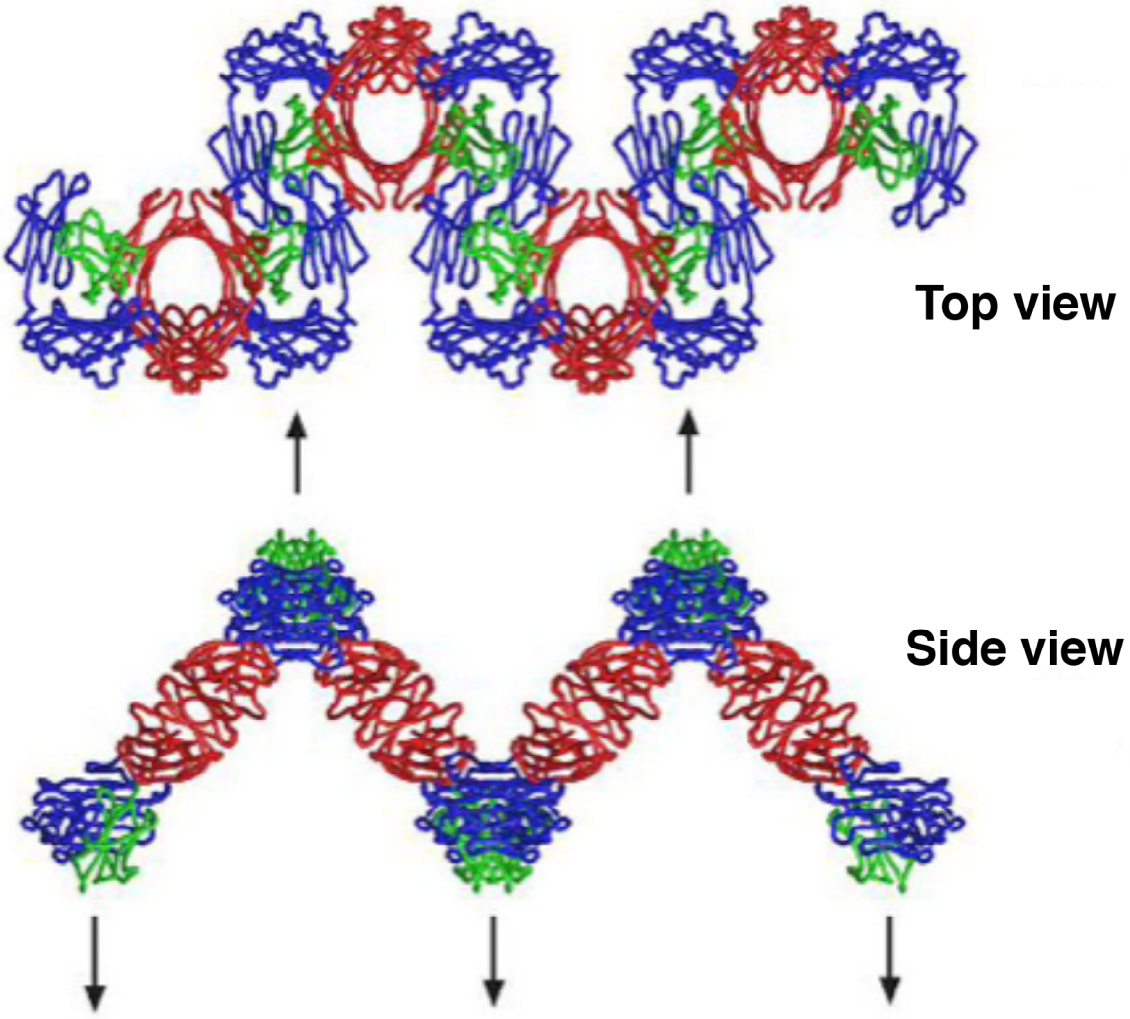

Figure 6. The "oligomeric ribbon" seen in the co-crystal structure of rat FcRn in complex with rat Fc. The structure is an array of FcRn dimers (α-chain in blue, β_2m in green) bridged by homodimeric Fc (red). In the top view the membrane would be in the plane of the page. The side view is rotated 90 degress towards the viewer. Arrows indicate where FcRn would attach to the membrane. (Adapted from Burmeister, et al. 1994)

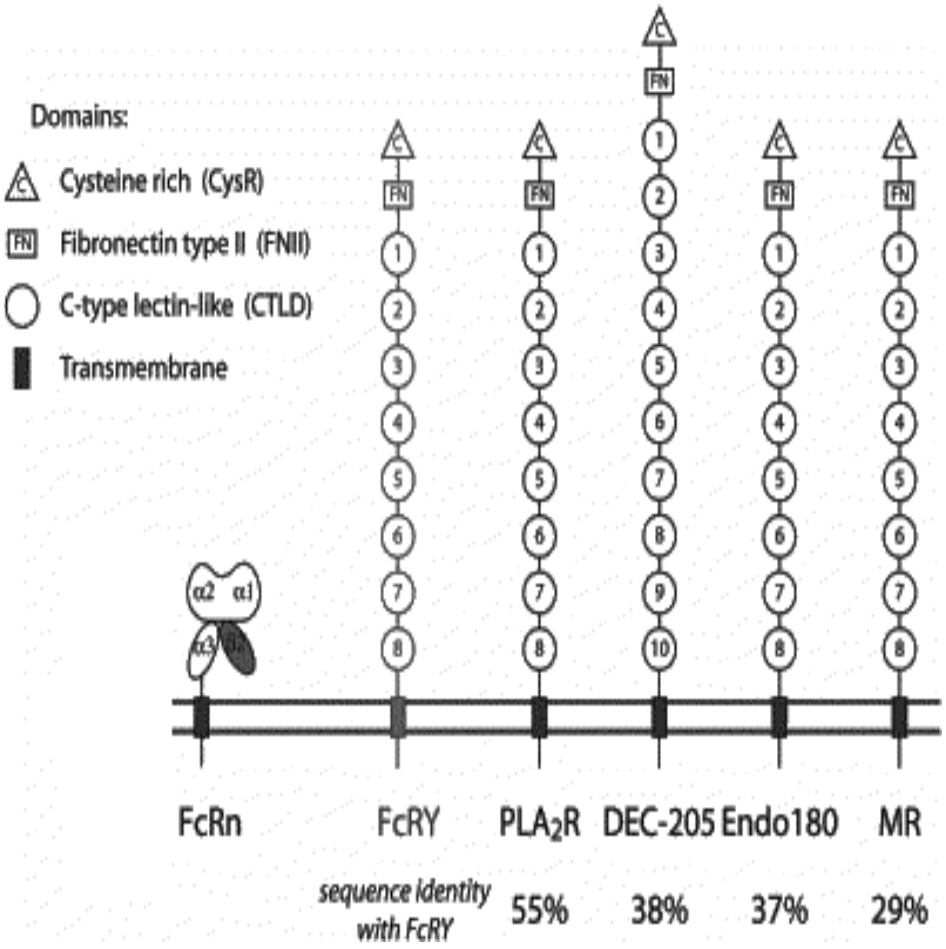

Figure 7. Structural comparison between FcRY and mannose receptor (MR) family members. FcRY exhibits a high degree of sequence identity to the mammalian PLA_2R. All MR family members contain multiple C-type lectin-like domains and N-terminal Fibronectin type II and cysteine-rich domains. FcRY is structurally distinct from the class I MHC-related FcRn. (West, A.P., 2002)

	Transmission of passive immunity		Route of transmission	
Species	**Prenatal**	**Postnatal**	**Prenatal**	**Postnatal**
Horse	-	++++ (24 hrs)	None	Gut
Pig	-	+++ (24-36 hrs)	None	Gut
Ruminants (ox, goat, sheep)	-	+++ (24 hrs)	None	Gut
Wallaby	-	+++ (180 days)	None	Gut
Dog, cat	+	++ (1-2 days)	Unknown (yolk sac?)	Gut
Chicken	++	++ (<5 days)	Yolk sac	Yolk sac
Hedgehog	+	++ (40 days)	Unknown	Gut
Mouse	+	++ (16 days)	Yolk sac	Gut
Rat	+	++ (20 days)	Yolk sac	Gut
Guineapig	+++	-	Yolk sac	None
Rabbit	+++	-	Yolk sac	None
Human, primates	+++	-	Placenta	None
Fish (carp)	+	++	Yolk sac	Yolk sac
Reptiles (desert tortoise)	+	++	Yolk sac	Yolk sac

Table 1. Timeframes and transmission routes of passive immunity across different species.

Chapter 2:

Ligand Valency Affects Transcytosis, Recycling, and Intracellular Trafficking Mediated by the Neonatal Fc Receptor

In the paper we describe the importance of ligand bivalency for the efficient FcRn-mediated transport of Fc and IgG. Noreen Tiangco assisted in the isolation and maintenance of cell lines used in the transport experiments and in the production of recombinant Fc proteins.

Traffic 2006; **7:** 1–16
Blackwell Munksgaard

© 2006 The Authors

doi: 10.1111/j.1600-0854.2006.00457.x

Ligand Valency Affects Transcytosis, Recycling and Intracellular Trafficking Mediated by the Neonatal Fc Receptor

OnlineOpen: This article is available free online at www.blackwell-synergy.com

Devin B. Tesar[1], Noreen E. Tiangco[1,2,3] and Pamela J. Bjorkman[1,2]*

[1]Division of Biology and [2]Howard Hughes Medical Institute, California Institute of Technology, Pasadena, CA 91125, USA
[3]Present address: Division of Graduate Medical Sciences, Boston University, Boston, MA, 02118, USA
** Corresponding author: Pamela J. Bjorkman, bjorkman@caltech.edu*

The neonatal Fc receptor (FcRn) transports IgG across epithelial cell barriers to provide maternal antibodies to offspring and serves as a protection receptor by rescuing endocytosed IgG and albumin from lysosomal degradation. Here we describe the generation of polarized Madin–Darby canine kidney (MDCK) cells expressing rat FcRn (rFcRn) to investigate the potential requirement for ligand bivalency in FcRn-mediated transport. The rFcRn-MDCK cells bind, internalize and bidirectionally transcytose the bivalent ligands IgG and Fc across polarized cell monolayers. However, they cannot be used to study FcRn-mediated transport of the monovalent ligand albumin, as we observe no specific binding, internalization or transcytosis of rat albumin. To address whether ligand bivalency is required for transport, the ability of rFcRn to transcytose and recycle wild-type Fc homodimers (wtFc; two FcRn-binding sites) and a heterodimeric Fc (hdFc; one FcRn-binding site) was compared. We show that ligand bivalency is not required for transcytosis or recycling, but that wtFc is transported more efficiently than hdFc, particularly at lower concentrations. We also demonstrate that hdFc and wtFc have different intracellular fates, with more hdFc than wtFc being trafficked to lysosomes and degraded, suggesting a role for avidity effects in FcRn-mediated IgG transport.

Key words: apical, basolateral, FcRn, FcRn-GFP, heterodimeric Fc (hdFc), IgG, Madin–Darby canine kidney (MDCK) cells, transcytosis

Received 10 December 2005, revised and accepted for publication 25 May 2006

The plasma membranes of epithelial cell barriers are segregated into two spatially and functionally distinct domains that serve as a means for complex organisms to distinguish between the external environment and the underlying tissue. A vital characteristic of such cellular barriers is their ability to selectively allow the passage of materials, such as ions, small molecules, peptides, lipids and proteins, either by passive or active (receptor mediated) transport mechanisms. The neonatal Fc receptor (FcRn), a class I major histocompatibility complex (MHC)-related protein that associates with the MHC light chain β_2-microglobulin (β_2m), mediates the transfer of maternal IgG across epithelial cell barriers to the fetus or newborn (1,2). In newborn suckling rodents, FcRn is expressed in the polarized epithelium of the intestine. The FcRn present at the apical surface of the intestinal cells binds to maternal IgG from ingested milk, transcytoses it across the epithelium and releases it into circulation from the basolateral cell surface (1). This process confers passive humoral immunity to the newborn during the first weeks of independent life. The difference in pH between the intestinal lumen (~pH 6.0) and the bloodstream (~pH 7.4) promotes the efficient unidirectional transport of IgG, as FcRn binds IgG at pH values $\leq$6.5, but not at neutral or higher pH (1,3).

The FcRn-mediated transport of IgG can also occur in the absence of a pH gradient. In gestating primates, IgG in the maternal bloodstream is transferred to the fetal bloodstream in a process that consists of passive uptake of IgG by syncitiotrophoblast cells, followed by transcytotic delivery to the fetal bloodstream on the opposite surface (4–6). In adult mammals, FcRn plays a key role in serum IgG homeostasis by protecting IgG taken up by vascular endothelial cells from a default degradative pathway (7–9). For both these functions, it is believed that IgG internalized at pH 7.4 via fluid-phase endocytosis is bound by FcRn in acidic endosomes. This results in FcRn–IgG complexes being transcytosed in the case of maternofetal IgG transfer, or returned to the cell surface rather than catabolized in the case of serum IgG homeostasis.

We previously described a structure-based hypothesis to account for the ability of cells to distinguish endosomes containing FcRn–IgG complexes destined for recycling or transcytosis from endosomes destined for a degradative pathway (10). The hypothesis suggests that an oligomeric ribbon of FcRn dimers bridged by the homodimeric Fc regions of IgG molecules, as seen in the crystal structure of an rFcRn/Fc complex (11), forms inside acidic trafficking vesicles. Formation of the oligomeric ribbon between the

Re-use of this article is permitted in accordance with the Creative Commons Deed, Attribution 2.5, which does not permit commercial exploitation.

adjacent membranes of a tubular endosome could act as an intracellular trafficking signal, designating vesicles containing such complexes for entry into the transcytotic or recycling pathways. A requirement for the formation of the oligomeric ribbon is a homodimeric Fc or IgG molecule capable of bridging between FcRn proteins on opposing membrane faces. Consistent with this hypothesis, previous studies demonstrated that a heterodimeric Fc molecule (hdFc), which contains one FcRn-binding chain and one non-FcRn-binding chain, is less efficiently transcytosed across neonatal mouse intestine (12) and exhibits a shorter serum half-life (13) than a wild-type homodimeric Fc molecule (wtFc). These results indicate that two FcRn-binding sites on a ligand are required for the purposeful movement of vesicles containing FcRn–ligand complexes through the transcytotic and protection pathways. However, recent studies have demonstrated that human and rodent FcRn bind a monomeric ligand, serum albumin, with a similar pH dependency as the FcRn–IgG interaction, and that mice lacking either the FcRn heavy or light chain exhibit a shortened half-life for albumin in the circulation (14,15). These studies support a model in which FcRn acts as a protection receptor for a monomeric protein, albumin, as well as for dimeric IgG and Fc ligands.

Here we describe an *in vitro* system using transfected Madin–Darby canine kidney (MDCK) cells to compare the transport of dimeric and monomeric FcRn ligands. The MDCK cells expressing rat FcRn (rFcRn) transcytose Fc and IgG in both the apical to basolateral and basolateral to apical directions, consistent with previous studies of human FcRn (hFcRn) and rFcRn expressed in MDCK cells or other polarized cell lines (16–23). We do not observe specific binding, uptake or transcytosis of a naturally occurring monovalent FcRn ligand, rat albumin. We therefore used variant forms of rat Fc containing two, one or zero FcRn-binding site (24) to assess the effects of ligand valency on FcRn-mediated transport. We show that the presence of two binding sites on the internalized Fc is not strictly required for the transcytosis or recycling to occur, but a bivalent Fc with two FcRn-binding sites (wtFc) is trafficked more efficiently than its monovalent cognate (hdFc), particularly at lower concentrations. Analysis by confocal microscopy of wtFc and hdFc trafficking following internalization reveals that the two ligands have different intracellular fates such that more internalized hdFc than wtFc colocalizes with markers for early endosomes (EEA1) and lysosomes, consistent with quantitative studies demonstrating that more hdFc than wtFc is degraded after internalization. These results suggest that avidity effects play a key role in FcRn-mediated ligand transport.

Results

Functional expression of rFcRn in MDCK cells

Our laboratory previously described the generation of MDCK cell lines expressing rFcRn and an rFcRn-green fluorescent protein (GFP) chimeric protein (25). In the course of conducting new experiments with the previously described rFcRn-GFP-MDCK cell line, we discovered that we could not replicate some of the published properties of the cell line (26). It had been reported that the rFcRn-GFP-MDCK cells functioned in transport of Fc when ligand was added at both permissive (acidic) and nonpermissive (basic) pH values for the rFcRn–IgG interaction and that rFcRn-GFP fluorescence underwent a striking redistribution upon addition of ligand at either pH (25). In recent experiments, however, we found that the rFcRn-GFP-MDCK cell line, although positive by antibody staining for both the rFcRn heavy and light chains (data not shown), did not take up significant amounts of Fc or IgG at basic pH, and the distribution of rFcRn-GFP did not change upon ligand addition (26).

To resolve these discrepancies, we generated new MDCK cell lines stably expressing rat β_2m (rβ_2m) together with the full-length rFcRn heavy chain or with an rFcRn-GFP chimera in which GFP was added C-terminal to the rFcRn cytoplasmic tail. Drug-resistant transfected cells were screened by Western blot and by pH-dependent uptake of fluorescent rat Fc. A drug-resistant cell line transfected with an empty expression vector (vector-only MDCK) was used as a negative control. The rFcRn-MDCK and rFcRn-GFP-MDCK cells used in the present studies exhibited transepithelial electrical resistance (TEER) values of ~250–300 Ωcm^2 when grown as polarized monolayers on filter supports. The high TEER value is important, as the rFcRn-GFP-MDCK cell line described previously (25) was subsequently found to have low TEER values (~50–75 Ωcm^2), consistent with our later finding that the cells were leaky to radiolabeled ligands (our unpublished results).

Expression of rFcRn and rFcRn-GFP in the newly generated MDCK cell lines was verified in cell lysates by Western blot. An anti-rFcRn antiserum detected two bands migrating with apparent molecular masses of ~50 and ~65 kDa in the rFcRn-MDCK cell lysate and ~80 and ~95 kDa in the rFcRn-GFP-MDCK cell lysate (Figure 1A). The upper and lower bands likely represent mature and incompletely glycosylated forms of rFcRn, respectively, as previously observed for hFcRn expressed in MDCK (16) cells and rFcRn expressed in rat inner medullary collecting duct (IMCD) cells (22). To verify IgG binding by rFcRn in MDCK cells, whole-cell lysates were incubated with human IgG-Sepharose beads at acidic or basic pH, and the bound proteins were eluted and analyzed by Western blot. The rFcRn and rFcRn-GFP were detected in IgG pull-downs conducted at acidic but not at basic pH (Figure 1B), although both proteins were detectable in blots of total cell lysates from rFcRn-MDCK and rFcRn-GFP-MDCK at both pH 6 and 8 (data not shown). Additionally, no rFcRn or rFcRn-GFP is detected in IgG pull-downs performed at pH 6 and subsequently washed at pH 8 (data not shown), demonstrating that both forms of rFcRn bind IgG at pH 6 and dissociate from the ligand at pH 8.

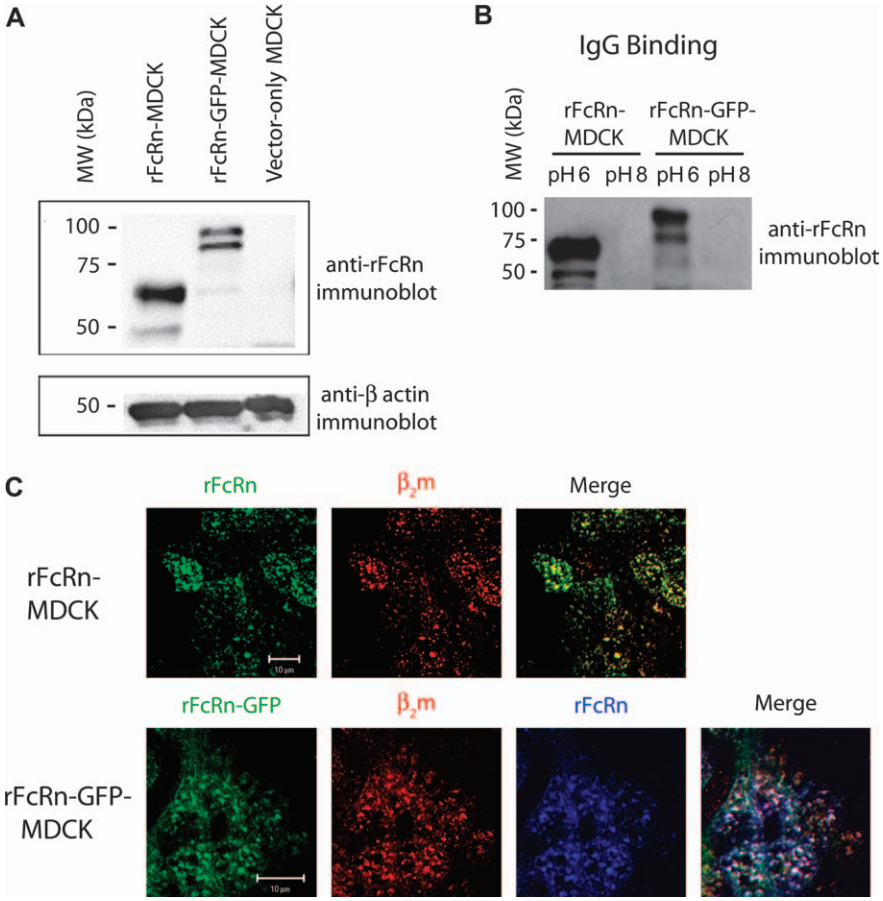

Figure 1: Expression of rFcRn and rFcRn-GFP in MDCK cells. (A) Western blot using anti-rFcRn antiserum of detergent lysates from rFcRn-MDCK, rFcRn-GFP-MDCK and vector-only MDCK cells. Two bands, likely representing the mature and incompletely glycosylated rFcRn heavy chains, are detected in rFcRn-expressing cells, but not in control cells. (B) Western blot of detergent lysates after a pull-down with human IgG-Sepharose at pH 6 or pH 8. Bands corresponding to the rFcRn and rFcRn-GFP heavy chains are present in samples from pull-downs at pH 6. No bands are detected in samples pulled down at pH 6 and subsequently washed at pH 8 (data not shown). (C) Confocal images of rFcRn-MDCK and rFcRn-GFP cells stained with fluorescently labeled anti-rFcRn (green or blue) or anti-rβ_2m (red) antibodies. Staining of rFcRn-MDCK cells shows that rFcRn-positive compartments colocalize with rβ_2m-positive compartments, and staining of rFcRn-GFP-MDCK cells shows that fluorescence from GFP colocalized with fluorescence from both the anti-rFcRn and anti-rβ_2m antibodies.

Confocal analyses of rFcRn-MDCK and rFcRn-GFP-MDCK cells showed intracellular compartments that are labeled by antibodies against the heavy and light chains of rFcRn (Figure 1C). The stainings for rFcRn and rβ_2m are colocalized, consistent with proper association between the two chains, and both the anti-rFcRn and the anti-rβ_2m fluorescence colocalize with GFP fluorescence in the rFcRn-GFP-MDCK cell line, indicating that GFP can be used as a marker for rFcRn expression in this cell line.

The ability of rFcRn-MDCK and rFcRn-GFP-MDCK cells to uptake wtFc, a recombinant rat Fc (24), was evaluated by a quantitative radioligand endocytosis assay. As shown in Figure 2, rFcRn-MDCK and rFcRn-GFP-MDCK cells internalized a significant amount of [^{125}I]wtFc at pH 6 but not at pH 8. Internalization was saturable, as inclusion of the unlabeled wtFc or IgG reduced the uptake to background levels, and was also specific, as significant uptake of a recombinant rat Fc with substitutions in both chains that prevent binding to rFcRn (nonbinding Fc; nbFc) (24) was not observed in either the rFcRn-MDCK or the rFcRn-GFP-MDCK cells. Labeled hdFc, a recombinant rat Fc composed of one wild-type Fc chain and one nbFc chain (24), was also endocytosed by the rFcRn-MDCK cells in a saturable and pH-dependant manner, although at lower levels than wtFc (Figure 2). Taken together, these results show that rFcRn expressed in MDCK cells undergoes proper posttranslational modifications, binds IgG with the expected pH dependence and mediates specific and saturable uptake of Fc ligands at acidic pH.

To observe the subcellular localization of endocytosed Fc, the apical surfaces of polarized rFcRn-MDCK, rFcRn-GFP-MDCK or vector-only MDCK cell monolayers were incubated with wtFc (1 μM) at acidic or basic pH and processed for immunofluorescence microscopy. Confocal images

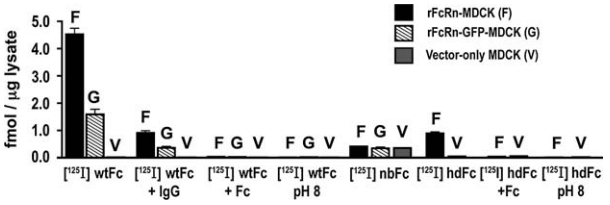

Figure 2: Endocytosis of rFcRn ligands by rFcRn and rFcRn-GFP expressed in MDCK cells. Subconfluent rFcRn-MDCK, FcRn-GFP-MDCK or vector-only MDCK were incubated with radiolabeled Fc ligands (recombinant wtFc, hdFc and nbFc derived from rat IgG2a at a concentration of 20 nM) at pH 6 or pH 8 in the presence or absence of a 500-fold excess of unlabeled competitor protein, and levels of radioactivity were determined in cell lysates.

(Figure 3) show that internalized wtFc (red fluorescence) is present in rFcRn-positive compartments (green fluorescence) in rFcRn-MDCK and rFcRn-GFP-MDCK cells incubated with ligand at pH 6. The distribution of rFcRn and rFcRn-GFP was not significantly different in the absence of wtFc or IgG compared to when these ligands were present at concentrations ranging from 20 nM to 1 μM (data not shown), contradicting the previous report (25). Also in contrast to the previous study (25), substantially less uptake was observed when the cells were incubated with wtFc at basic pH (pH 7.4) versus at acidic pH (shown for rFcRn-MDCK; Figure 3), indicating that an acidic extracellular environment greatly enhances uptake by allowing Fc to bind rFcRn at the cell surface prior to internalization. The vector-only MDCK cells did not stain with the 1G3 antibody and showed only low levels of internalized wtFc (Figure 3), likely resulting from trace internalization via the fluid phase.

Bidirectional transcytosis of IgG and Fc

Radiolabeled rat wtFc (20 nM) was added to the apical surface of the polarized rFcRn-MDCK or rFcRn-GFP-MDCK monolayers at pH 6, while the basolateral surface was maintained at pH 8. The amount of transcytosed ligand in the basolateral reservoir was measured after 90 min. Significantly more wtFc is transported by the rFcRn-MDCK cells than the control MDCK cells (Figure 4A). The presence of a 500-fold excess of competitor (unlabeled rat IgG or wtFc) reduces transcytosis to background levels observed for [^{125}I]nbFc.

Surprisingly, rFcRn-GFP-MDCK cells do not mediate specific transport of [^{125}I]wtFc (Figure 4A). This lack of detectable transport was observed in at least three other clones of rFcRn-GFP-MDCK cells, and in transcytosis experiments performed in both the apical to basolateral and basolateral to apical directions (data not shown). Because the rFcRn-GFP-MDCK cells do appear to function in a pH-dependent uptake of wtFc (Figure 2), these data suggest that addition of the GFP tag to the rFcRn cytoplasmic tail does not prevent endocytosis, but interferes with post-internalization trafficking events. Further experiments were therefore conducted using only the rFcRn-MDCK cells and vector-only control MDCK cells.

We next compared the ability of rFcRn-MDCK cells to transcytose IgG and Fc ligands in both the apical to basolateral and basolateral to apical directions (Figure 4B). These experiments were conducted using [^{125}I]human IgG and [^{125}I]human Fc because radiolabeled human IgG is transcytosed more efficiently than radiolabeled versions of other commercially available IgGs (data not shown). We find that both IgG and Fc are transcytosed bidirectionally across the rFcRn-MDCK cells when the loading surface is maintained at pH 6 and the nonloading surface is maintained at pH 8 (Figure 4B). When either ligand is prevented from binding to cell-surface rFcRn by maintaining the loading surface at pH 8, or by saturating surface receptors with unlabeled ligand, we see only background levels of transcytosis. Fc is transported more efficiently than intact IgG in both directions. The lower efficiency of IgG transcytosis as compared with Fc transcytosis may result from steric effects, i.e., the Fab arms present on intact IgG could clash with the membrane when rFcRn is in a 'standing up' conformation (11). This is consistent with our observation that intact rat IgG competes less efficiently for endocytosis and transcytosis of [^{125}I]wtFc than does wtFc (Figures 2 and 4A).

Binding, endocytosis and transport studies using rat albumin as an rFcRn ligand

IgG and Fc are both bivalent ligands of FcRn, that is, each contains two potential FcRn-binding sites. To determine whether rFcRn expressed in MDCK cells can act as a functional receptor for a monovalent ligand, rat serum albumin (RSA), we conducted binding, endocytosis and transcytosis assays using [^{125}I]RSA. Because RSA has a more acidic pH optimum than IgG for binding to rFcRn (14,27), cell-surface binding assays were performed at pH 5.0. Although rFcRn-MDCK cells incubated at pH 5 specifically bind [^{125}I]wtFc (data not shown), cells incubated with [^{125}I]RSA and then washed at pH 5 do not bind more RSA than cells washed at pH 8 (Figure 5A); thus, we see no specific binding of RSA to rFcRn-MDCK cells.

We next tested the possibility that binding to cell-surface rFcRn that is undetectable in a binding assay could promote endocytosis of RSA into rFcRn-MDCK cells. A high concentration (3 μM) of [^{125}I]RSA was added at pH 5 or 8 to rFcRn-MDCK or to vector-only MDCK cells in the presence or absence of a 100-fold excess of unlabeled RSA. We find that both the rFcRn-MDCK and vector-only cells internalize a high level of labeled RSA at pH 5 and at pH 8, with the greatest amount of internalization being observed when [^{125}I]RSA is added at pH 5 without competitor (Figure 5B). Although slightly more RSA is internalized at pH 5 by the rFcRn-MDCK cells than by the vector-only MDCK cells, perhaps representing rFcRn-mediated endocytosis of RSA, the difference is very small compared to the absolute amount of RSA internalized by either cell line.

We also investigated whether the rFcRn-MDCK cells can transcytose RSA. To account for the relatively low affinity of the RSA–rFcRn interaction (14,27), a high concentration of [^{125}I]RSA (10 μM) was incubated at the apical surface of

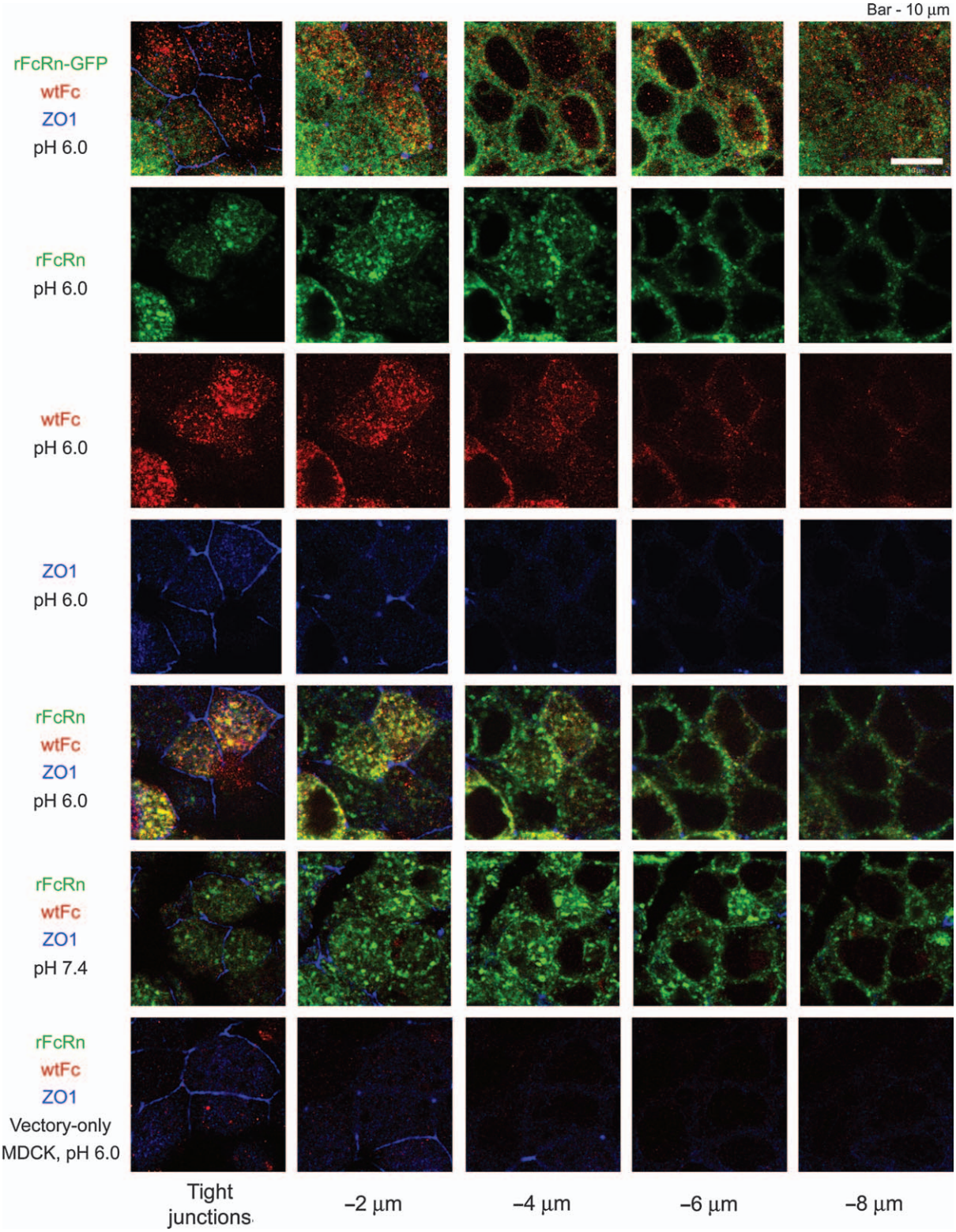

Figure 3: Distribution of internalized wtFc in rFcRn-MDCK, rFcRn-GFP-MDCK and vector-only MDCK cells. Filter-grown monolayers were incubated with 1 μM wtFc (recombinant Fc derived from rat IgG2a) for 1 h at pH 6 or pH 7.4 and processed for immunofluorescence using antibodies against wtFc (red) and the tight junction marker ZO-1 (blue). The heavy chain of rFcRn (green) was detected using GFP fluorescence (rFcRn-GFP-MDCK cells) or an antibody against the rFcRn heavy chain (rFcRn-MDCK and vector-only MDCK cells). Optical sections were taken every 2 μm below the level of the tight junctions.

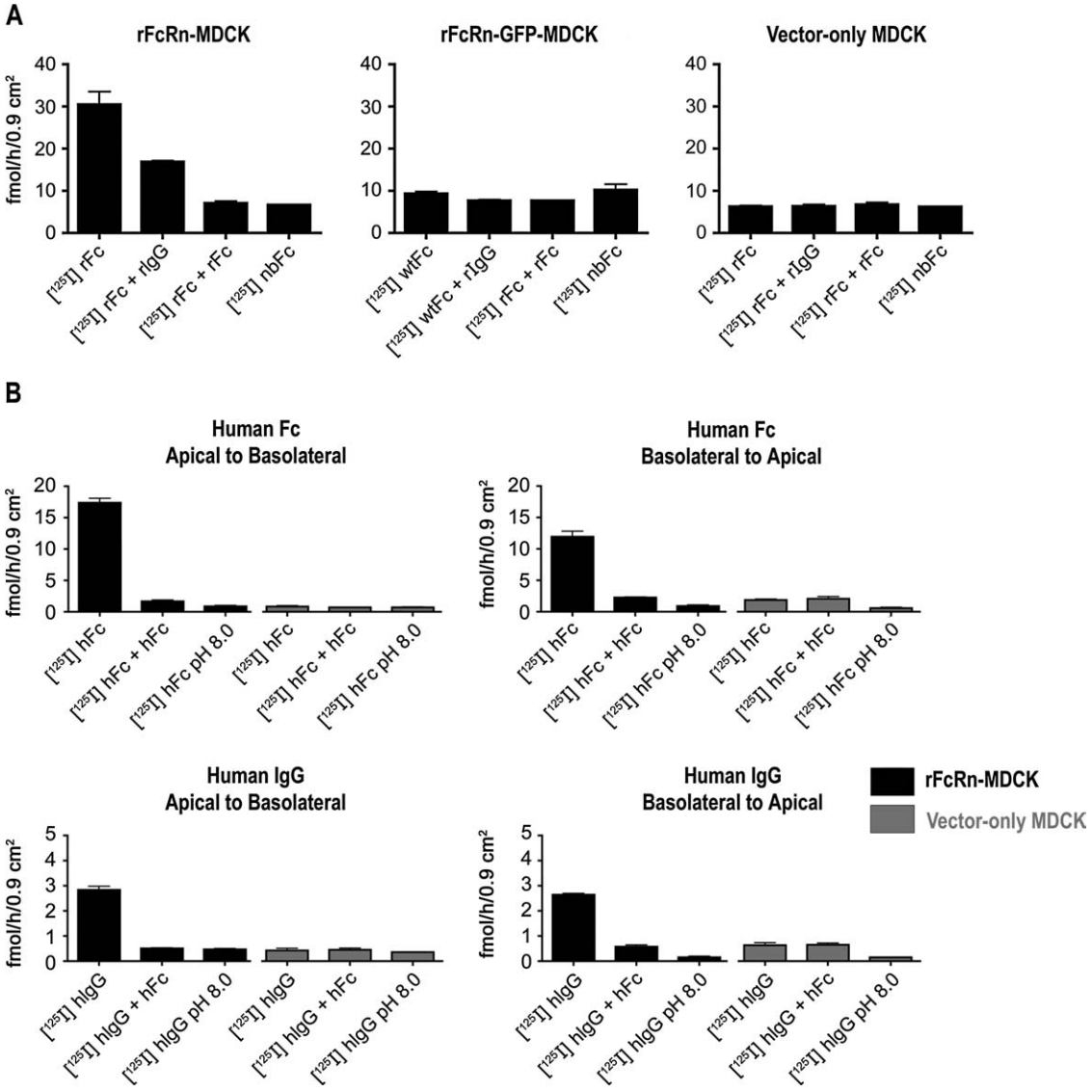

Figure 4: Bidirectional transcytosis of Fc and IgG ligands by rFcRn-MDCK cells. Radiolabeled Fc or IgG was added to the loading surface (apical in panel A and apical or basolateral in panel B) of polarized cell monolayers and levels of radioactivity in the media from the nonloading surface were measured after 90 min. Bars represent the mean and standard deviation of triplicate filters. (A) Comparison of apical to basolateral transcytosis of wtFc in three different cell lines. rFcRn-MDCK, rFcRn-GFP-MDCK and vector-only MDCK cells were incubated on the apical surface with 20 nM of [^{125}I]wtFc (recombinant Fc derived from rat IgG2a), [^{125}I]wtFc plus 500-fold excess unlabeled wtFc or rat IgG (rIgG), or [^{125}I]nbFc. (B) Comparison of bidirectional transcytosis of Fc and IgG. rFcRn-MDCK and vector-only MDCK cells were incubated with 20 nM [^{125}I]human Fc (hFc) or [^{125}I]human IgG (hIgG) on the apical or basolateral surface. Control experiments were performed in the presence of 500-fold excess unlabeled hFc or at pH 8 as indicated.

rFcRn-MDCK or vector-only-MDCK cells at pH 5 or pH 8. Control experiments using labeled wtFc and nbFc demonstrated that incubation at pH 5 does not disrupt transcytosis of a functional ligand (wtFc) or result in leakage of nbFc across the monolayer (Figure 5C). In the experiments using labeled RSA, we see no evidence of rFcRn-mediated transcytosis. Instead, we observe a high level of transport across both the rFcRn-MDCK and control cells at both acidic and basic pH, with transport being slightly higher for both cell lines at basic pH (Figure 5C). Similar results were obtained in experiments using lower concentrations of [^{125}I]RSA (data not shown). The lack of observed transcytosis of RSA in the rFcRn-MDCK cells is consistent with a previous demonstration that little or no albumin is transcytosed across the proximal intestine of neonatal rats under conditions in which 10–35% of the administered IgG is transported into the blood (28).

Relative affinities of wtFc and hdFc for cell-surface rFcRn

Because we did not observe binding or transyctosis of albumin, a naturally occurring monovalent ligand for FcRn,

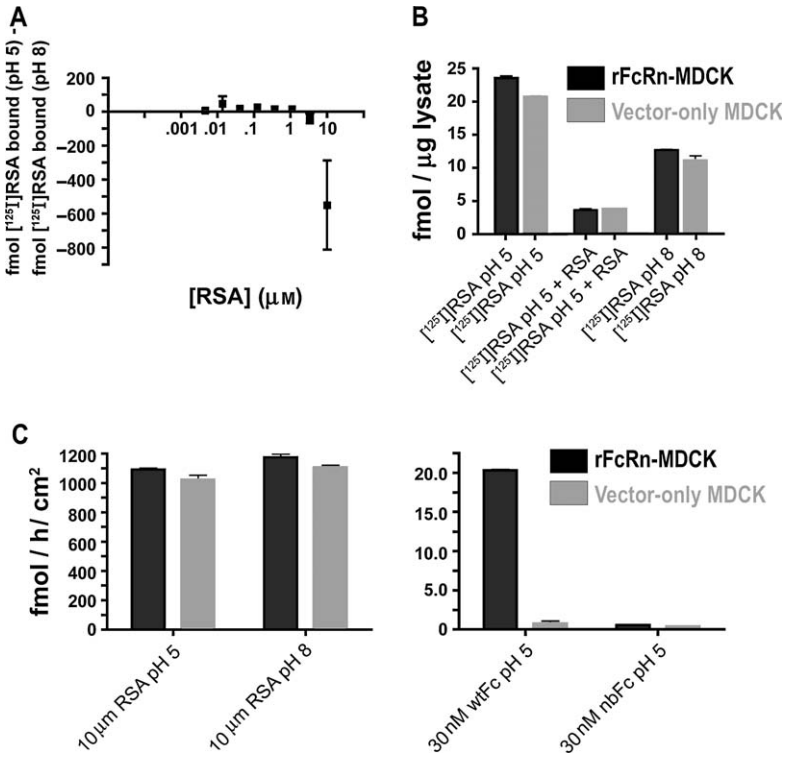

Figure 5: Albumin binding, endocytosis and transport experiments. (A) Cell-surface binding. rFcRn-MDCK cells were incubated at pH 5 with [^{125}I]RSA at a range of concentrations. For each concentration of labeled RSA, quadruplicate samples were washed at either pH 8 or pH 5 after the incubations, and the radioactivity bound at basic pH was subtracted from the radioactivity bound at acidic pH to determine the amount of specifically bound RSA at each concentration. (B) Endocytosis of RSA. Subconfluent rFcRn-MDCK and vector-only MDCK cells were incubated with 3 μM [^{125}I]RSA at pH 5 in the presence or absence of 2 mM unlabeled RSA, or at pH 8, and levels of radioactivity were determined in cell lysates. (C) Apical to basolateral transcytosis of RSA. The apical surfaces of filter-grown cell monolayers were incubated with 10 μM [^{125}I]RSA at pH 5 or pH 8 as indicated. Some filters were treated with 30 nM [^{125}I]wtFc or [^{125}I]nbFc as positive and negative controls, respectively. The levels of radioactivity in the basolateral media were determined after 90 min.

we used hdFc as a monovalent ligand for comparative studies with wtFc, a bivalent ligand. We first compared the binding of radiolabeled wtFc and hdFc to rFcRn on the surface of rFcRn-MDCK cells. Equilibrium dissociation constants (K_D) were determined by nonlinear regression analysis from plots of bound Fc as a function of Fc concentration (Figure 6A). The wtFc binding data were fit to a two-site binding model assuming two independent classes of binding sites (a high-affinity class, which takes avidity effects into account, and a low-affinity class), yielding K_D values of 1.6 and 13 nM. The hdFc binding data cannot be fit to a two-site binding model (data not shown), consistent with its single FcRn-binding site. These data were therefore fit to a 1:1 binding model, from which a K_D of 120 nM was derived.

Transcytosis and recycling efficiencies of monovalent and bivalent Fc proteins

We next compared the transcytosis and recycling efficiencies of the two forms of rat Fc. First, radiolabeled versions of wtFc and hdFc were added at pH 6 to the apical surface of rFcRn-MDCK monolayers at a range of concentrations. The amount of transcytosed Fc released into the basolateral medium after 90 min was plotted as a function of Fc concentration (Figure 6B), yielding curves that are analogous to the binding isotherms in Figure 6A. At concentrations below 1 μM, wtFc is transported in significantly greater amounts than hdFc. Transcytosis of both proteins is comparable at approximately 1 μM, and for values greater than 1 μM, more hdFc than wtFc is transported to the basolateral media. Nonlinear regression analysis performed on the trancytosis data was used to extract the concentration at which half-maximal transcytosis occurs ($T_{1/2max}$), which is analogous to a K_D, the concentration at which half-maximal binding of a ligand to its receptor occurs. As described for the binding data, the wtFc transcytosis data were fit to a two-site model, yielding two $T_{1/2max}$ values, 5.2 nM (high-affinity population) and 26 nM (low-affinity population), and the data for hdFc were fit to a one-site model, yielding a single $T_{1/2max}$ value (1.6 μM). The fact that the $T_{1/2max}$ value for the high-affinity population of receptors that bind wtFc (5.2 nM) is lower than the $T_{1/2max}$ value for hdFc (1.6 μM) indicates that bivalency of the Fc ligand contributes to the efficient transcytosis of cargo, particularly at lower ligand concentrations, but that ligand bivalency is not absolutely required for FcRn-mediated transcytosis.

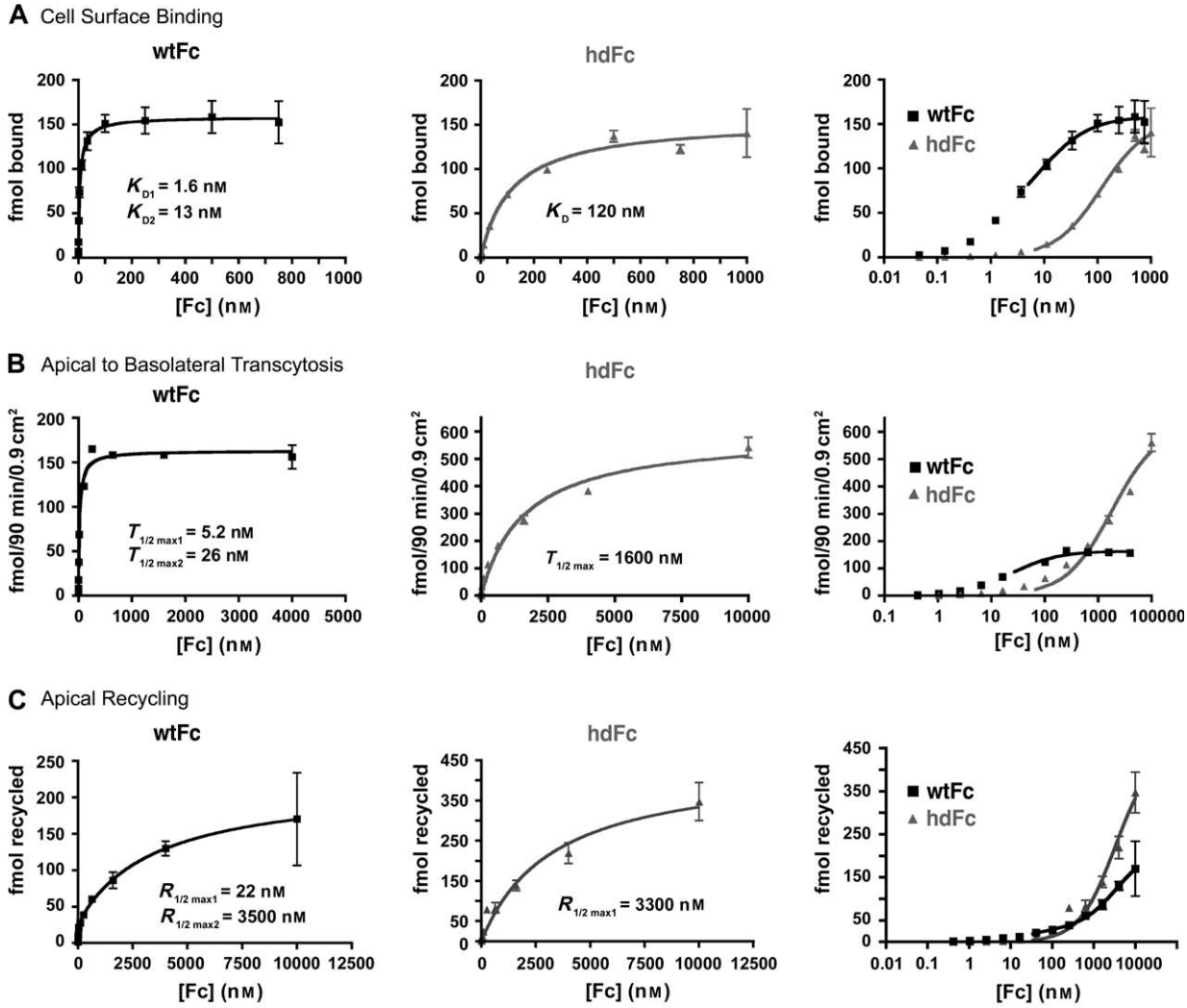

D

	$T_{1/2\,max}$	$R_{1/2\,max}$	K_D	$T_{1/2\,max}/K_D$	$R_{1/2\,max}/K_D$
wtFc	5.2 nM	22 nM	1.6 nM	3.2	14
hdFc	1600 nM	3300 nM	120 nM	14	28

Figure 6: Comparison of binding and transport of wtFc and hdFc by rFcRn-MDCK cells. Binding, transcytosis and recycling data are presented separately for wtFc and hdFc (recombinant Fc proteins derived from rat IgG2a) as a linear function of concentration (left and center graphs in panels A–C), and together as a function of the logarithm of the input concentration (right graphs in panels A–C). Data points represent the mean and standard error for quadruplicate (panel A) or triplicate (panels B and C) measurements. The data for wtFc were fit to a two-site binding model, therefore yielding two half-maximal values per graph: half-maximal binding (K_D), half-maximal transport ($T_{1/2max}$) or half-maximal recycling ($R_{1/2max}$). The data for hdFc were fit to a one-site binding model, yielding one half-maximal value per graph (see *Materials and Methods*). (A) Cell-surface binding of wtFc and hdFc. The amounts of wtFc and hdFc bound to cell-surface rFcRn were determined using ~500 000 cells at each input concentration. Assuming that each wtFc or hdFc molecule is bound by a single rFcRn molecule at saturating concentrations, there are ~150 fmol of ligand binding sites in each binding experiment, which corresponds to ~180 000 surface-accessible sites/cell. (B) Apical to basolateral transcytosis of wtFc and hdFc. (C) Apical recycling of wtFc and hdFc. (D) Comparison of $T_{1/2max}$ to K_D and $R_{1/2max}$ to K_D ratios for wtFc and hdFc. These ratios are predicted to be 1.0 in a perfectly efficient transport or recycling system.

Apical recycling was evaluated by measuring the amount of radioligand returned to the apical media after internalization from the apical surface of rFcRn-MDCK cells. As described for the transcytosis assay, the amounts of recycled wtFc and hdFc were plotted as a function of concentration, and the concentrations at which half-maximal recycling occurs ($R_{1/2max}$) were determined from the data by nonlinear regression analyses using a two-site

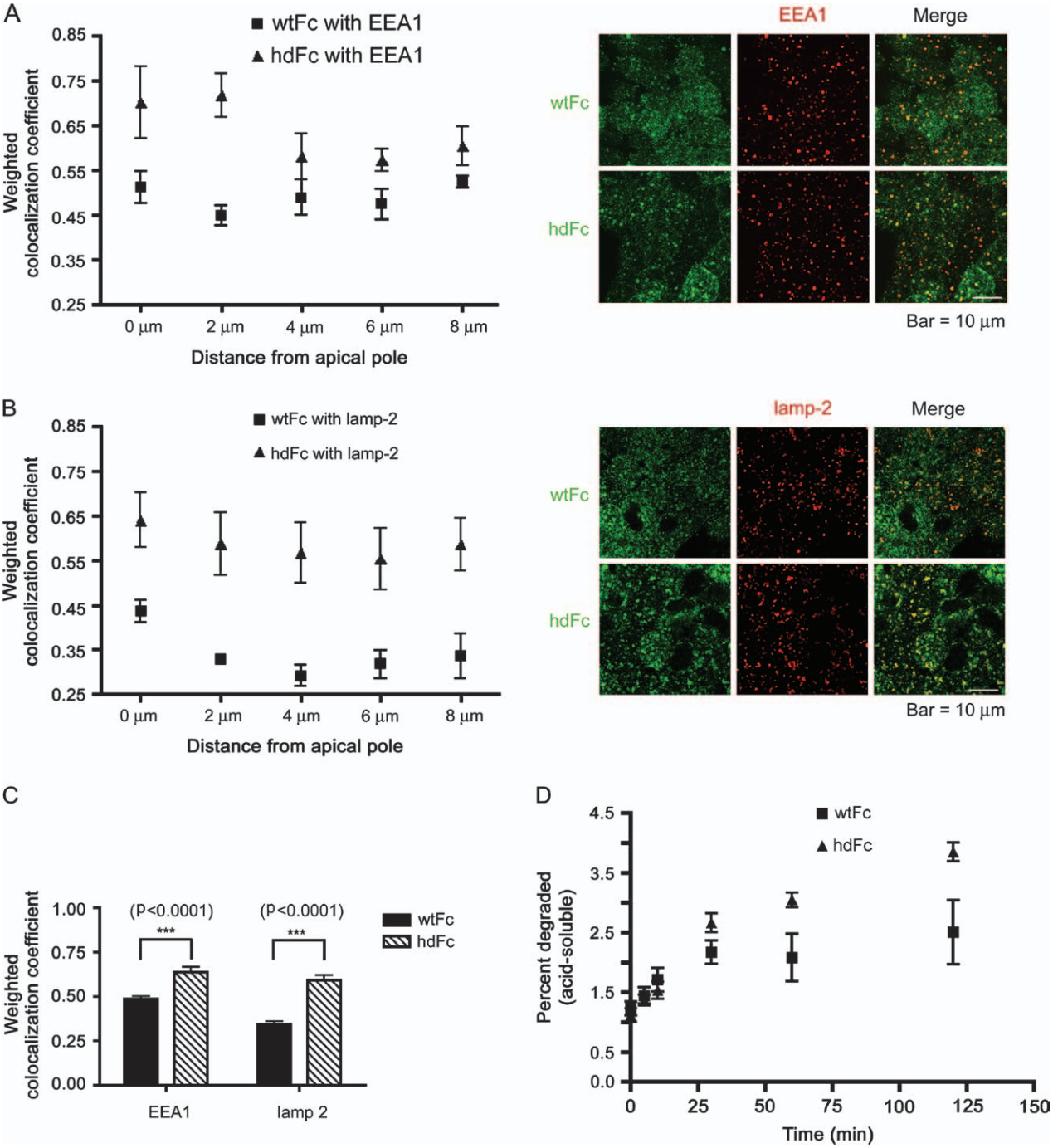

Figure 7: Comparison of intracellular localization and degradation of wtFc and hdFc. (A and B) The apical surface of rFcRn-MDCK cells was incubated with 1 μM wtFc or hdFc (recombinant Fcs derived from rat IgG2a) at pH 6 for 1 h, then fixed and processed for immunofluorescence using labeled antibodies against rat Fc and specific markers. The degree of colocalization of the Fcs with EEA1 (panel A) or LAMP-2 (panel B) is shown as a function of distance from the apical pole on the left of each panel ($n = 3$ or 4 for each data point). The percentage of above-threshold Fc pixels colocalizing with above-threshold EEA1 or LAMP-2 pixels was determined in each optical section as described in the *Materials and Methods*. Confocal images of the distributions of wtFc or hdFc (green) and EEA1 (red) (panel A) or wtFc or hdFc (green) and canine LAMP-2 (red) (panel B) are shown for a subapical optical section on the right of each panel. Regions of colocalization appear yellow in the merged images. (C) Averages of the colocalization coefficients for five optical sections spanning the whole cell. Significantly more ($p < 0.0001$) hdFc than wtFc colocalizes with EEA1 ($n = 15$ and $n = 19$, respectively) and with LAMP-2 ($n = 20$). (D) Comparison of degradation of wtFc and hdFc. [^{125}I]labeled wtFc or hdFc was internalized at pH 6 from the apical surface of rFcRn-MDCK cells for 1 h, after which the cells were washed at pH 8. The cells were returned to 37°C for the indicated time points, after which acid-soluble radioactivity in the media was measured. The percent of each Fc that was degraded was determined as described in the *Materials and Methods*.

binding model (wtFc) or a one-site binding model (hdFc) (Figure 6C). The $R_{1/2max}$ values for recycling of wtFc ($R_{1/2max1}$) and hdFc are 22 nM and 3.3 μM, respectively, indicating that bivalency of the Fc ligand also contributes to the efficiency of the recycling process.

To compare the affinities of the two forms of Fc to their transport efficiencies, we calculated the $T_{1/2max}/K_D$ and $R_{1/2max}/K_D$ ratios for each Fc. For comparisons of wtFc transcytosis and recycling with binding, we are interested in the K_D, $T_{1/2max}$ and $R_{1/2max}$ values representing the high-affinity population of receptors that are affected by avidity (K_{D1}, $T_{1/2max1}$ and $R_{1/2max}$ in Figure 6A–C). The $T_{1/2max1}/K_{D1}$ ratio for wtFc is 3.2, which is significantly smaller than the $T_{1/2max}/K_D$ ratio for hdFc (~14) (Figure 6D); thus, the less efficient transport of hdFc versus wtFc is not fully explained by the differences in affinity. Similarly, the $R_{1/2max1}/K_{D1}$ ratio for wtFc (~14) is smaller than the $R_{1/2max}/K_D$ ratio for hdFc (~28) (Figure 6D).

Although the $T_{1/2max}$ and $R_{1/2max}$ values demonstrate that higher concentrations of hdFc than wtFc are required to achieve half-maximal transcytosis or recycling rates, the absolute amounts of hdFc that are transcytosed and recycled are higher than the analogous amounts of wtFc as the concentration of Fc approaches saturation (values above ~1 μM) (Figure 6B,C). The reason for the higher levels of hdFc transport is unclear. It may result from the fact that a given number of receptors can transport twice as many hdFc molecules as wtFc because hdFc can be bound and transported by only one receptor, whereas wtFc can be bound and transported by two receptors. In addition, allowing each receptor to act as an independent trafficking unit may increase the overall rate at which individual receptors can complete one full round of ligand internalization and transport as compared to when the receptors are required to transport cargo in sets of two.

Comparison of localization of wtFc and hdFc in rFcRn-MDCK cells

To address whether the increased efficiency of wtFc over hdFc transport results from different intracellular fates of the two forms of Fc, we compared the intracellular localizations of internalized wtFc and hdFc with a marker for early endosomes (EEA1) and with a marker for lysosomes (the lysosomal membrane protein LAMP-2).

After 1 h of internalization from the apical surface, both wtFc and hdFc are present in discrete compartments throughout the cell (Figure 7A,B), including EEA1-positive compartments (Figure 7A), demonstrating that rFcRn-bound Fc proteins enter the endosomal network after being endocytosed. Although the mean intensity of the wtFc and hdFc staining is similar (see *Materials and Methods*), more hdFc than wtFc is colocalized with EEA1, as demonstrated by quantitative analysis of the confocal image data to determine the percent colocalization of above-threshold fluorescence for each type of Fc with EEA1 (see *Materials and Methods*). The degree of hdFc colocalization with EEA1 is consistently higher throughout the cell than the colocalization of wtFc with EEA1, with the most significant differences observed in the apical sections of the monolayer (left, Figure 7A). Averaged over the entire cell, 64 ± 3.0% of the hdFc fluorescence colocalizes with EEA1-positive compartments compared with 49 ± 1.4% of the wtFc fluorescence (Figure 7C). A more striking difference is observed for colocalization of the two Fcs with the lysosomal marker LAMP-2 (Figure 7B), in which 59 ± 2.8% of hdFc fluorescence colocalizes with LAMP-2-positive compartments compared with 34 ± 1.7% of wtFc fluorescence (Figure 7C).

The observation that more hdFc than wtFc is present in LAMP-2-positive compartments suggests that more hdFc than wtFc is degraded following internalization. To test this possibility, we measured the amounts of degraded Fc (acid-soluble radioactivity) released as a function of time by cells incubated with 1 μM wtFc or hdFc. As shown in Figure 7D, more degraded radioligand is released from hdFc-treated cells than from wtFc-treated cells. This difference is significant for postincubation times of 30 min or more, confirming that a substantially greater fraction of a single cohort of internalized hdFc is degraded compared to wtFc.

Discussion

Ligand valency is a critical feature of many receptor–ligand interactions. While many receptors that mediate intracellular signal transduction bind bivalent ligands to form 2:1 receptor:ligand complexes (e.g., platelet-derived growth factor receptor, colony-stimulating factor 1 receptor and stem cell factor receptor) [reviewed by Heldin (29)], receptors involved in ligand transcytosis and transport more commonly bind monovalent ligands to form 1:1 complexes (e.g., pIgR, low-density lipoprotein receptor and transferrin receptor) [reviewed by Tuma and Hubbard (30)]. FcRn was first identified as a receptor for IgG, a bivalent ligand, and the crystal structure of rFcRn in complex with wtFc showed that two FcRn molecules can bind simultaneously to a dimeric Fc (11). Studies of purified proteins in solution confirmed a 2:1 FcRn:Fc stoichiometry (24,31–33), and *in vivo* studies in mice showed that both FcRn-binding sites on Fc are required for efficient transcytosis and protection from catabolism (12,13). However, the discovery that FcRn also serves as a protection receptor for serum albumin (14,34), a monovalent ligand, suggests that ligand bivalency is not a general requirement for FcRn-mediated ligand trafficking.

Here we investigate the effects of valency on FcRn-mediated ligand trafficking to determine whether bivalency of an FcRn ligand is a strict requirement for proper trafficking, or if it merely acts to increase the efficiency

of the trafficking process. In the former case, one would expect the binding of the Fc or IgG ligand by two FcRn molecules to act as a signal, perhaps by bringing the receptors into close spatial proximity to facilitate interactions with cytosolic trafficking components. In the latter case, the binding of each ligand by two receptors would facilitate transport through an avidity effect, ensuring that the ligand molecule, once bound and internalized, remains in complex with its receptor throughout the transport process.

To evaluate the effects of ligand valency on FcRn-mediated transport, we generated stable MDCK cell lines expressing rFcRn that can be used as a model system for studies of FcRn-mediated transport of IgG and Fc ligands. Two cell lines were generated: rFcRn-MDCK, which expresses full-length rFcRn and the rFcRn light chain rβ_2m, and rFcRn-GFP-MDCK, which expresses an rFcRn-GFP chimeric protein together with rβ_2m. The expressed rFcRn proteins both bind to IgG at acidic but not at basic pH (Figure 1B), the characteristic pH dependency of the FcRn–IgG interaction (3). Functional binding and internalization of Fc ligands were demonstrated in polarized rFcRn-MDCK and rFcRn-GFP-MDCK monolayers at acidic pH (Figure 2). We observe only background amounts of wtFc internalized at pH 8, suggesting that fluid-phase uptake at basic pH is not significant at the relatively low concentration (20 nM) used for these experiments. Thus, an acidic extracellular environment greatly enhances the efficiency of ligand uptake, most likely by allowing IgG or Fc to bind rFcRn molecules transiently exposed to the cell surface prior to reinternalization. However, confocal analyses of rFcRn-MDCK cells that have internalized Fc ligands at a significantly higher concentration (1 μM) indicate that a low, but detectable, amount of wtFc is internalized at pH 7.4 (Figure 3), consistent with the assumption that non-receptor-mediated uptake of IgG at basic pH occurs in FcRn-mediated placental transport and in FcRn-mediated recycling of IgG by vascular endothelial cells (35). In these *in vivo* situations, the high concentration of IgG in the blood (50–100 μM) (36) likely facilitates fluid-phase uptake of IgG.

The rFcRn-MDCK cells transport IgG and Fc in both the apical to basolateral and basolateral to apical directions when the loading surface is incubated at acidic pH (Figure 4) as previously observed for hFcRn-transfected MDCK cells (16–18), rFcRn-transfected IMCD cells (20–22) and rat alveolar cells (23). Interestingly, in contrast to the studies on hFcRn in MDCK cells, in which higher levels of transcytosis occurred in the basolateral to apical direction (16,17), rFcRn expressed in IMCD and rat alveolar cells transports more ligand in the apical to basolateral direction (20,23). Consistent with these results, the rFcRn-MDCK cells described here transport more Fc in the apical to basolateral direction and roughly equal amounts of IgG bidirectionally (Figure 4), suggesting fundamental differences in the preferred directionality of ligand transport by the rat and human receptors.

Although the rFcRn-MDCK cells function in transcytosis of IgG and Fc ligands, we do not observe significant levels of wtFc transport in the rFcRn-GFP-MDCK cells (Figure 4A). The most likely explanation is that the addition of GFP to the C-terminus of the rFcRn cytoplasmic tail interferes with the binding of downstream effectors responsible for mediating intracellular trafficking processes. This is surprising, as a C-terminal GFP fusion of hFcRn has been shown to function in recycling of IgG ligands in the human endothelial cell line HMEC-1.CDC (35,37). Whether this discrepancy is due to differences in the interactions required for transcytosis versus recycling, differences in the behavior of the receptors when expressed in HMEC-1.CDC versus MDCK cells or fundamental differences between the hFcRn and rFcRn proteins is not clear. However, the fact that rFcRn-GFP-MDCK cells function in specific uptake of Fc ligands (Figure 2) suggests that signals responsible for endocytosis are intact, implying different signaling mechanisms for endocytosis versus transcytosis, or that rFcRn can internalize bound ligand via non-specific membrane flow after binding to ligand molecules at the cell surface.

Having demonstrated that rFcRn expressed in MDCK cells functions in binding, endocytosis and transcytosis of Fc and IgG ligands, both of which are naturally bivalent, we sought to study the interaction of rFcRn with RSA, a monovalent ligand that binds to rFcRn with the same pH dependency as the FcRn–IgG interaction and for which FcRn acts as a protection receptor *in vivo* (14,34). Despite using high ligand concentrations (10 μM) and low pH (pH 5) to facilitate binding (14,27), we were not able to detect specific binding of radiolabeled RSA to rFcRn (Figure 5A). We note, however, that although the experiments were performed at concentrations near or above the K_D of hFcRn for albumin (~1–5 μM) (27), we could not perform experiments at the concentration of albumin in serum (~270 μM) (38) because of background problems. When incubated at 3 μM, rFcRn-MDCK cells did not internalize significantly more RSA than control cells that do not express rFcRn (Figure 5B). However, both cell lines internalized less labeled RSA in the presence of competing unlabeled RSA, suggesting that much of the observed internalization was due to non-rFcRn-dependent binding of the labeled RSA to constituents of the cell surface. In addition, the levels of apical to basolateral transport of labeled RSA were similar in rFcRn-expressing and control cell lines, and the degree of transport was not significantly altered in either cell line by incubating the loading surface at pH 8 rather than at pH 5 (Figure 5C). Taken together, these results suggest that RSA binds non-specifically to components present on the surface of MDCK cells; thus, these cells are not an appropriate system in which to study the interaction of rFcRn with RSA.

To investigate the potential requirement for two FcRn-binding sites on an FcRn ligand, we compared the ability of rFcRn-MDCK cells to transcytose and recycle monovalent and bivalent forms of rat Fc (hdFc and wtFc, which

contain one and two FcRn-binding sites, respectively) (Figure 6B,C). The experiments were performed over a wide range of concentrations (0.15 nM–10 μM) to compensate for avidity affects that favor binding of wtFc over hdFc at low concentrations. The results revealed that hdFc is specifically transcytosed and recycled by rFcRn, but that more wtFc than hdFc is transported at low concentrations (<1 μM). Previous studies suggesting that two FcRn-binding sites on mouse Fc are required for FcRn-mediated rescue from catabolism (13) and transcytosis across the intestine of neonatal mice (12) are consistent with the present results if the Fc concentrations used in the *in vivo* studies fell within the range in which wtFc is more efficiently transported by FcRn than hdFc. The present study reveals that the amount of wtFc transcytosed reaches a relatively constant level at concentrations above 150 nM, whereas the amount of hdFc transcytosed continues to increase with concentration, such that more hdFc than wtFc is transcytosed at concentrations above 1 μM (Figure 6B). At a concentration of 10 μM, at least twice as much hdFc is transcytosed or recycled as wtFc. This suggests that two rFcRn molecules are bound to each wtFc during the transport process, whereas only one rFcRn molecule is bound to each hdFc, resulting in twice as many available receptors to transport the monovalent hdFc as there are for the transport of the bivalent wtFc.

To determine how the differences in rFcRn-mediated transport of wtFc versus hdFc are related to the apparent affinity of rFcRn for each ligand, we compared the concentrations of each protein that result in half-maximal binding to cell-surface rFcRn (K_D) with the concentrations that result in half-maximal transcytosis across a polarized monolayer ($T_{1/2max}$) and with the concentrations that result in half-maximal recycling of ligand back to the apical surface ($R_{1/2max}$). In a perfectly efficient transcytosis system, each binding event would result in a single transcytosis event, and $T_{1/2max}$ would equal K_D. In the present study, we observe that the $T_{1/2max}/K_D$ ratio for wtFc transcytosis is ~3, whereas the ratio for hdFc transcytosis is ~14 (Figure 6D). For the recycling experiments, the $R_{1/2max}/K_D$ ratio for wtFc is ~14, whereas the ratio for hdFc is ~28. Thus, a greater number of individual binding events result in successful transcytosis or recycling of the bivalent wtFc, whereas transcytosis or recycling of the monovalent hdFc requires the input of more ligand to achieve saturation of the transport system. Interestingly, the $T_{1/2max}/K_D$ and $R_{1/2max}/K_D$ values suggest that a given Fc molecule, once bound to FcRn at the apical surface, is more likely to be transcytosed than recycled.

The observed differences in the relative efficiencies of transport of the bivalent and monovalent Fcs could be related to differences in the subcellular fates of the two molecules during rFcRn-mediated trafficking. For example, a higher proportion of endocytosed hdFc molecules may enter a degradative pathway, whereas a higher proportion of wtFc molecules are transcytosed or recycled. Consistent with this hypothesis, we observed a greater amount of hdFc in both lysosomal (LAMP-2 positive) and early endosomal (EEA1 positive) compartments as compared to wtFc (Figure 7), suggesting that more wtFc than hdFc is transported to compartments downstream of the early endosomes and that less wtFc than hdFc is sent to degradative compartments. The quantitative colocalization experiments were conducted using a ligand concentration of 1 μM, a concentration at which roughly equal amounts of wtFc and hdFc are bound and transported by rFcRn-expressing MDCK cells (Figure 6A–C). Under these conditions, we presume that all wtFc or hdFc molecules on the cell surface are initially bound by a single rFcRn molecule prior to internalization and that the amount of each ligand entering the cell is approximately equal. Consistent with this assumption, digital image analysis shows that the average mean pixel intensities for Fc fluorescence in all images used in these experiments are similar (see *Materials and Methods*). Therefore, the higher proportion of hdFc seen in LAMP-2- and EEA1-positive structures is not the result of greater absolute amounts of hdFc entering into the cell. Instead, the data are consistent with a model whereby equal amounts of both wtFc and hdFc initially enter the cell but, subsequent to internalization and delivery to EEA1-positive early endosomes, a greater proportion of wtFc than hdFc molecules remain bound to FcRn and are transported to downstream compartments involved in transcytosis and/or recycling. Conversely, a greater proportion of hdFc molecules remain in early endosomes prior to being transferred to the lysosomal degradation pathway along with other fluid-phase components. This model is also supported by our demonstration that, following internalization of a single cohort of wtFc or hdFc ligand, a higher percentage of hdFc is released from rFcRn-MDCK cells as degraded (acid-soluble) material (Figure 7D).

The observation that an Fc ligand containing only one FcRn-binding site is preferentially trafficked to lysosomes and degraded compared with a bivalent Fc ligand can be explained by an avidity effect; because the hdFc cannot be cross-linked by adjacent FcRn molecules, it is predicted to dissociate more readily from FcRn inside endosomes, and unbound hdFc could then enter a default degradative pathway with other molecules in the fluid phase. The present demonstration that FcRn-mediated transcytosis and recycling of hdFc occur, although at a lower efficiency than transcytosis and recycling of wtFc, does not address whether an oligomeric structure of FcRn dimers linked by homodimeric Fc or IgG molecules (10,11) is present inside endosomes, but rules out that it is required for proper transport of vesicles containing FcRn–IgG or FcRn–Fc complexes.

Materials and Methods

Construction of expression vectors

The gene encoding rFcRn was modified by polymerase chain reaction (PCR) to incorporate 5′ *Asp*718 and 3′ *Hin*dIII restriction sites and subsequently

subcloned with an *Asp*718/*Hin*dIII double digest into the mammalian cell expression vector pCB6-*Hin*dIII (kindly provided by Ira Mellman, Yale University), which carries a neomycin resistance gene for G418 selection. To make the FcRn–GFP fusion construct, the enhanced GFP (EGFP) gene was amplified from the pEGFP-1 vector (Clontech, Mountain View, CA, USA) via PCR to remove the start codon and to introduce a 5′ in-frame *Xho*I site and a 3′ *Hin*dIII site and subcloned into the pBluescript II SK− vector (Stratagene, La Jolla, CA, USA). Polymerase chain reaction was used to introduce a 5′ *Asp*718 site and an in-frame 3′ *Xho*I site at the 3′ end of the rFcRn gene, which was then subcloned into the EGFP Bluescript vector. The resulting open reading frame, which encoded the entire rFcRn amino acid sequence, a leucine-glutamate linker region and EGFP without its N-terminal methionine, was subcloned with a *Asp*718/*Hin*dIII double digest into the expression vector pCB6-*Hin*dIII. We used a previously described rβ_2m expression vector (39), which does not contain a selectable marker, to coexpress rβ_2m along with full-length rFcRn and the rFcRn-GFP chimeric protein.

Antibodies

The mouse monoclonal antibodies 1G3 (anti-rFcRn heavy chain) and 4C9 (anti-rβ_2m) were generated in our laboratory (40) and can be purchased from the American Tissue Culture Collection. 2B10C11, a mouse monoclonal antibody against rβ_2m, was the kind gift of Lennart Lögdberg. 1G3, 4C9 and 2B10C11 were directly conjugated to AlexaFluor488-NHS, AlexaFluor546-NHS or AlexaFluor633-NHS (Molecular Probes, Carlsbad, CA, USA) according to the manufacturer's protocol and used for immunofluorescence (1G3 and 4C9) and flow cytometry (2B10C11) experiments. Labeled antibodies were separated from unconjugated dye using 10 000-kDa cutoff dextran desalting columns (Pierce, Rockford, IL, USA), and the concentration and degree of labeling were determined spectrophotometrically using an extinction coefficient at 280 nm of 202 000 M^{-1} cm^{-1} for the antibodies. A polyclonal rabbit antiserum used for Western blotting was raised against purified rFcRn/rβ_2m heterodimers. Polyclonal rabbit anti-ZO1 was from Zymed (San Francisco, CA, USA). Mouse monoclonal anti-EEA1 was from BD Transduction Labs (San Jose, CA, USA), and the mouse monoclonal antibody AC17 against the canine lysosomal membrane protein lamp-2 (41,42) was a kind gift from Dr E. Rodriguez-Boulan (Weill Medical College, Cornell University). AlexaFluor488-, 546-, and 647-labeled secondary antibodies (goat anti-mouse, goat anti-rabbit and goat anti-rat) were purchased from Molecular Probes.

Maintenance and transfection of cell lines

MDCK type II cells (generously provided by Keith Mostov, UCSF) were maintained in MEM (GibcoBRL, Carlsbad, CA, USA) supplemented with 10% FBS (HyClone, Logan, UT, USA) at 37°C, 5% CO_2. Cells were fed every other day and passaged once weekly. MDCK II cells were cotransfected with expression vectors encoding full-length rFcRn or rFcRn-GFP and rβ_2m using Lipofectamine 2000 (Invitrogen, Carlsbad, CA, USA) and selected with 0.5 mg/mL G418 (Invitrogen). Resistant colonies were tested for uptake of fluorescently labeled rat Fc at pH 6.0. Colonies from each transfection were picked with cloning cylinders and expanded for further analysis. Colonies were analyzed by flow cytometry for binding to Alexa488-conjugated 1G3 (anti-rFcRn) (40) and/or Alexa633-conjugated 2B10C11 (anti-rβ_2m). At least three clones from each transfection were assayed by immunofluorescence for expression of both the heavy and light chains of rFcRn as well as for the ability to endocytose and transcytose radiolabeled rat Fc at acidic pH. We also generated MDCK II cells transfected with the pCB6H vector lacking an inserted gene to serve as a negative control (vector-only MDCK cells). All cell lines were maintained under constant drug selection.

The integrity of filter-grown, cell-transfected MDCK monolayers was evaluated by seeding cells at superconfluent density on filter supports and recording daily measurements of the TEER. The TEER typically plateaued after 3 or 4 days at ~250–300 Ωcm^2, a characteristic range for polarized MDCK II cells (43).

For experiments requiring polarized cell monolayers, cells were seeded at superconfluent density (1×10^6 cells/mL) onto 12-mm Transwell polyester filters (Corning Costar, Acton, MA, USA), with 0.5 and 1.5 mL of media in the apical and basolateral reservoirs, respectively. Cells were fed daily beginning 2 days after initial seeding and used for experiments on the fourth or fifth day postplating.

Western blot and IgG binding analyses

Western blot analyses to evaluate FcRn expression were performed after denaturing lysis of transfected cells by boiling in 0.5% SDS and vortexing. After centrifuging to remove insoluble material, samples of each lysate [10 μg of total protein as determined by bicinchoninic acid (BCA) assay from Pierce] were loaded onto a 15% SDS polyacrylamide gel and run under reducing conditions. Proteins were transferred to nitrocellulose, probed with a 1:2000 dilution of a polyclonal rabbit antiserum against the rFcRn ectodomain and then treated with peroxidase-conjugated goat anti-mouse secondary antibody (Jackson Immunoresearch Laboratories, West Grove, PA, USA) and detected by enhanced chemiluminescence (Amersham, Piscataway, NJ, USA).

For evaluations of IgG binding, cells were lysed in 5 mg/mL 3-[(3-Cholamidopropyl)dimethylammonia]-1-propanesulfonate (CHAPS), 130 mM NaCl, 20 μM ethylenediaminetetraacetic acid (EDTA), pH 5.9 (15 mM 2-(N-Morpholino)ethanesulfonic acid [MES]) or pH 8.0 (15 mM 4-(2-Hydroxyethyl)piperazine-1-ethanesulfonic acid [HEPES]), supplemented with a protease inhibitor cocktail for mammalian cells (Sigma, St Louis, MO, USA). After centrifuging to remove insoluble material, lysates were incubated with 50 μL human IgG-Sepharose (Amersham) pre-equilibrated to pH 5.9 or pH 8.0 in lysis buffer overnight at 4°C. The complexes were washed four times with 1 mg/mL CHAPS, 30 mM NaCl, 20 μM EDTA, pH 5.9 or 8.0. Bound proteins were eluted by boiling in double-strength sample buffer and processed for SDS-PAGE and Western blotting to detect rFcRn as described above.

Preparation of FcRn ligands for uptake and transport assays

Rat FcRn binds all four subclasses of rat, human and mouse IgGs with roughly equal affinities (44); therefore, IgGs and Fcs from these three species were used for different experiments based on availability or convenience.

Three forms of rat Fc, wtFc, hdFc and nbFc, were expressed in Chinese hamster ovary (CHO) cells and purified as previously described (45). The Fc-expressing CHO cell line was generated by transfection of expression vectors encoding wtFc (rat IgG2a residues 223–447) and nbFc (IgG2a residues 223–447 with mutations that disrupt FcRn binding (Thr-252 to Gly, Ile-253 to Gly, Thr-254 to Gly, His-310 to Glu, His-433 to Glu and His-435 to Glu) and a C-terminal factor Xa cleavage site and 6x-His tag). The hdFc and nbFc were purified from supernatants of CHO cells secreting a mixture of wtFc, hdFc and nbFc as described (24). Briefly, CHO supernatants were first passed over a nickel-nitrilotriacetic acid (Ni-NTA) column, allowing separation of wtFc from 6x-His tagged species. The hdFc and nbFc were eluted from the Ni-NTA column, then passed over an FcRn affinity column at pH 6.0. The hdFc was eluted from the FcRn column at pH 8.0, and nbFc was recovered from the flowthrough.

Human Fc and rat and human IgGs, each a mixture of the four IgG subclasses, were purchased from Jackson Immunoresearch Laboratories. Purified samples of the monoclonal antibodies 12C7 (anti-*Drosophila* methuselah) and 1C5 (anti-Zn-α2-glycoprotein) (46) were used as mouse IgG1 proteins. Rat serum albumin was purchased from Sigma. All proteins were passed over a Superdex 200 gel filtration column (Amersham) to remove oligomeric species prior to experiments.

Human IgG, rat IgG, mouse IgG1 monoclonal antibodies, human Fc, the recombinant rat Fcs (wtFc, hdFc and nbFc) and RSA were iodinated to a specific activity of 2–5 μCi/μg using Na[^{125}I] (MP Biomedicals, Irvine, CA, USA) and IODO-GEN (Pierce). Radiolabeled ligands were buffer exchanged into HEPES buffered saline (25 mM HEPES, 150 mM NaCl, pH 7.4) by two subsequent passages over Bio-Spin 30 prepacked acrylamide columns

(30 000 molecular weight cutoff) (BioRad, Hercules, CA, USA). Protein concentrations were determined by BCA assay (Pierce) using bovine serum albumin or bovine γ-globulin as standards.

Quantitative endocytosis assay

Cells were grown in 12-well tissue culture plates until ~80–90% confluent. Prior to incubations with ligand, the cells were serum starved for 20–30 min in Hanks' balanced salt solution, 1.3 mM $CaCl_2$, 0.8 mM $MgSO_4$ (HBSS+) adjusted to either pH 5.9 or pH 8.0 with MES or HEPES (10 mM each), respectively. [^{125}I]wtFc was added to a final concentration of 20 nM in HBSS+ pH 5.9, and plates were incubated in a 37°C circulating water bath for the indicated amounts of time. For competitor studies, 10 μM unlabeled wtFc or rat IgG was added during the preincubation. The cells were cooled on ice, washed four times with ice-cold HBSS+ pH 8.0 to remove surface-bound ligand and then lysed in 0.1 N NaOH. The radioactivity present in the lysates was counted on a Beckman 5500 γ-counter and converted to fmoles of protein using the specific activity of the radiolabeled ligand.

Quantitative endocytosis assays involving [^{125}I]RSA were done as described above, except that the concentrations of [^{125}I]RSA and unlabeled RSA were 3 μM and 2 mM, respectively, and the incubations were performed at pH 5.0.

Cell-surface binding assay

For assays of Fc binding to cell-surface FcRn, subconfluent rFcRn-MDCK cells were lifted from plates by incubating in calcium/magnesium-free HBSS and 4 mM EDTA. Cells were washed twice in binding buffer (HBSS+/1% ovalbumin/1 mM KI/10 mM MES, pH 5.9), and triplicate samples of ~500 000 cells were incubated with serial threefold dilutions of radiolabeled Fc (0.4–900 nM) in a 100 μL volume for 1 h at 4°C with shaking. The binding reactions were collected onto a 96-well filter plate (Durapore membrane, 0.65- μm pore size) (Millipore, Billerica, MA, USA) by centrifugation at 1500 × *g* for 1 min. The filter wells were washed four times with 250 μL of binding buffer at pH 5.9, and the filter circles were punched out into glass vials and counted for radioactivity. A duplicate set of binding reactions performed in parallel were washed four times with HBSS+/1% ovalbumin/1 mM KI/10 mM HEPES, pH 8.0, to serve as a control for non-specific binding. The amount of radioactivity bound to samples washed at pH 8 was subtracted from the corresponding values for samples washed at acidic pH to yield values for specific binding of the radiolabeled ligand.

The RSA binding assays were conducted as described above, except that the binding reactions were performed at pH 5.0 and washed at pH 5.0 or 8.0 (control experiments), and the concentration of [^{125}I]RSA ranged from 4 nM to 10 μM.

Radioligand transcytosis and recycling assays

For transport assays involving only Fc (Figure 4A), we used radiolabeled rat wtFc. For assays comparing IgG and Fc transport, we used radiolabeled human IgG and human Fc (Figure 4B) because radiolabeled human IgG was transported more efficiently than radiolabeled versions of either rat IgG or two different mouse monoclonal antibodies (data not shown). Human IgG binds as well as rat IgG to rFcRn (44).

For transcytosis experiments involving IgG and Fc ligands, polarized cell monolayers were washed once with HBSS+/1% ovalbumin/1 mM KI buffered to pH 5.9 (loading surface) or pH 8.0 (nonloading surface or loading surface for pH 8 control experiments). Filters were preincubated for 20 min with HBSS+ pH 5.9 on the loading surface (or pH 8.0 for control experiments) and HBSS+ pH 8.0 on the nonloading surface. For competition experiments, the unlabeled competing ligand was present in the loading surface medium during the preincubation step. [^{125}I]Fc (rat or human) or [^{125}I]IgG (rat or human) was added directly to the loading media to a final concentration of 20 nM at pH 5.9 or 8.0. Plates were incubated for 90 min in a 37°C circulating water bath, after which media from the nonloading surface were collected and precipitated at 4°C with 10% (vol/vol) trichloroacidic acid (TCA). The TCA-insoluble (intact ligand) fractions were counted on a Beckman 5500 γ-counter. For experiments comparing the relative transport efficiencies of [^{125}I]wtFc, -hdFc or -nbFc, the radiolabeled proteins were added at concentrations ranging from 0.15 nM to 10 μM. The amount of [^{125}I]nbFc that moved across the monolayers for a given concentration was assumed to represent non-specific transport or leakage across the monolayer and was subtracted from the corresponding values for wtFc and hdFc to yield values for specific rFcRn-mediated transport.

Quantitative transcytosis assays involving [^{125}I]RSA were done as described above, except that the concentration of [^{125}I]RSA was 10 μM, and the apical surface was maintained at pH 5.0 or at pH 8.0 (control experiments). Filters incubated with 30nM [^{125}I]nbFc at pH 5.0 served as a control for the integrity of the monolayer, and filters incubated with 30 nM [^{125}I]wtFc at pH 5.0 served as a positive control for the ability of the cells to function in FcRn-mediated transcytosis at pH 5.0.

For apical recycling experiments involving labeled Fcs, filter-grown monolayers were washed and preincubated as described above for the IgG and Fc transcytosis assays. [^{125}I]labeled wtFc, hdFc or nbFc was added to the apical surface at pH 5.9 at concentrations ranging from 0.15 nM to 10 μM, while the basolateral surface was maintained at pH 8.0. After a 30-min incubation at 37°C, the cells were cooled on ice and washed rapidly five times with ice-cold HBSS+ pH 8.0. Prewarmed HBSS+ pH 8.0 was then added to the apical and basolateral surfaces. After a 60-min incubation at 37°C, media from the apical surface were collected and TCA precipitated, and the TCA-insoluble fractions were counted as described above.

Analyses of data for binding and transport assays

The amount of specifically bound or transported Fc was plotted as a function of concentration, and nonlinear regression analyses of the data were performed using GraphPad Prism version 4.0b for Macintosh (GraphPad Software, San Diego, CA, USA). As previously described for biosensor-based binding data (24), half-maximal binding (K_D), transcytosis ($T_{1/2max}$) or recycling ($R_{1/2max}$) values were derived by fitting the wtFc data to a two-site model, which assumes two independent classes of receptors (a high-affinity class and a low-affinity class), and the hdFc data to a one-site model.

Preparation of samples for immunofluorescence experiments

Cells were grown on permeable filter supports for 3–4 days to allow formation of a polarized monolayer. The filters were preincubated in HBSS+ pH 8.0 for 20–30 min. The loading surface was then washed with HBSS+ pH 5.9, and ligands were added to the loading surface at the indicated concentrations in the same buffer. The nonloading surface was maintained in HBSS+ pH 7.4 throughout the experiment. Filter plates were incubated at 37°C in a circulating water bath for the indicated times after which the cells were placed on ice and processed for immunofluorescence.

For immunofluorescence staining, cells were washed briefly with ice-cold PBS+ (PBS supplemented with 1 mM $CaCl_2$, 0.5 mM $MgCl_2$ and 0.25 mM $MgSO_4$) and fixed using a pH-shift protocol (47). Briefly, cells were incubated for 5 min at room temperature in 4% paraformaldehyde (PFA) in 80 mM 1,4-piperazinebis-(ethanesulphonic acid) (PIPES), pH 6.5, 5 mM EGTA and 2.0 mM $MgCl_2$, and then transferred to 4% PFA, 100 mM sodium borate, pH 11.0 for 10 min. After quenching excess aldehyde with freshly prepared 75 mM NH_4Cl and 20 mM glycine in PBS for 10 min, the cells were washed twice with PBS and blocked for 30 min at room temperature in PBS containing 8% normal goat serum and 0.025% saponin. Cells were then incubated overnight at 4°C in blocking buffer containing one or more of the following primary antibodies: fluorescently conjugated 1G3 or 4C9 (5 μg/mL), mouse anti-EEA1 (1:100 dilution), rabbit anti-ZO1 (1:25 dilution) or AC17 (1:500). Cells were washed and then incubated with the appropriate AlexaFluor-conjugated secondary antibodies diluted 1:500 in blocking buffer for 1 h at room temperature. For experiments involving localization of internalized Fc proteins, unlabeled ligands

were detected after internalization using AlexaFluor-conjugated goat anti-rat IgG antibodies. After extensive washing with PBS, cells were treated with 0.1% Triton X-100 for 5 min, washed once with PBS and then postfixed with 4% PFA in 100 mM sodium cacodylate, pH 7.4 for 30 min at room temperature. The cells were washed twice more with PBS, and the filters were cut out of their holders using a scalpel and a fine-tipped pair of forceps. Excised filters were mounted on glass slides using ProLong Gold antifade medium (Molecular Probes), sealed with beeswax and stored at −20°C until viewing on a confocal microscope.

Confocal microscopy

All experiments were conducted using an inverted Zeiss LSM META confocal microscope equipped with a Zeiss Plan-Apochromat 100× oil objective (numerical aperture 1.4). Green fluorophores were excited with the 488-nm line of an argon ion laser. Orange and far-red dyes were excited with the 543 and 633- nm lines of a He-Ne laser, respectively. Fluorescence was detected through a variable confocal pinhole set to 1.0 Airy units for the longest wavelength used within a given experiment, and the pinholes of other channels were adjusted to maintain a constant optical section thickness across all channels. The gain and offset of the photomultipliers was adjusted for each channel individually so that the observed fluorescence signal filled the linear range of the detectors, with the background being slightly positive and saturation being minimized.

Image processing and quantitative colocalization studies

Image processing was performed using the Zeiss LSM Examiner software (version 3.2). Quantitative colocalization measurements were performed using the colocalization tool within the Zeiss LSM Examiner package. Four colocalization experiments were conducted: wtFc with EEA1 and with AC17, and hdFc with EEA1 and with AC17. For each experiment, we analyzed five optical sections from approximately five different regions, each containing 5–10 cells. Different optical sections within the same region were spaced 2 μm apart to ensure that each represented a unique image plane within the volume. Thresholds for the two channels in each image were set to be 2 standard deviations above the mean pixel intensity. Weighted colocalization coefficients (*M*) were calculated by summing the intensities of the above-threshold Fc-positive pixels that colocalized with above-threshold marker-positive pixels and dividing that number by the sum of all above-threshold Fc pixel intensities as follows:

$$M = \frac{\sum_i \mathrm{Fc}_{i,\mathrm{coloc}}}{\sum_i \mathrm{Fc}_{i,\mathrm{total}}},$$

where $\mathrm{Fc}_{i,\mathrm{coloc}}$ represents the intensity of a colocalized above-threshold pixel in the Fc channel, and $\mathrm{Fc}_{i,\mathrm{total}}$ represents the intensity of any above-threshold pixel in the Fc channel. The value of *M* can range from 0 (no colocalization) to 1.0 (all pixels colocalize). The mean intensities of the labeled proteins were calculated to rule out that potential differences in colocalization coefficients resulted from higher levels of one labeled protein relative to another. The mean intensity values were wtFc and hdFc in the EEA1 colocalization: 1969 ± 342 and 2055 ± 713; wtFc and hdFc in the lamp-2 colocalization: 2088 ± 476 and 2346 ± 436; EEA1 in the wtFc and hdFc colocalizations: 1472 ± 414 and 1332 ± 454; lamp-2 in the wtFc and hdFc colocalizations: 1473 ± 629 and 1433 ± 396.

Degradation assay

The apical surface of rFcRn-MDCK monolayers were incubated for 1 h with 1 μM [^{125}I]labeled wtFc or hdFc at pH 5.9 as described for the immunofluorescence and transcytosis assays. Cells were cooled on ice and then washed four times with ice-cold pH 8.0 buffer. Prewarmed pH 8.0 buffer was added, and the cells were returned to 37°C for various times, after which cells were again cooled on ice. Media from the apical and basolateral surfaces were pooled and TCA precipitated, and the levels of radioactivity in TCA-soluble and TCA-insoluble fractions were determined. Cell-associated radioactivity was determined after lysis of cells in 0.1 N NaOH. The percent of an Fc ligand that was degraded at each time point was derived as $[\mathrm{c.p.m.}_{\text{TCA-soluble}}/(\mathrm{c.p.m.}_{\text{TCA-soluble}} + \mathrm{c.p.m.}_{\text{TCA-insoluble}} + \mathrm{c.p.m.}_{\text{cell-associated}})] \times 100$.

Acknowledgments

We thank W. Lance Martin for construction of expression vectors, Shelley Diamond of the Caltech Cell Sorting Facility for assistance in the analysis of cell lines, Enrique Rodriguez-Boulan and Lennart Lögdberg for the AC17 and 2B10C11 antibodies, Keith Mostov for the MDCK II cells, and Elaine Bearer and members of the Bjorkman lab for critical reading of the manuscript. This work was supported by the National Institutes of Health (2 R37 AI041239-06A1 to P. J. B.).

References

1. Rodewald R, Kraehenbuhl JP. Receptor-mediated transport of IgG. J Cell Biol 1984;99:159s–164s.
2. Simister NE, Rees AR. Isolation and characterization of an Fc receptor from neonatal rat small intestine. Eur J Immunol 1985;15:733–738.
3. Simister NE, Mostov KE. An Fc receptor structurally related to MHC class I antigens. Nature 1989;337:184–187.
4. Simister NE, Story CM, Chen HL, Hunt JS. An IgG-transporting Fc receptor expressed in the syncytiotrophoblast of human placenta. Eur J Immunol 1996;26:1527–1531.
5. Kristoffersen EK. Human placental Fc gamma-binding proteins in the maternofetal transfer of IgG. APMIS Suppl 1996;64:5–36.
6. Leach JL, Sedmak DD, Osborne JM, Rahill B, Lairmore MD, Anderson CL. Isolation from human placenta of the IgG transporter, FcRn, and localization to the syncytiotrophoblast: implications for maternal-fetal antibody transport. J Immunol 1996;157:3317–3322.
7. Ghetie V, Hubbard JG, Kim JK, Tsen MF, Lee Y, Ward ES. Abnormally short serum half-lives of IgG in beta 2-microglobulin-deficient mice. Eur J Immunol 1996;26:690–696.
8. Israel EJ, Wilsker DF, Hayes KC, Schoenfeld D, Simister NE. Increased clearance of IgG in mice that lack beta 2-microglobulin: possible protective role of FcRn. Immunology 1996;89:573–578.
9. Junghans RP, Anderson CL. The protection receptor for IgG catabolism is the beta2-microglobulin-containing neonatal intestinal transport receptor. Proc Natl Acad Sci U S A 1996;93:5512–5516.
10. Raghavan M, Bjorkman PJ. Fc receptors and their interactions with immunoglobulins. Annu Rev Cell Dev Biol 1996;12:181–220.
11. Burmeister WP, Huber AH, Bjorkman PJ. Crystal structure of the complex of rat neonatal Fc receptor with Fc. Nature 1994;372:379–383.
12. Kim JK, Tsen MF, Ghetie V, Ward ES. Localization of the site of the murine IgG1 molecule that is involved in binding to the murine intestinal Fc receptor. Eur J Immunol 1994;24:2429–2434.
13. Kim JK, Tsen MF, Ghetie V, Ward ES. Catabolism of the murine IgG1 molecule: evidence that both CH2-CH3 domain interfaces are required for persistence of IgG1 in the circulation of mice. Scand J Immunol 1994;40:457–465.
14. Chaudhury C, Mehnaz S, Robinson JM, Hayton WL, Pearl DK, Roopenian DC, Anderson CL. The major histocompatibility complex-related Fc receptor for IgG (FcRn) binds albumin and prolongs its lifespan. J Exp Med 2003;197:315–322.
15. Koltun M, Nikolovski J, Strong KJ, Nikolic-Paterson DJ, Comper WD. Mechanism of hypoalbuminemia in rodents. Am J Physiol Heart Circ Physiol 2004; 288:1604–1610.
16. Claypool SM, Dickinson BL, Yoshida M, Lencer WI, Blumberg RS. Functional reconstitution of human FcRn in Madin-Darby canine kidney

cells requires co-expressed human beta 2-microglobulin. J Biol Chem 2002;277:28038–28050.
17. Claypool SM, Dickinson BL, Wagner JS, Johansen FE, Venu N, Borawski JA, Lencer WI, Blumberg RS. Bidirectional transepithelial IgG transport by a strongly polarized basolateral membrane Fcgamma-receptor. Mol Biol Cell 2004;15:1746–1759.
18. Yoshida M, Claypool SM, Wagner JS, Mizoguchi E, Mizoguchi A, Roopenian DC, Lencer WI, Blumberg RS. Human neonatal Fc receptor mediates transport of IgG into luminal secretions for delivery of antigens to mucosal dendritic cells. Immunity 2004;20:769–783.
19. Dickinson BL, Badizadegan K, Wu Z, Ahouse JC, Zhu X, Simister NE, Blumberg RS, Lencer WI. Bidirectional FcRn-dependent IgG transport in a polarized human intestinal epithelial cell line. J Clin Invest 1999;104: 903–911.
20. McCarthy KM, Yoong Y, Simister NE. Bidirectional transcytosis of IgG by the rat neonatal Fc receptor expressed in a rat kidney cell line: a system to study protein transport across epithelia. J Cell Sci 2000;113 (Pt 7):1277–1285.
21. McCarthy KM, Lam M, Subramanian L, Shakya R, Wu Z, Newton EE, Simister NE. Effects of mutations in potential phosphorylation sites on transcytosis of FcRn. J Cell Sci 2001;114:1591–1598.
22. Wu Z, Simister NE. Tryptophan- and dileucine-based endocytosis signals in the neonatal Fc receptor. J Biol Chem 2001;276:5240–5247.
23. Kim KJ, Fandy TE, Lee VH, Ann DK, Borok Z, Crandall ED. Net absorption of IgG via FcRn-mediated transcytosis across rat alveolar epithelial cell monolayers. Am J Physiol Lung Cell Mol Physiol 2004; 287:L616–L622.
24. Martin WL, Bjorkman PJ. Characterization of the 2:1 complex between the class I MHC-related Fc receptor and its Fc ligand in solution. Biochemistry 1999;38:12639–12647.
25. Ramalingam TS, Detmer SA, Martin WL, Bjorkman PJ. IgG transcytosis and recycling by FcRn expressed in MDCK cells reveals ligand-induced redistribution. EMBO J 2002;21:590–601.
26. Detmer SA, Martin WL, Bjorkman PJ. Retraction of: Ramalingam TS, Detmer SA, Martin WL, Bjorkman PJ. (2002) EMBO J.15:590–601. IgG transcytosis and recycling by FcRn expressed in MDCK cells reveals ligand-induced redistribution. EMBO J 2002;21:5953.
27. Chaudhury C, Brooks CL, Carter DC, Robinson JM, Anderson CL. Albumin binding to FcRn: distinct from the FcRn-IgG interaction. Biochemistry 2006;45:4983–4990.
28. Jones EA, Waldmann TA. The mechanism of intestinal uptake and transcellular transport of IgG in the neonatal rat. J Clin Invest 1972; 51:2916–2927.
29. Heldin CH. Dimerization of cell surface receptors in signal transduction. Cell 1995;80:213–223.
30. Tuma PL, Hubbard AL. Transcytosis: crossing cellular barriers. Physiol Rev 2003;83:871–932.
31. Huber AH, Kelley RF, Gastinel LN, Bjorkman PJ. Crystallization and stoichiometry of binding of a complex between a rat intestinal Fc receptor and Fc. J Mol Biol 1993;230:1077–1083.
32. Sanchez LM, Penny DM, Bjorkman PJ. Stoichiometry of the interaction between the major histocompatibility complex-related Fc receptor and its Fc ligand. Biochemistry 1999;38:9471–9476.
33. Schuck P, Radu CG, Ward ES. Sedimentation equilibrium analysis of recombinant mouse FcRn with murine IgG1. Mol Immunol 1999;36: 1117–1125.
34. Kim J, Bronson CL, Hayton WL, Radmacher MD, Roopenian DC, Robinson JM, Anderson CL. Albumin turnover: FcRn-mediated recycling saves as much albumin from degradation as the liver produces. Am J Physiol Gastrointest Liver Physiol 2005;290:352–360.
35. Ober RJ, Martinez C, Vaccaro C, Zhou J, Ward ES. Visualizing the site and dynamics of IgG salvage by the MHC class I-related receptor, FcRn. J Immunol 2004;172:2021–2029.
36. Janeway C. Immunobiology: The Immune System in Health and Disease, 6th edn. New York: Garland Science; 2005.
37. Ober RJ, Martinez C, Lai X, Zhou J, Ward ES. Exocytosis of IgG as mediated by the receptor, FcRn: an analysis at the single-molecule level. Proc Natl Acad Sci U S A 2004;101:11076–11081.
38. Monks J, Neville MC. Albumin transcytosis across the epithelium of the lactating mouse mammary gland. J Physiol 2004;560:267–280.
39. Gastinel LN, Simister NE, Bjorkman PJ. Expression and crystallization of a soluble and functional form of an Fc receptor related to class I histocompatibility molecules. Proc Natl Acad Sci U S A 1992; 89:638–642.
40. Raghavan M, Chen MY, Gastinel LN, Bjorkman PJ. Investigation of the interaction between the class I MHC-related Fc receptor and its immunoglobulin G ligand. Immunity 1994;1:303–315.
41. Nabi IR, Le Bivic A, Fambrough D, Rodriguez-Boulan E. An endogenous MDCK lysosomal membrane glycoprotein is targeted basolaterally before delivery to lysosomes. J Cell Biol 1991;115:1573–1584.
42. Nabi IR, Rodriguez-Boulan E. Increased LAMP-2 polylactosamine glycosylation is associated with its slower Golgi transit during establishment of a polarized MDCK epithelial monolayer. Mol Biol Cell 1993; 4:627–635.
43. Fuller SD, Simons K. Transferrin receptor polarity and recycling accuracy in ''tight'' and ''leaky'' strains of Madin-Darby canine kidney cells. J Cell Biol 1986;103:1767–1779.
44. Vaughn DE, Bjorkman PJ. High-affinity binding of the neonatal Fc receptor to its IgG ligand requires receptor immobilization. Biochemistry 1997;36:9374–9380.
45. Martin WL, West AP Jr, Gan L, Bjorkman PJ. Crystal structure at 2.8 A of an FcRn/heterodimeric Fc complex: mechanism of pH-dependent binding. Mol Cell 2001;7:867–877.
46. Sanchez LM, Lopez-Otin C, Bjorkman PJ. Biochemical characterization and crystalization of human Zn-alpha2-glycoprotein, a soluble class I major histocompatibility complex homolog. Proc Natl Acad Sci U S A 1997;94:4626–4630.
47. Apodaca G, Katz LA, Mostov KE. Receptor-mediated transcytosis of IgA in MDCK cells is via apical recycling endosomes. J Cell Biol 1994;125:67–86.

Chapter 3:

Immunoglobulin Transcytosis and Recycling by an Avian Functional Equivalent of FcRn

This chapter has been published as Devin B. Tesar, Evelyn J. Cheung, and Pamela J. Bjorkman (2008) The Chicken Yolk Sac IgY Receptor, a Mammalian Mannose Receptor Family Member, Transcytoses IgY across Polarized Epithelial Cells, Molecular Biology of the Cell, Vol. 19, Issue 4, 1587–1593, April 2008. Evelyn Cheung assisted in immunofluorescence experiments and in the maintenance of cell lines.

Molecular Biology of the Cell
Vol. 19, 1587–1593, April 2008

The Chicken Yolk Sac IgY Receptor, a Mammalian Mannose Receptor Family Member, Transcytoses IgY across Polarized Epithelial Cells

Devin B. Tesar,* Evelyn J. Cheung,*† and Pamela J. Bjorkman*‡

*Division of Biology and ‡Howard Hughes Medical Institute, California Institute of Technology, Pasadena, CA 91125

Submitted September 27, 2007; Revised January 4, 2008; Accepted January 30, 2008
Monitoring Editor: Keith Mostov

In mammals the transfer of passive immunity from mother to young is mediated by the MHC-related receptor FcRn, which transports maternal IgG across epithelial cell barriers. In birds, maternal IgY in egg yolk is transferred across the yolk sac to passively immunize chicks during gestation and early independent life. The chicken yolk sac IgY receptor (FcRY) is the ortholog of the mammalian phospholipase A2 receptor, a mannose receptor family member, rather than an FcRn or MHC homolog. FcRn and FcRY both exhibit ligand binding at the acidic pH of endosomes and ligand release at the slightly basic pH of blood. Here we show that FcRY expressed in polarized mammalian epithelial cells functioned in endocytosis, bidirectional transcytosis, and recycling of chicken FcY/IgY. Confocal immunofluorescence studies demonstrated that IgY binding and endocytosis occurred at acidic but not basic pH, mimicking pH-dependent uptake of IgG by FcRn. Colocalization studies showed FcRY-mediated internalization via clathrin-coated pits and transport involving early and recycling endosomes. Disruption of microtubules partially inhibited apical-to-basolateral and basolateral-to-apical transcytosis, but not recycling, suggesting the use of different trafficking machinery. Our results represent the first cell biological evidence of functional equivalence between FcRY and FcRn and provide an intriguing example of how evolution can give rise to systems in which similar biological requirements in different species are satisfied utilizing distinct protein folds.

INTRODUCTION

The transfer of maternal antibodies to the gestating fetus or neonate allows for the passive acquisition of humoral immunity to antigens encountered by the mother. In mammals, this process is mediated by the neonatal Fc receptor (FcRn). FcRn was first isolated from the neonatal rodent gut (Simister and Rees, 1985) and was later shown by sequence analysis to be related to class I major histocompatibility complex (MHC) molecules (Simister and Mostov, 1989). Subsequent structural analyses demonstrated that FcRn has a narrowed and nonfunctional counterpart of the MHC peptide-binding groove and interacts with Fc in a manner that differs from MHC interactions with peptides, T-cell receptors, and other macromolecules (Burmeister *et al.*, 1994; Martin *et al.*, 2001). FcRn has since been identified in other mammals, including humans (Leach *et al.*, 1996), nonhuman primates (Spiekermann *et al.*, 2002), ruminants (Mayer *et al.*, 2002, 2004), and marsupials (Western *et al.*, 2003). FcRn also plays a key role in serum IgG homeostasis by serving as a protection receptor for IgG internalized via fluid phase endocytosis by the vascular endothelium, causing it to be recycled and released at the plasma membrane rather than lysosomally degraded (for review see Ghetie and Ward, 2002). The expression of FcRn across many different mammalian species coupled with its roles in bidirectional transcytosis and recycling have made it a widely used model for studies of intracellular transport (Praetor *et al.*, 1999; McCarthy *et al.*, 2000, 2001; Zhu *et al.*, 2002; Ward *et al.*, 2003; Claypool *et al.*, 2004; Ober *et al.*, 2004a,b; Lencer and Blumberg, 2005; Tesar *et al.*, 2006).

Transfer of maternal immunoglobulin to offspring has long been known to occur in birds as well as mammals (Brambell, 1970). IgY, the avian and reptilian counterpart of IgG, is packaged into egg yolk and transported across yolk sac membranes during development (Kowalczyk *et al.*, 1985). Yolk sac membranes isolated from chicken exhibit IgY-binding properties similar to those of FcRn for IgG—high-affinity binding at acidic pH and no observable binding at neutral or basic pH (Linden and Roth, 1978; Tressler and Roth, 1987)—suggesting the existence of a functionally equivalent receptor in avian species. Recently, our laboratory isolated a chicken yolk sac IgY receptor (FcRY) that exhibits pH-dependent binding to IgY (West *et al.*, 2004). Surprisingly, FcRY shared no homology with class I MHC molecules or FcRn, but was instead a homolog of the mammalian phospholipase A_2 receptor (PLA_2R), a member of the mannose receptor (MR) family (East and Isacke, 2002). Mammalian MR family members mediate a variety of functions, including roles in the innate and adaptive immune systems (MR), internalization of soluble PLA_2 enzymes (PLA_2R), presentation of antigens to T-cells (DEC-205), and remodeling of the extracellular matrix (Endo180). FcRY shares a common domain organization with other MR family members, which consists of an N-terminal cysteine-rich domain, a single fibronectin type II (FNII) domain, 8 to 10 tandem C-type lectin-like domains (CTLDs), a single-pass

This article was published online ahead of print in *MBC in Press* (http://www.molbiolcell.org/cgi/doi/10.1091/mbc.E07–09–0972) on February 6, 2008.

† Present address: Division of Health Sciences and Technology, Harvard Medical School, Boston, MA 02115.

Address correspondence to: Pamela J. Bjorkman (bjorkman@caltech.edu).

© 2008 by The American Society for Cell Biology

transmembrane region and a short cytoplasmic tail (East and Isacke, 2002). The presence of tandem lectin-like domains does not necessarily imply lectin activity because only the MR and Endo180 bind to monosaccharides. Indeed, the CTLDs in PLA_2R mediate a protein-protein interaction independently of carbohydrates (East and Isacke, 2002), and FcRY is thought to recognize IgY through a protein–protein interaction (West *et al.*, 2004).

None of the mammalian MR family members are known to function as immunoglobulin and/or transcytotic receptors, but all exhibit clathrin-mediated endocytosis, resulting in either recycling back to the plasma membrane or delivery of cargo to the late endosome/lysosomal pathway (East and Isacke, 2002). The cytoplasmic tails of mammalian MR family members contain two putative internalization motifs: an acid-based dihydrophobic motif (Exxx$\phi\phi$) and a low density lipoprotein receptor (LDLR)-like tyrosine-based internalization motif (ϕxNxxY; East and Isacke, 2002). The cytoplasmic tail of FcRY also includes these motifs, although the tyrosine in the LDL-like motif is substituted by a phenylalanine. Although FcRY appeared to fill all criteria for being the functional equivalent of mammalian FcRn (West *et al.*, 2004), it had not been directly demonstrated to endocytose and transcytose IgY. Here we report creation of a cell-based model system to probe questions regarding the function of FcRY in relation to other known members of the MR family and present direct evidence that FcRY functions in endocytosis and transcytosis of IgY. These studies establish FcRY as an intriguing model of receptor-mediated transport in polarized cells and demonstrate an increased diversity of functional possibilities within the MR family.

MATERIALS AND METHODS

Antibodies and Proteins

Mouse monoclonal anti-Rab11, anti-clathrin heavy chain, and anti-EEA1 antibodies were purchased from BD Transduction Laboratories (San Jose, CA). Alexa Fluor 546– and 568—conjugated goat anti-mouse and Alexa Fluor 647–conjugated goat anti-chicken secondary antibodies were from Molecular Probes (Eugene, OR). Chicken IgY and FcY were obtained from Jackson ImmunoResearch Laboratories (West Grove, PA) and passed over a Superdex 200 column to remove aggregates.

The purified FcRY ectodomain, expressed in baculovirus-infected insect cells and purified as described (West *et al.*, 2004), was used as an immunogen for the production of polyclonal ascites as described previously (Ou *et al.*, 1993). The Fc fragment of rat IgG2a (Fcγ) was expressed in Chinese hamster ovary cells and purified from culture supernatants as described (Martin and Bjorkman, 1999). For quantitative endocytosis and transport experiments, FcY and Fcγ were iodinated to a specific activity of 30 μCi/μg using Na[^{125}I] (MP Biomedicals, Solon, OH) and IODO-GEN (Pierce, Rockford, IL). Radiolabeled ligands were buffer exchanged into HBS (25 mM HEPES, 150 mM NaCl, pH 7.4) by two subsequent passages over Zeba Desalting spin columns (Pierce). Protein concentrations were determined by BCA assay (Pierce) using bovine γ-globulin as a standard.

Cell Culture and Generation of Stable Cell Lines

Rat inner medullary collecting duct (IMCD) cells (a kind gift from Neil Simister, Brandeis University) were cultured in DMEM supplemented with 10% fetal bovine serum (FBS), 100 U/ml penicillin, and 100 mg/ml streptomycin under 5% CO_2. Cells were fed every other day and passaged weekly. The cDNA encoding the full-length FcRY gene was subcloned into the pIRES2-EGFP mammalian expression vector (Clontech, Mountain View, CA) and transfected into IMCD cells using Lipofectamine 2000 (Invitrogen, Carlsbad, CA). Stable clones were selected with 500 μg/ml G418 (Invitrogen). For experiments requiring polarized cell monolayers, cells were seeded at superconfluent density (1×10^6 cells/ml) onto 12-mm Transwell polyester filters (0.4-μm pores; Corning Costar, Acton, MA) with 0.5 and 1.5 ml of media in the apical and basolateral reservoirs, respectively. Cells were fed daily beginning 2 d after initial seeding and used for experiments on the fourth or fifth day after plating.

Quantitative Endocytosis Assay

Cells were grown to near-confluence in 12-well tissue culture plates until ~80–90% confluent. Before incubations with ligand, the cells were serum-starved for 20 min in Hank's balanced salt solution (HBSS), 1.3 mM $CaCl_2$, 0.8 mM $MgSO_4$ (HBSS+), 1% bovine serum albumin (BSA; Sigma, St. Louis, MO), 1 mM KI adjusted to either pH 5.9 or 8.0 with MES or HEPES (20 mM each), respectively. [^{125}I]FcY or [^{125}I]Fcγ was added to a final concentration of 100 nM in HBSS+ at pH 5.9 or 8.0, and plates were incubated in a 37°C circulating water bath for 45 min. For competitor studies, 20 μM unlabeled IgY was added during the preincubation and kept present throughout the experiment. After incubation with the radioligand the cells were cooled on ice, washed four times with ice-cold HBSS+ at pH 8.0 to remove surface-bound ligand, and then lysed in 0.1 N NaOH. Total protein concentration in the lysates was determined by BCA assay and the radioactivity present in the lysates was counted on a Beckman 5500 γ-counter (Fullerton, CA) and converted to picograms of protein using the specific activity of the radiolabeled ligand.

Transcytosis Assay

FcRY-IMCD and untransfected IMCD cell monolayers were grown on permeable filter supports as described previously (McCarthy *et al.*, 2000). Polarization of monolayers was confirmed by measuring a transepithelial electrical resistance (TEER) of 350–500 Ωcm^2. Filters were preincubated for 20 min with HBSS+/BSA/KI at pH 5.9 on the loading surface and HBSS+/BSA/KI at pH 8.0 on the nonloading surface. For competition experiments, unlabeled IgY (20 μM) was present in the loading surface medium during the preincubation step. Where indicated, cells were incubated with nocodazole (33 μM) for 1 h at 37°C in both the loading and nonloading surface medium. Nocodazole treatment did not alter the TEER values across the monolayers (data not shown). [^{125}I]FcY or [^{125}I]Fcγ was added directly to the loading media to a final concentration of 100 nM. Plates were incubated for 90 min in a 37°C circulating water bath. Media from the nonloading surface were collected and precipitated with 10% trichloroacetic acid (TCA) at 4°C. TCA-insoluble (intact ligand) fractions were counted on a Beckman 5500 γ-counter.

Recycling Assay

Filter-grown FcRY-IMCD and untransfected IMCD cells were treated as described above for the transcytosis assay. After 90 min of incubation with ^{125}I-ligand, the filters were cooled on ice and washed six times with ice-cold HBSS+/BSA at pH 8. Prewarmed HBSS+/BSA at pH 8 was added, and the cells were returned to 37°C for 1 h. The media from the loading surface were collected, precipitated with TCA, and counted as described above.

Immunofluorescence and Microscopy

For immunofluorescence colocalization studies, FcRY-IMCD cells were grown until polarized on permeable filters. Monolayers were washed once with HBSS+/BSA and treated with IgY or FcY (500 nM in HBSS+/BSA, pH 5.9 or 8.0) for 45 min at 37°C. Cells were cooled on ice, washed twice with HBSS+/BSA, pH 8, and fixed with 4% paraformaldehyde before immunostaining. Immunofluorescence was carried out as described previously (Tesar *et al.*, 2006). Commercial antibodies (anti-EEA1, anti-clathrin heavy chain, and anti-Rab11) were used at 1:100 dilutions. The anti-FcRY polyclonal ascites was used at 10 μg/ml. Secondary antibodies were used at a 1:500 dilution. Samples were imaged on an inverted Zeiss LSM 510 confocal microscope equipped with a Zeiss Plan-Apochromat 100× oil immersion objective (NA 1.4; Thornwood, NY). Green fluorophores were excited with the 488-nm line of an argon ion laser. Orange and far-red dyes were excited with the 543- and 633-nm lines of a He-Ne laser, respectively. Image processing was performed using the Zeiss LSM Examiner software (v. 3.2) and arranged for presentation in Photoshop 7.0 (Adobe Systems, San Jose, CA).

Potassium Depletion

Potassium depletion of FcRY-IMCD cells was performed essentially as described (McGraw and Subtil, 1999). Briefly, filter-grown FcRY-IMCD monolayers were shocked in hypotonic medium (1:1 vol/vol MEM/water) for 10 min before being incubated in potassium-free HBSS+/BSA, pH 5.9, for 30 min. Cells were then incubated for with 500 nM IgY in potassium-free HBSS+/BSA, pH 5.9, for 45 min and processed for immunofluorescence as described above.

RESULTS

Functional Expression of FcRY in IMCD Cells

To study the behavior of FcRY in a cellular context, we prepared a polarized cell line stably expressing the full-length FcRY gene. Because an appropriate avian epithelial cell line is not presently available, we considered two mammalian cell lines for FcRY expression: Madin-Darby canine kidney (MDCK) cells and rat IMCD cells. Both cell lines can be grown as polarized monolayers on filter supports and have been used as model systems for studying transcytosis and recycling by FcRn and other receptors (Praetor *et al.*,

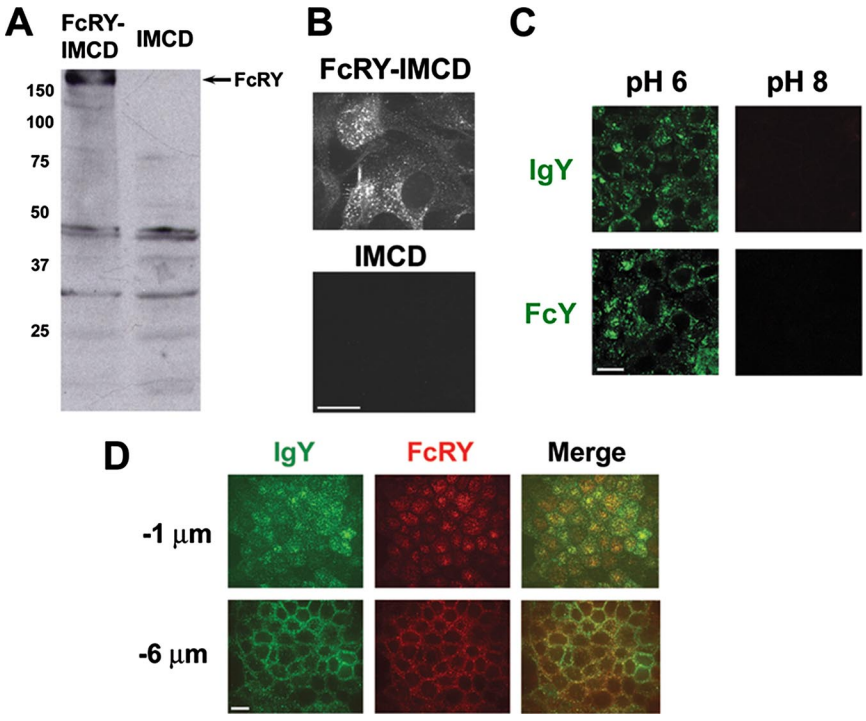

Figure 1. Functional expression of FcRY in IMCD cells. (A) Anti-FcRY Western blot of detergent lysates from FcRY-transfected IMCD and untransfected IMCD cells using a polyclonal ascites raised against the FcRY ectodomain. (B) Confocal immunofluorescence of FcRY-IMCD and untransfected IMCD cells stained with anti-FcRY polyclonal ascites. Images were collected with the same laser power, exposure times, and detector settings. (C) Confocal images of FcRY-IMCD cells incubated with 500 nM Alexa 488–labeled IgY or FcY at pH 6 and 8. Internalized ligand was seen only when incubated at acidic pH. (D) Confocal images demonstrating colocalization of FcRY and IgY. Filter-grown monolayers of FcRY-IMCD cells were incubated with Alexa 488–labeled IgY at pH 6 and stained with anti-FcRY. Optical sections were taken ~1 μm below the tight junctions (top panels) or ~6 μm below the tight junctions (bottom panels). Scale bars, 10 μm.

1999; McCarthy *et al.*, 2000, 2001; Wu and Simister, 2001; Claypool *et al.*, 2002, 2004; Tesar *et al.*, 2006). We were able to obtain expression of FcRY in IMCD cells, but not MDCK cells (data not shown); thus we proceeded to study FcRY function in IMCD cells using untransfected IMCD cells as a negative control. Western blot analysis of lysates of transfected IMCD cells (hereafter abbreviated as FcRY-IMCD) using a polyclonal ascites raised against the FcRY ectodomain detected a prominent band with an apparent molecular mass of 180 kDa (Figure 1A), corresponding to the anticipated molecular weight of FcRY. Although two nonspecific bands of ~30 and 45 kDa were detected in FcRY-IMCD and untransfected IMCD cell lysates, confocal immunofluorescence analysis of fixed cells showed that only FcRY-IMCD cells were positively stained by the ascites under identical treatment and imaging conditions (Figure 1, B and D, red fluorescence) and that FcRY-positive staining colocalized with internalized IgY (Figure 1D, green fluorescence and merged panels). Untransfected IMCD cells do not internalize detectable amounts of IgY or FcY when subjected to the same treatment and imaging conditions as FcRY-IMCD cells (data not shown).

We also examined pH-dependent binding and internalization of FcRY ligands by FcRY-IMCD cells. FcRY-IMCD cells were incubated with intact IgY or the Fc fragment of IgY (FcY) at pH 6 or 8 at a concentration of 500 nM. Fixed cells were imaged by confocal microscopy (Figure 1C). Both IgY and FcY were efficiently internalized at pH 6, but not at pH 8. This is consistent with previous surface plasmon resonance-based binding studies, which showed that FcRY bound to these ligands at acidic, but not basic, pH (West *et al.*, 2004), analogous to the pH-dependent binding properties of FcRn.

Quantitative Analysis of FcRY-mediated Endocytosis

Having demonstrated that FcY and IgY could be internalized by FcRY-IMCD cells (Figure 1, C and D), we next sought to quantify endocytosis using radiolabeled FcY ([^{125}I]FcY). Endocytosis of 100 nM [^{125}I]FcY was observed in FcRY-expressing cells, but not in untransfected cells (Figure 2A) when incubated at pH 6 (see *Materials and Methods*), but not at pH 8, consistent with our confocal analysis (Figure 1C). FcRY-mediated endocytosis was specific, as we observed no endocytosis of a recombinant Fc fragment from rat IgG_{2a} (Fcγ), which binds to FcRn but not to FcRY (West *et al.*, 2004). As expected for a receptor-mediated process, endocytosis was saturable by addition of a 200-fold excess of unlabeled IgY to the incubation medium (Figure 2A).

Clathrin-mediated Internalization and Delivery to Early Endosomes

To investigate the potential involvement of clathrin in FcRY-mediated endocytosis and the postendocytic fate of IgY, we performed confocal immunofluorescence experiments on polarized FcRY-IMCD monolayers. After incubation with 500 nM FcY at pH 6, cells were fixed and stained with an antibody against chicken IgY to visualize the internalized ligand and with antibodies against either the clathrin heavy chain or the early endosome marker EEA1. As shown in Figure 2, B and C, endocytosed IgY (green fluorescence) is present in discrete compartments throughout the cell. A single confocal section through a medial region of the monolayer showed that some clathrin-positive compartments (Figure 2B, red fluorescence) contained endocytosed IgY (yellow signal in merged image). Some of these doubly-labeled structures may represent clathrin-coated vesicles that had pinched off from the plasma membrane and were en route to deliver their contents to the subcellular endosomal network. To confirm that FcRY-mediated ligand internalization was via a clathrin-dependent pathway, we performed IgY internalization experiments using cells in which clathrin-mediated endocytosis was blocked by potassium depletion (Larkin *et al.*, 1983). When potassium-depleted cells are treated with IgY and imaged under the same con-

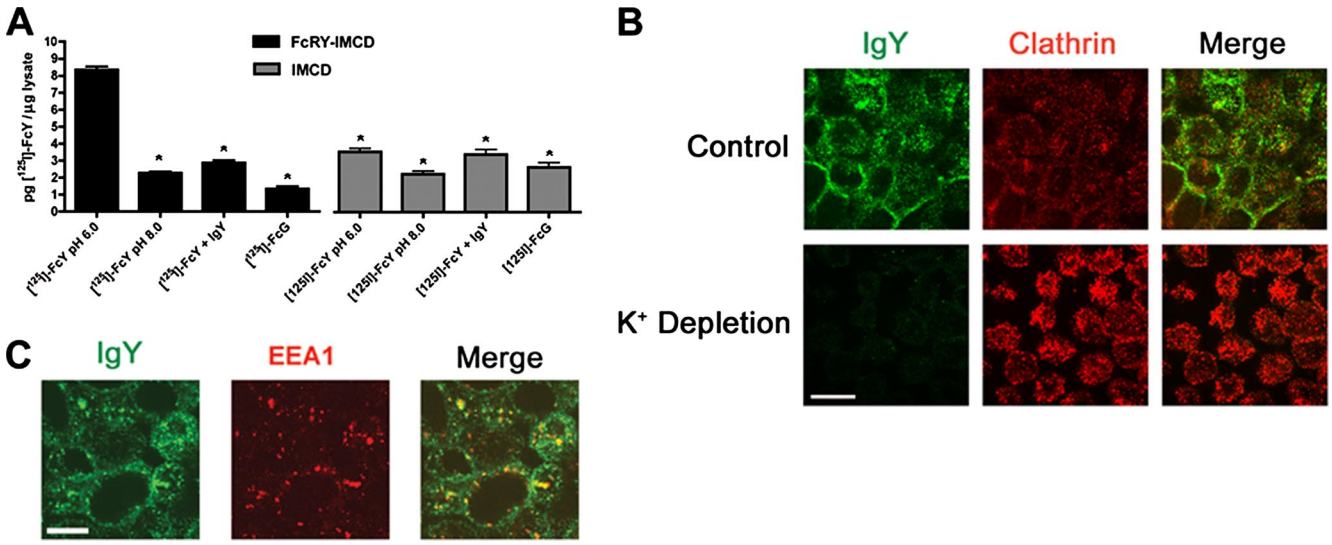

Figure 2. Quantitative endocytosis of FcY and delivery to clathrin- and EEA1-positive compartments. (A) Endocytosis of [^{125}I]FcY by FcRY-IMCD cells. FcRY-IMCD and untransfected IMCD cells were grown to near-confluence in 12-well plates. Cells were incubated at pH 6 or 8 with 100 nM [^{125}I]FcY or [^{125}I]Fcγ in the presence or absence of a 200-fold excess of unlabeled IgY. After washing at pH 8 to remove surface bound ligand, cells were lysed and counted for ^{125}I radioactivity. Bars, the mean ± SEM of triplicate measurements. *$p < 0.001$ relative to [^{125}I]FcY, pH 6.0. (B) Clathrin-dependent endocytosis of IgY. Control or potassium-depleted FcRY-IMCD cells were incubated with 500 nM IgY at pH 6 and then fixed and stained with antibodies against IgY (left panels, green fluorescence) and clathrin heavy chain (center panels, red fluorescence). (C) Delivery of endocytosed IgY to EEA1-positive endosomes. IgY-treated cells were stained with antibodies against IgY (green fluorescence) and EEA1 (red fluorescence). Scale bars, 10 μm.

ditions as the FcRY-IMCD cells, little or no intracellular IgY was detected (Figure 2B, bottom-left panel). Staining of IgY-treated cells with anti-EEA1 (Figure 2C, red fluorescence) showed many double-positive compartments (yellow signal in merged image). Taken together, these results demonstrated that FcRY ligands were internalized via a clathrin-mediated mechanism and subsequently entered the endosomal trafficking network, most likely through postendocytotic delivery to early endosomes.

FcRY Mediates Bidirectional Transcytosis

We next asked if FcRY expressed in IMCD cells could recapitulate transcytosis, a canonical in vivo function of its mammalian cognate, FcRn. Radiolabeled FcY was added to the loading surface of filter-grown monolayers, and cells were allowed to transport [^{125}I]-FcY into the nonloading surface medium for 90 min. Transcytosis of [^{125}I]FcY was observed in both the apical-to-basolateral and basolateral-to-apical directions of FcRY-IMCD cells, but not the control untransfected cells (Figure 3, A and B). Buffering the loading surface to pH 8 diminished transcytosis in FcRY-expressing cells to the background levels observed for untransfected cells, as did inclusion of a 200-fold excess of unlabeled competitor IgY. Radiolabeled Fcγ, which does not bind to FcRY (West *et al.*, 2004), was not significantly transcytosed in either direction. Pretreatment of cells with the microtubule-depolymerizing agent nocodazole reduced observable transcytosis in both directions to approximately one-half of the corresponding specific (above-background) level. The reduction was statistically significant in the apical-to-basolateral direction ($p = 0.0007$), but not in the basolateral-to-apical direction ($p = 0.0943$). These results suggest that directed movement of cargo-loaded vesicles along microtubule tracts is required for efficient FcRY-mediated apical-to-basolateral transport across polarized cell monolayers.

Ligand Recycling by FcRY

Having shown that FcRY was capable of ligand transport across polarized monolayers, we next sought to determine if endocytosed ligands could be recycled from either the apical or basolateral surfaces. Filter-grown cell monolayers were treated with [^{125}I]FcY as described for the transcytosis assay. Cell were washed and returned to 37°C to allow recycling of internalized ligands back into the loading surface media. As shown in Figure 4A, we observed recycling at both the apical and basolateral surfaces of FcRY-expressing cells that had been incubated with ligand at pH 6. Consistent with these results, confocal immunofluorescence of fixed, IgY-treated cells using a mAb against the recycling endosome marker Rab11 (Figure 4B, red fluorescence) confirmed the presence of internalized IgY (green fluorescence) in Rab11-positive recycling compartments in FcRY-IMCD cells (Figure 4B), but not in untransfected cells (data not shown). No significant amount of recycling was observed when cells were incubated with ligand at pH 8 or in the presence of competitor IgY (Figure 4A). In addition, no recycling was observed in untransfected IMCD cells. Interestingly, treatment with nocodazole had no significant effect on [^{125}I]FcY recycling (Figure 4A), suggesting that recycling of FcY, unlike transcytosis, does not rely on an intact microtubule network.

DISCUSSION

The transfer of passive immunity from mother to young is a pervasive feature of most, if not all, orders of mammals. The mammalian neonatal Fc receptor, FcRn, has served as the central model for nearly all biochemical and cell biological investigations of this process to date, although it has been known for many years that this process is not unique to mammals (Brambell, 1970). The molecular characterization of the functional equivalent of FcRn in birds, the yolk sac IgY

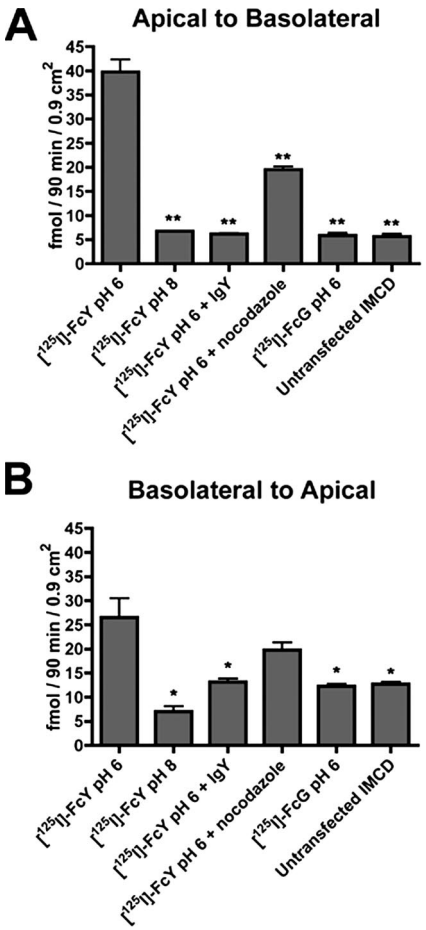

Figure 3. Bidirectional transcytosis of FcY. FcRY-IMCD and untransfected IMCD cells were grown as polarized monolayers on permeable filter supports. [^{125}I]FcY or [^{125}I]Fcγ was added to the loading surface to a final concentration of 100 nM with or without unlabeled competitor or nocodazole. Medium from the nonloading surface was collected after 90 min, and levels of [^{125}I] radioactivity in the acid-insoluble fraction were determined. (A) Apical-to-basolateral transcytosis. (B) Basolateral-to-apical transcytosis. Both sets of histograms represent the mean ± SEM of triplicate measurements from a representative experiment. Similar results were obtained in two independent experiments. *$p < 0.05$, **$p < 0.001$ relative to [^{125}I]FcY, pH 6.0.

receptor FcRY, yielded the unexpected result that FcRn and FcRY were structurally distinct; FcRn being a homolog of class I MHC molecules, and FcRY being a homolog of the mammalian MR family member PLA_2R (West *et al.,* 2004). Biochemical experiments using a recombinant FcRY ectodomain showed that it bound to the Fc region of IgY with the expected pH dependence of an FcRn analog (West *et al.,* 2004), but whether FcRY could recapitulate FcRn function in a cellular context remained unclear. Here we describe the development of a cell culture model with which to study the cellular function of FcRY using stably-transfected IMCD cells.

Our FcRY-expressing IMCD cells specifically and saturably endocytosed FcY when it was added at pH 6, but not pH 8, as observed previously for endocytosis of Fcγ by FcRn expressed in transfected cell lines (Ellinger *et al.,* 1999; McCarthy *et al.,* 2000; Claypool *et al.,* 2004; Tesar *et al.,* 2006). In addition to specific endocytosis of FcY, FcRY-expressing IMCD cells bidirectionally transcytosed FcY across filter-grown polarized monolayers in a saturable and specific manner. To our knowledge, this represents the first observation of transcytosis by a member of the MR family. Additionally, our results suggest that key components of the cellular endocytotic/transcytotic machinery are conserved in avians and mammals.

FcRn is one of the few transcytotic receptors known to carry out physiologically relevant apical-to-basolateral transcytosis. Quantitative analyses of transcytosis mediated by rat FcRn expressed in IMCD (McCarthy *et al.,* 2000) and MDCK cells (Tesar *et al.,* 2006) have shown that rat FcRn transports significantly more ligand in the apical-to-basolateral than in the basolateral-to-apical direction, consistent with its role in transporting IgG in ingested milk from the luminal (apical) surface of the intestinal epithelium of newborn rodents, where the pH is acidic, to the serosal (basolateral) surface, which is exposed to the slightly basic pH of the bloodstream. By contrast, human FcRn transcytoses IgG more efficiently in the basolateral-to-apical direction when expressed in transfected cells (Claypool *et al.,* 2002, 2004), perhaps owing to its purported role in transferring antibodies from the host circulation into luminal secretions by basolateral-to-apical transcytosis. Once in the lumen, the antibodies can complex with antigens, which can then be presented to dendritic cells in the host circulation after reverse transcytosis (Yoshida *et al.,* 2004). Whether this difference between the human and rat receptors gives rise to differences in the functions of these molecules in their respective in vivo settings remains unclear. In the case of FcRY, a preferred apical-to-basolateral directionality makes sense in light of the fact that the pH-dependent interaction between FcRY and IgY would then dictate unidirectional transport from the apical surface of yolk sac membrane cells, where the pH of the yolk is ~6 (Cutting and Roth, 1973), to the basolateral surface leading to the circulation of the developing chick, where the pH is ~7.4 (Dawes and Simkiss, 1969). Accordingly, we have shown that FcRY-expressing IMCD cells transcytose more FcY in the apical-to-basolateral than in the basolateral-to-apical direction (Figure 3, A and B).

Biochemical and biophysical characterization of recombinant FcRY suggested that the molecule undergoes a conformational change at pH 6, assuming a more compact form that binds IgY compared with an elongated form at basic pH that does not bind IgY (West *et al.,* 2004). This is consistent with recent electron microscopy studies of the mannose receptor and Endo180, which revealed that these molecules undergo significant conformational changes upon incubation at acidic pH, with the mannose receptor in particular assuming a more compact conformation at low pH (Rivera-Calzada *et al.,* 2003; Boskovic *et al.,* 2006). Although the functional relevance of the conformational change is unclear for the mammalian MR family members, the body of evidence strongly suggests that the pH-dependent conformational change in FcRY is required for its function in delivery of maternal IgY to the chick. Thus acidic pH, either in endosomes or in egg yolk, would cause FcRY to adopt a conformation that allows IgY binding, whereas the slightly basic pH of the bloodstream would result in a conformation that promotes IgY release. In general, pH-dependent conformational changes in MR family members could serve as a driving force for activity modulation; e.g., by controlling binding and dissociation of a receptor-ligand complex, activation of signal cascades through the receptor, and/or mediation of downstream trafficking events. Unlike FcRY, mammalian MR family members must be capable of binding to their cognate ligands at the neutral/slightly basic pH of the extracellular environment; e.g., PLA_2R binds circulating PLA_2 at the cell surface. FcRY may be unique among MR

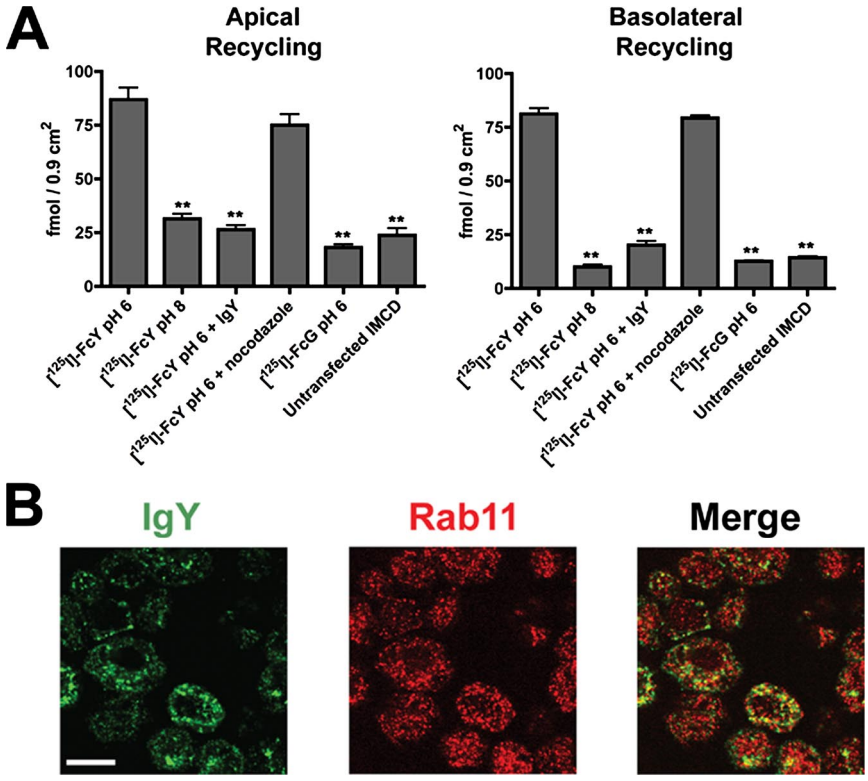

Figure 4. Recycling of FcY occurs at both the apical and basolateral surfaces. (A) Recycling of [^{125}I]FcY and [^{125}I]Fcγ by polarized FcRY-IMCD monolayers. Cells grown as polarized monolayers on permeable filters were treated as described for the bidirectional transcytosis assay. After a 90-min incubation with a ^{125}I-ligand, the cells were cooled on ice, washed to remove surface bound ^{125}I-ligand, and returned to 37°C to allow recycling of internalized ligands into the loading surface medium. Data are shown as the mean ± SEM of triplicate measurements from a representative experiment in both panels. **$p < 0.001$ relative to [^{125}I]FcY pH 6.0. (B) Confocal images demonstrating trafficking of IgY to Rab11-positive recycling endosomes. Filter-grown FcRY-IMCD cells were incubated with 500 nM IgY at pH 6. Cells were washed, fixed, and double-stained for IgY (green fluorescence) and the recycling endosome marker, Rab11 (red fluorescence). Scale bar, 10 μm.

family members in that the compact conformation assumed at acidic pH is the functional ligand-binding state, whereas the elongated conformation at neutral/basic pH is not permissive for ligand binding. Because the other MR family members retain binding of their ligands at the cell surface, the lack of a practical mechanism for ligand release makes it unlikely that the mammalian MR proteins function to transcytose ligands across polarized cells.

In addition to its function in bidirectional transcytosis, we found that FcRY promoted ligand recycling at both the apical and basolateral surfaces of IMCD cells (Figure 4A). Consistent with this observation, confocal immunofluorescence experiments showed that internalized IgY was present in Rab11-positive recycling compartments (Figure 4B). Given that recycling is a common feature of MR family members (East and Isacke, 2002), these results were not unexpected. However, combined with the evidence for immunoglobulin transcytosis by FcRY and the role of mammalian FcRn in serum IgG homeostasis (Ghetie and Ward, 2002), this raises the intriguing possibility that serum IgY homeostasis in avian species is regulated by FcRY. Indeed, the observation that a greater amount of FcY was recycled than transcytosed under the same conditions (Figures 3 and 4) suggests that ligand recycling is an important part of the in vivo function of FcRY. Although mammalian FcRn can recycle serum albumin as well as IgG, and is therefore proposed to serve as a protection receptor for both types of ligand (Chaudhury *et al.*, 2003; Kim *et al.*, 2006; Koltun *et al.*, 2005), FcRY does not appear to function as a protection receptor for albumin, as we observed no binding of FcRY to ovalbumin in surface plasmon resonance binding assays conducted at pH 5–6 and at concentrations of up to 10 μM (data not shown).

To investigate the importance of cytoskeletal elements in FcRY-mediated transport, we asked whether intact microtubules were required for FcRY transcytosis and recycling. Although treatment of FcRY-IMCD cells with the microtubule depolymerizing agent nocodazole appeared to reduced specific transcytosis by approximately one-half in both the apical-to-basolateral and basolateral-to-apical directions, only in the apical-to-basolateral direction was this reduction statistically significant. The incomplete inhibition of transcytosis in the absence of an intact microtubule network could indicate that diffusion allows for the proper delivery of some vesicles containing receptor-ligand complexes to the opposite plasma membrane, but that the efficiency of cargo delivery is increased by the presence of intact microtubule tracts. It should be noted, however, that in previous studies of rat FcRn expressed in IMCD cells, nocodazole treatment resulted in more complete inhibition of transcytosis in both directions (McCarthy *et al.*, 2000), perhaps reflecting a difference in the extent to which intact microtubules are required for transcytosis mediated by these two receptors. By contrast to its effect on transcytosis, treatment with nocodazole had no observable effect on the efficiency of FcRY-mediated recycling (Figure 4). Taken together, these results indicate that, in IMCD cells, FcRY mediates trafficking of endocytosed ligands into both a microtubule-dependent transcytotic pathway and a microtubule-independent recycling pathway.

FcRY is an intriguing model for the evolution and function of Fc receptors and of transcytotic receptors in general. Unlike other well-characterized transcytotic receptors, FcRY and its mammalian cognate FcRn are capable of bidirectional transcytosis, owing to the utilization of pH-dependent ligand binding as an efficient mechanism to allow for ligand release upon exposure to the neutral/slightly basic pH of the extracellular environment. Additionally, FcRY represents the incorporation of a new function, transcytosis, into the repertoire of functions performed by members of the MR family. Like its mammalian counterpart FcRn, FcRY evolved from a protein fold whose original function was of no apparent relation to immunoglobulin transport. The compari-

son of FcRY with other MR family members and with FcRn offers a fascinating glimpse into the evolution of cross-species functional equivalence in molecules that are structurally distinct, illustrating how the key protein player within an essential and intricate system can evolve from more than one functional protein fold and, conversely, how certain folds can evolve as versatile tools to be applied in more than one functional setting.

ACKNOWLEDGMENTS

We thank Anthony West for construction of expression vectors, the Caltech Protein Expression Center for baculovirus expression of FcRY, and members of the Bjorkman lab for critical reading of the manuscript. This work was supported by the National Institutes of Health (2 R37 AI041239-06A1 to P.J.B.).

REFERENCES

Boskovic, J., Arnold, J. N., Stilion, R., Gordon, S., Sim, R. B., Rivera-Calzada, A., Wienke, D., Isacke, C. M., Martinez-Pomares, L., and Llorca, O. (2006). Structural model for the mannose receptor family uncovered by electron microscopy of Endo180 and the mannose receptor. J. Biol. Chem. *281*, 8780–8787.

Brambell, F. W. (1970). The Transmission of Passive Immunity from Mother to Young, Amsterdam: North-Holland Company.

Burmeister, W. P., Gastinel, L. N., Simister, N. E., Blum, M. L., and Bjorkman, P. J. (1994). Crystal structure at 2.2 A resolution of the MHC-related neonatal Fc receptor. Nature *372*, 336–343.

Chaudhury, C., Mehnaz, S., Robinson, J. M., Hayton, W. L., Pearl, D. K., Roopenian, D. C., and Anderson, C. L. (2003). The major histocompatibility complex-related Fc receptor for IgG (FcRn) binds albumin and prolongs its lifespan. J. Exp. Med. *197*, 315–322.

Claypool, S. M., Dickinson, B. L., Wagner, J. S., Johansen, F. E., Venu, N., Borawski, J. A., Lencer, W. I., and Blumberg, R. S. (2004). Bidirectional transepithelial IgG transport by a strongly polarized basolateral membrane Fcgamma-receptor. Mol. Biol. Cell *15*, 1746–1759.

Claypool, S. M., Dickinson, B. L., Yoshida, M., Lencer, W. I., and Blumberg, R. S. (2002). Functional reconstitution of human FcRn in Madin-Darby canine kidney cells requires co-expressed human beta 2-microglobulin. J. Biol. Chem. *277*, 28038–28050.

Cutting, J. A., and Roth, T. F. (1973). Changes in specific sequestration of protein during transport into the developing oocyte of the chicken. Biochim. Biophys. Acta *298*, 951–955.

Dawes, C., and Simkiss, K. (1969). The acid-base status of the blood of the developing chick embryo. J. Exp. Biol. *50*, 79–86.

East, L., and Isacke, C. M. (2002). The mannose receptor family. Biochim. Biophys. Acta *1572*, 364–386.

Ellinger, I., Schwab, M., Stefanescu, A., Hunziker, W., and Fuchs, R. (1999). IgG transport across trophoblast-derived BeWo cells: a model system to study IgG transport in the placenta. Eur. J. Immunol. *29*, 733–744.

Ghetie, V., and Ward, E. S. (2002). Transcytosis and catabolism of antibody. Immunol. Res. *25*, 97–113.

Kim, J., Bronson, C. L., Hayton, W. L., Radmacher, M. D., Roopenian, D. C., Robinson, J. M., and Anderson, C. L. (2006). Albumin turnover: FcRn-mediated recycling saves as much albumin from degradation as the liver produces. Am. J. Physiol. Gastrointest. Liver Physiol. *290(2)*, G352–G360.

Koltun, M., Nikolovski, J., Strong, K., Nikolic-Paterson, D., and Comper, W. D. (2005). Mechanism of hypoalbuminemia in rodents. Am. J. Physiol. Heart Circ. Physiol. *288*, H1604–H1610.

Kowalczyk, K., Daiss, J., Halpern, J., and Roth, T. F. (1985). Quantitation of maternal-fetal IgG transport in the chicken. Immunology *54*, 755–762.

Larkin, J. M., Brown, M. S., Goldstein, J. L., and Anderson, R. G. (1983). Depletion of intracellular potassium arrests coated pit formation and receptor-mediated endocytosis in fibroblasts. Cell *33*, 273–285.

Leach, J. L., Sedmak, D. D., Osborne, J. M., Rahill, B., Lairmore, M. D., and Anderson, C. L. (1996). Isolation from human placenta of the IgG transporter, FcRn, and localization to the syncytiotrophoblast: implications for maternal-fetal antibody transport. J. Immunol. *157*, 3317–3322.

Lencer, W. I., and Blumberg, R. S. (2005). A passionate kiss, then run: exocytosis and recycling of IgG by FcRn. Trends Cell Biol. *15*, 5–9.

Linden, C. D., and Roth, T. F. (1978). IgG receptors on foetal chick yolk sac. J. Cell Sci. *33*, 317–328.

Martin, W. L., and Bjorkman, P. J. (1999). Characterization of the 2:1 complex between the class I MHC-related Fc receptor and its Fc ligand in solution. Biochemistry *38*, 12639–12647.

Martin, W. L., West, A. P., Jr., Gan, L., and Bjorkman, P. J. (2001). Crystal structure at 2.8 A of an FcRn/heterodimeric Fc complex: mechanism of pH-dependent binding. Mol. Cell *7*, 867–877.

Mayer, B., Kis, Z., Kajan, G., Frenyo, L. V., Hammarstrom, L., and Kacskovics, I. (2004). The neonatal Fc receptor (FcRn) is expressed in the bovine lung. Vet. Immunol. Immunopathol. *98*, 85–89.

Mayer, B., Zolnai, A., Frenyo, L. V., Jancsik, V., Szentirmay, Z., Hammarstrom, L., and Kacskovics, I. (2002). Redistribution of the sheep neonatal Fc receptor in the mammary gland around the time of parturition in ewes and its localization in the small intestine of neonatal lambs. Immunology *107*, 288–296.

McCarthy, K. M., Lam, M., Subramanian, L., Shakya, R., Wu, Z., Newton, E. E., and Simister, N. E. (2001). Effects of mutations in potential phosphorylation sites on transcytosis of FcRn. J. Cell Sci. *114*, 1591–1598.

McCarthy, K. M., Yoong, Y., and Simister, N. E. (2000). Bidirectional transcytosis of IgG by the rat neonatal Fc receptor expressed in a rat kidney cell line: a system to study protein transport across epithelia. J. Cell Sci. *113*(Pt 7), 1277–1285.

McGraw, T. E., and Subtil, A. (1999). Current Protocols in Cell Biology, John Wiley & Sons.

Ober, R. J., Martinez, C., Lai, X., Zhou, J., and Ward, E. S. (2004a). Exocytosis of IgG as mediated by the receptor, FcRn: an analysis at the single-molecule level. Proc. Natl. Acad. Sci. USA *101*, 11076–11081.

Ober, R. J., Martinez, C., Vaccaro, C., Zhou, J., and Ward, E. S. (2004b). Visualizing the site and dynamics of IgG salvage by the MHC class I-related receptor, FcRn. J. Immunol. *172*, 2021–2029.

Ou, S. K., Hwang, J. M., and Patterson, P. H. (1993). A modified method for obtaining large amounts of high titer polyclonal ascites fluid. J. Immunol. Methods *165*, 75–80.

Praetor, A., Ellinger, I., and Hunziker, W. (1999). Intracellular traffic of the MHC class I-like IgG Fc receptor, FcRn, expressed in epithelial MDCK cells. J. Cell Sci. *112*(Pt 14), 2291–2299.

Rivera-Calzada, A., Robertson, D., MacFadyen, J. R., Boskovic, J., Isacke, C. M., and Llorca, O. (2003). Three-dimensional interplay among the ligand-binding domains of the urokinase-plasminogen-activator-receptor-associated protein, Endo180. EMBO Rep. *4*, 807–812.

Simister, N. E., and Mostov, K. E. (1989). An Fc receptor structurally related to MHC class I antigens. Nature *337*, 184–187.

Simister, N. E., and Rees, A. R. (1985). Isolation and characterization of an Fc receptor from neonatal rat small intestine. Eur. J. Immunol. *15*, 733–738.

Spiekermann, G. M., Finn, P. W., Ward, E. S., Dumont, J., Dickinson, B. L., Blumberg, R. S., and Lencer, W. I. (2002). Receptor-mediated immunoglobulin G transport across mucosal barriers in adult life: functional expression of FcRn in the mammalian lung. J. Exp. Med. *196*, 303–310.

Tesar, D. B., Tiangco, N. E., and Bjorkman, P. J. (2006). Ligand valency affects transcytosis, recycling and intracellular trafficking mediated by the neonatal Fc receptor. Traffic *7*, 1127–1142.

Tressler, R. L., and Roth, T. F. (1987). IgG receptors on the embryonic chick yolk sac. J. Biol. Chem. *262*, 15406–15412.

Ward, E. S., Zhou, J., Ghetie, V., and Ober, R. J. (2003). Evidence to support the cellular mechanism involved in serum IgG homeostasis in humans. Int. Immunol. *15*, 187–195.

West, A. P., Jr., Herr, A. B., and Bjorkman, P. J. (2004). The chicken yolk sac IgY receptor, a functional equivalent of the mammalian MHC-related Fc receptor, is a phospholipase A2 receptor homolog. Immunity *20*, 601–610.

Western, A. H., Eckery, D. C., Demmer, J., Juengel, J. L., McNatty, K. P., and Fidler, A. E. (2003). Expression of the FcRn receptor (alpha and beta) gene homologues in the intestine of suckling brushtail possum (*Trichosurus vulpecula*) pouch young. Mol. Immunol. *39*, 707–717.

Wu, Z., and Simister, N. E. (2001). Tryptophan- and dileucine-based endocytosis signals in the neonatal Fc receptor. J. Biol. Chem. *276*, 5240–5247.

Yoshida, M., Claypool, S. M., Wagner, J. S., Mizoguchi, E., Mizoguchi, A., Roopenian, D. C., Lencer, W. I., and Blumberg, R. S. (2004). Human neonatal Fc receptor mediates transport of IgG into luminal secretions for delivery of antigens to mucosal dendritic cells. Immunity *20*, 769–783.

Zhu, X., Peng, J., Raychowdhury, R., Nakajima, A., Lencer, W. I., and Blumberg, R. S. (2002). The heavy chain of neonatal Fc receptor for IgG is sequestered in endoplasmic reticulum by forming oligomers in the absence of beta2-microglobulin association. Biochem. J. *367*, 703–714.

Chapter 4:

A Freeze Substitution Fixation-Based Gold Enlarging Technique for EM Studies of Endocytosed Nanogold-Labeled Molecules

In this paper we report the development of gold labeling and enhancement techniques for visualization of FcRn-mediated transcytosis in neonatal rat intestine. My contribution was developing the initial conditions for the chemical labeling of recombinant Fc proteins with commercially available 1.4 nm Nanogold clusters. This involved determining the proper conditions for gentle reduction of the hinge disulfides for reaction with mono-maleimido-1.4 nm gold clusters and subsequent purification of the reaction products.

Available online at www.sciencedirect.com
ScienceDirect
Journal of Structural Biology 160 (2007) 103–113
Journal of Structural Biology
www.elsevier.com/locate/yjsbi

A freeze substitution fixation-based gold enlarging technique for EM studies of endocytosed Nanogold-labeled molecules

Wanzhong He [a,1], Christine Kivork [a], Suman Machinani [a,2], Mary K. Morphew [b], Anna M. Gail [a,3], Devin B. Tesar [a], Noreen E. Tiangco [a], J. Richard McIntosh [b], Pamela J. Bjorkman [a,c,*]

[a] Division of Biology 114-96, California Institute of Technology, 1200 East California Boulevard, Pasadena, CA 91125, USA
[b] Boulder Laboratory for 3D Electron Microscopy of Cells, Department of Molecular, Cellular and Developmental Biology, University of Colorado, Boulder, CO 80309, USA
[c] Howard Hughes Medical Institute, California Institute of Technology, 1200 East California Boulevard, Pasadena, CA 91125, USA

Received 16 March 2007; received in revised form 5 July 2007; accepted 17 July 2007
Available online 25 July 2007

Abstract

We have developed methods to locate individual ligands that can be used for electron microscopy studies of dynamic events during endocytosis and subsequent intracellular trafficking. The methods are based on enlargement of 1.4 nm Nanogold attached to an endocytosed ligand. Nanogold, a small label that does not induce misdirection of ligand–receptor complexes, is ideal for labeling ligands endocytosed by live cells, but is too small to be routinely located in cells by electron microscopy. Traditional pre-embedding enhancement protocols to enlarge Nanogold are not compatible with high pressure freezing/freeze substitution fixation (HPF/FSF), the most accurate method to preserve ultrastructure and dynamic events during trafficking. We have developed an improved enhancement procedure for chemically fixed samples that reduced auto-nucleation, and a new pre-embedding gold enlarging technique for HPF/FSF samples that preserved contrast and ultrastructure and can be used for high-resolution tomography. We evaluated our methods using labeled Fc as a ligand for the neonatal Fc receptor. Attachment of Nanogold to Fc did not interfere with receptor binding or uptake, and gold-labeled Fc could be specifically enlarged to allow identification in 2D projections and in tomograms. These methods should be broadly applicable to many endocytosis and transcytosis studies.
© 2007 Elsevier Inc. All rights reserved.

Keywords: Electron microscopy; Endocytosis; Fc receptor; Freeze substitution fixation; Gold enhancement; High pressure freezing; IgG; Nanogold; Electron tomography; Transcytosis

1. Introduction

Electron microscopy (EM) of cells often requires the use of labeled proteins to identify particular intracellular compartments. For example, gold-labeled antibodies are used to label compartment-specific antigens by immuno-EM. For thick cells that require sectioning, such studies are usually limited to the visualization of antigen near the top and bottom surfaces of a section (e.g., Griffiths et al., 1984; Ladinsky et al., 2002). In studies of systems involving endocytosis, labeled ligands are found in all depths of the cell, thus labeling is not limited to the section surfaces. Recent

* Corresponding author. Address: Division of Biology 114-96, California Institute of Technology, 1200 East California Boulevard, Pasadena, CA 91125, USA. Fax: +1 626 792 3683.
E-mail address: bjorkman@caltech.edu (P.J. Bjorkman).
[1] Present address: Department of Biological Sciences, National University of Singapore, 14 Science Drive 4, Singapore 117543, Singapore.
[2] Present address: Student Affairs, David Geffen School of Medicine, Los Angeles, CA 90095-1722, USA.
[3] Present address: Molecular Metabolic Control A170, German Cancer Research Center Heidelberg, 69120 Heidelberg, Germany.

1047-8477/$ - see front matter © 2007 Elsevier Inc. All rights reserved.
doi:10.1016/j.jsb.2007.07.004

advances in EM tomography of cells allow cell sections to be investigated in 3D rather than with 2D projections, and methods for sample preparation that quickly immobilize all structures involved in dynamic trafficking events, such as rapid freezing, can generate a snapshot of complex cellular events (McIntosh et al., 2005). With high pressure freezing combined with freeze substitution fixation (HPF/FSF), one can obtain ice crystal-free freezing of cultured cells or small tissue samples (Sartori et al., 1993) and a fixation that preserves many aspects of cell ultrastructure (Kellenberger, 1991). Thus studies of intracellular trafficking of labeled ligands by EM tomography have the potential to accurately reveal the 3D itineraries of endocytosed molecules.

Various labeling methods have or could be used to label ligands for EM studies of endocytosis, including attachment of large, electron-dense labels such as colloidal gold (Harding et al., 1983; Murk et al., 2003), ferritin (Rodewald, 1973), or cadmium selenide quantum dots (Glepmans et al., 2005). Other methods involve attachment of labels that are visualized after photooxidation of diaminobenzidine (DAB) and metal deposition (e.g., peroxidase (Rodewald, 1980) and fluorescent labels for correlative light and electron microcopy (Deerinck et al., 1994; Gaietta et al., 2002)). None of these commonly used labels is well-suited for high-resolution studies of dynamic events in intracellular trafficking. For example, colloidal gold binds to its ligand non-specifically and non-covalently, binds multiple proteins at once, and tends to aggregate. Smaller colloidal gold particles (1–3 nm) are especially prone to aggregation, leading to large oligomeric gold-antibody structures (Hainfeld and Powell, 2000). The large diameter of ferritin (~14 nm) and its multimeric nature promote undefined ligand–ferritin stoichiometries and cross-linking, which can interfere with the proper trafficking of a ligand (Slade and Wild, 1971). Quantum dots, although promising for correlated fluorescent and electron microscopic studies (Glepmans et al., 2005), are often large ($\geqslant$10 nm) and most methods for attaching them to proteins of interest either lead to random attachment or, in the case of streptavidin quantum dots, require biotinylation of the ligand and can cause cross-linking resulting from binding to tetrameric streptavidin. Although the labels visualized after photooxidation and metal deposition are generally smaller than colloidal gold, ferritin or quantum dots, the stain that develops from these tags tends to be diffuse, reducing their resolution. Moreover, they are currently incompatible with HPF/FSF methods of sample preservation.

The ideal tracer for a study of endocytosis by electron tomography is a small compound that binds covalently to a ligand without blocking receptor binding, is non-toxic, and does not alter trafficking after being taken up by live cells through endocytosis. A tag with the potential to satisfy these requirements is 1.4 nm Nanogold, a gold cluster that can be conjugated covalently to macromolecules of interest (Hainfeld and Furuya, 1992). However, Nanogold is too small to see by EM in most cellular samples, so it must be enlarged after it has been internalized and the cells have been fixed. Methods to enhance Nanogold by deposition of silver or gold atoms on clusters in chemically fixed samples are available (Danscher, 1981; Hacker et al., 1988; Hainfeld and Furuya, 1995; Scopsi, 1989), but when we applied them to chemically fixed tissue samples containing an endocytosed 1.4 nm Nanogold–ligand, they resulted in high backgrounds due to auto-nucleation, and none of these techniques is compatible with HPF/FSF samples. Thus, there is a need for methods for enhancing small gold particles after either HPF/FSF or an optimized chemical fixation and before cells are embedded in plastic for microtomy.

Here we evaluated methods to enlarge 1.4 nm Nanogold clusters bound to IgG Fc, a ligand of the neonatal Fc receptor (FcRn). FcRn displays a binding affinity transition that is strongly pH-dependent, such that FcRn binds ligand at the acidic pH found in the gut and intracellular endosomes (pH $\leqslant$ 6.5) but not at the pH of blood (pH 7.4). This behavior is critical for FcRn's functions both in transporting maternal IgG across epithelial cell barriers, which provides immunity to offspring, and in rescuing serum IgG from degradation (Ghetie and Ward, 2000). We verified that Fc proteins covalently labeled with 1.4 nm Nanogold (Au–Fc) are appropriate ligands to follow FcRn trafficking inside cells by several tests. First, we demonstrated that Au–Fc retains pH-dependent binding to FcRn, is monodisperse, and is endocytosed normally into FcRn-expressing cells. We then used these tagged ligands to develop pre-embedding gold enlarging techniques that are compatible with chemical fixation or with HPF/FSF of tissue samples. Our chemical fixation enhancement method resulted in reduced auto-nucleation, and our HPF/FSF method extended a new FSF-based silver enhancement method (Morphew et al., in press) by using gold enhancement to gradually enlarge Nanogold and render it impervious to osmium compounds used during fixation. The resulting methods produced heavy metal labels that were large enough to be visible in 2D projections and tomograms but small enough to provide a spatial resolution that was about as good as EM tomography itself; thus we could reliably identify individual FcRn ligands inside intracellular vesicles in cells expressing FcRn. These methods should also be applicable to a wide range of EM tomography studies of endocytosis in other systems.

2. Methods

2.1. Preparation of 1.4 nm gold-labeled Fc (Au–Fc)

The Fc fragment from rat IgG2a was expressed in Chinese hamster ovary cells and purified as described (Martin and Bjorkman, 1999). Conditions to selectively reduce hinge disulfides were obtained by evaluating the results of different reduction protocols using Ellman's Reagent (Pierce Chemicals). 1.0–1.5 mg of Fc was reduced with 12–18 mg of mercaptoethylamine hydrochloride in 1 ml of 0.1 M $NaPO_4$, pH 6.0, 5 mM EDTA for 1.5 h at

37 °C, then passed over a Superdex 75 size exclusion column (Pharmacia) in 20 mM $NaPO_4$, pH 6.5, 150 mM NaCl, 1 mM EDTA.

After concentration, the reduced Fc was labeled with 1.4 nm monomaleimido Nanogold® (Nanoprobes, Inc.), which reacts specifically with reduced sulfhydryls (Hainfeld and Furuya, 1992), following the manufacturer's protocol for labeling IgG. Briefly, ~30 nmol of 1.4 nm monomaleimido Nanogold was suspended in 1 ml deionized water, then immediately incubated with the reduced Fc for 2–4 h at room temperature. Labeled Fc (Au–Fc) was separated from unlabeled Fc and free Nanogold by passage over the Superdex 75 gel filtration column. Labeled Fc was further purified by passage over an FcRn affinity column at pH 6, followed by elution at pH 8, as described (Huber et al., 1993). The molar concentrations of Nanogold and Fc were determined spectrophotometrically at 420 and 280 nm, respectively, using extinction coefficients of 155,000 $M^{-1}\,cm^{-1}$ for Nanogold and 60,900 $M^{-1}\,cm^{-1}$for Fc. The A_{280} for Fc was corrected for Nanogold absorption at 280 nm as described in the Nanoprobes protocol.

2.2. Au–Fc uptake in neonatal rats

11- to 13-day suckling rats born to Sprague–Dawley rats were separated from their mothers for ~3 h, then fed 3 × 100 μl (at 45–60 min intervals) of Au–Fc (~2 μM) in 20 mM $NaPO_4$, 1.2 mM $CaCl_2$, 0.5 mM $MgCl_2$, 0.25 mM $MgSO_4$, pH 6.0 at 37 °C. After 2–3 h, rats were anesthetized with CO_2, sacrificed, and the small intestine was removed by dissection. From each intestine, a 4–5 cm segment of proximal small intestine, starting ~2 cm from the pylorus, and a 4–5 cm segment of the distal small intestine (ileum), located ~2 cm from the ileocecal valve, were removed for chemical fixation or high pressure freezing. Within the proximal small intestine, the jejunum can be distinguished from the duodenum by the presence of the characteristic suspensory muscle of the duodenum (the ligament of Treitz).

2.3. Gold enhancement of chemically fixed intestinal samples

Small intestine segments were quickly cut into small pieces, then immediately fixed in 3% glutaraldehyde and 1% formaldehyde (Electron Microscopy Sciences) in 0.1 M sodium phosphate, pH 6.0, 2 mM $CaCl_2$, 1 mM $MgCl_2$, 0.5 mM $MgSO_4$ for 30 min at 20 °C. Fixation was continued for 3–4 h at 4 °C in the same buffer at pH 7.4, and then segments were rinsed with 0.1 M sodium phosphate, pH 7.4, before gold enhancing.

Initially, we used a gold enhancement kit, GoldEnhance-EM 2113 (Nanoprobes, Inc.), to enlarge Nanogold internalized by the cells in intestinal segments, but the solutions and protocol supplied by the manufacturer resulted in rapid enhancement (2–3 min) and substantial levels of auto-nucleation. Our modified protocol was as follows: samples were washed 3 × 5 min with PBS including glycine (20 mM sodium phosphate, pH 7.4, 150 mM NaCl, 50 mM glycine) to remove aldehydes, 3 × 5 min with PBS–BSA–Tween (PBS containing 1% BSA and 0.05% Tween 20), and then 3 × 5 min with 5 mM sodium phosphate, pH 5.5, 100 mM NaCl (Solution E). For gold enhancement, we placed 1–5 intestinal samples (~1 mm × ~1 mm) in a mixture of the manufacturer's Solutions A and B at a 2:1 ratio (~80 μl of A and ~40 μl of B). After 5 min, we added ~200 μl of Solution E with 20% gum arabic (Sigma–Aldrich) and then ~80 μl of Solution C. After 7–15 min of development, samples were transferred to 1–2% sodium thiosulfate to stop the enhancement. Samples were then washed 3 × 5 min with buffer E. This protocol resulted in slower development, reduced background and improved uniformity of enhanced particle size, especially when the enhancement was conducted at 4 °C rather than room temperature. In the absence of gum arabic, there were variations in the sizes of enlarged gold particles (Fig. 3b, left panel), perhaps resulting from differences in the time it took for the sodium thiosulfate stopping solution to reach different portions of the cell.

Gold-enhanced, chemically fixed samples were incubated in 1% OsO_4 in 0.1 M sodium phosphate, pH 6.1, for 60 min, and then rinsed with distilled H_2O prior to 1 h staining *en bloc* with 2% uranyl acetate. Samples were dehydrated with progressive lowering of temperature as described (Berryman and Rodewald, 1990; Gounon and Rolland, 1998) in a Leica EM AFS machine (Leica Microsystems).

2.4. HPF/FSF of intestinal samples

Intestinal samples were rapidly frozen with a BAL-TEC HPM 010 High Pressure Freezing Machine (Bal-Tec, AG). An intestinal segment was transferred into the 200 μm deep side of a 100 μm/200 μm specimen carrier that was ~2 mm in diameter (Engineering Office M. Wohlwend GmbH, Switzerland). The specimen chamber was filled with 1-hexadecene (Sigma–Aldrich) and then sandwiched against the flat side of a 300 μm specimen carrier. This sandwiched carrier was placed in the sample holder, then high pressure frozen at 2100 bar and transferred to liquid nitrogen for storage. The time interval between initial cutting of the sample and freezing was 30–40 s.

For conventional FSF of unenhanced samples, the specimen carriers with frozen samples were transferred to 1.5 ml microcentrifuge tubes (Fisher Scientific, USA) containing a frozen solution of acetone with 1% OsO_4 and 0.1% uranyl acetate under liquid nitrogen. Tubes were placed in a Leica EM AFS machine (Leica Microsystems) at −140 °C and gradually warmed to −90 °C in 4 h. The temperature was then gradually raised in 6 h transitions in the Leica AFS system as follows: −90 °C for 24–48 h, −60 °C for 24 h, and −30 °C for 18 h. After slowly warming to 0 °C over 2 h, samples were washed three times in pure acetone and warmed to room temperature.

2.5. Silver enhancement/gold-toning/gold enhancement during FSF of HPF samples

The FSF procedure described above was modified to include a pre-embedding gold enlarging technique for HPF cells by adapting approaches that involve silver or gold enhancement at room temperature (Danscher, 1981; Hacker et al., 1988; Hainfeld and Furuya, 1995; Scopsi, 1989), gold-toning (Sawada and Esaki, 2000), seed-mediated gold enlarging (Busbee et al., 2003; Daniel and Astruc, 2004; Gole and Murphy, 2004; Handley, 1989; Jana et al., 2001; Meltzer et al., 2001; Okitsu et al., 2005; Zou et al., 2006) and a FSF-based silver enhancement procedure (Morphew et al., in press). To avoid the background that results from spontaneous auto-nucleation, we designed a three-step enlarging protocol in which silver enhancement was used to slightly enlarge the Nanogold, the silver shell was coated by gold-toning to make it insoluble in osmium, and the particles were further enlarged to 10–16 nm using gold enhancement.

Samples were first added to a 1.2 ml solution of acetone including 0.5% glutaraldehyde and the temperature was raised from −140 to −60 °C as described above for the conventional FSF protocol. Samples were then washed with acetone at −60 °C (3 × 4 h each) to remove unreacted glutaraldehyde. An HQ or LI silver enhancing solution (Nanoprobes, Inc.) was prepared at 4 °C according to the manufacturer's instructions. Immediately after preparation, 20 μl of enhancing solution was quickly frozen by injection into liquid nitrogen. A silver enhancing mixture was prepared by adding 50 μl of saturated sodium citrate (0.1 g sodium citrate added to 10 ml of acetone at 4 °C) and 50 μl of saturated Na_2CO_3 (0.1 g Na_2CO_3 added to 10 ml of acetone at 4 °C) to 1 ml of saturated $AgNO_3$ (0.1 g $AgNO_3$ added to 10 ml of acetone–methanol solution (98%:2%) in a foil-covered tube) on dry ice, then adding the frozen drop of HQ or LI silver enhancing solution. After mixing in a foil-sealed tube, 1.2 ml of the silver enhancing mixture was added to the intestinal samples at −60 °C and incubated for 8–12 h.

After rinsing samples with acetone (3 × 2 h) at −60 °C, gold-toning was done by incubating the samples in 1.2 ml of a gold-toning mixture, 0.1% $HAuCl_4{\cdot}3H_2O$ (Sigma–Aldrich) in acetone–methanol (98%:2%), for 8–12 h at −60 °C. The gold enhancement procedure used a frozen 20 μl sample of a room temperature gold enhancement reagent, GoldEnhance-EM 2113 (Nanoprobes, Inc.), prepared by freezing 20 μl in liquid nitrogen as described for Silver LI and Silver HQ above. Saturated solutions of L-ascorbic acid (kept in the dark) and K_2CO_3 (Sigma–Aldrich) were prepared by adding 0.1 g of the relevant chemical to 10 ml acetone–methanol solution on ice. A fresh solution of saturated $NaBH_4$ (Sigma–Aldrich) was prepared similarly on dry ice in the dark. The gold enhancing mixture was prepared by adding the frozen drop of gold enhancement reagent plus 80 μl of the ascorbic acid solution, 50 μl of the K_2CO_3 solution, and 20–50 μl of $NaBH_4$ solution to 1 ml of 0.01–0.1% $HAuCl_4{\cdot}3H_2O$ in acetone–methanol (98%:2%) on dry ice. The gold enhancing mixture was applied to samples for 24 h at −60 °C. Samples were then rinsed with 1.2 ml acetone at the same temperature (3 × 4 h), and then 1.2 ml of 1% OsO_4 and 0.1% uranyl acetate in acetone was added to samples, followed by warming to −30 °C. Warming to room temperature was done as described above for unenhanced FSF samples.

Further optimization of the protocol might result in increased reliability and a decrease in the number of steps and/or reagents involved. For example, it might be possible to replace the silver enhancement step described above with the optimized protocol described in Morphew et al. (in press). However, the current protocol usually resulted in enlargement of 1.4 nm Nanogold while avoiding significant background auto-nucleation. If auto-nucleation did occur, it could usually be prevented by diluting the saturated reducing solution and/or reducing the development time in each of the three steps. To prevent nucleation due to deposition of silver or gold onto metal contaminants, we avoided any external sources of metal particles during the HPF/FSF and gold enlarging steps. Enlarged gold particles resulting from external seed particles were found on rare occasions, but these were larger and more irregular in shape than enhanced 1.4 nm Nanogold. A quantitative analysis of gold particles in >50 tomograms in HPF/FSF/enhanced intestinal cell samples revealed that ⩾98% of enlarged gold particles represented Au–Fc bound to FcRn (He et al., in preparation).

2.6. Embedding and electron microscopy

Chemically fixed or HPF/FSF intestinal samples were infiltrated, embedded, polymerized, sectioned and stained as previously described (He et al., 2003). Selected regions of 70–200 nm sections were examined using an FEI T12 G2 Electron Microscope operating at 120 kV, and projection images were recorded on a Gatan 894 2 K × 2 K CCD camera (Gatan Corporation). Tilt series (±70°, 1.0° angular increments) were digitally recorded at 6500× (pixel size = 1.57 nm) and at 700 nm underfocus about two orthogonal axes on the Gatan camera, using the microscope control program SerialEM as described (Mastronarde, 2005). Tomograms were computed for each tilt axis using the enlarged gold particles as markers for alignment, and then aligned to each other and combined using the IMOD software package (Kremer et al., 1996; Mastronarde, 1997).

Additional methods. Further information on methods and results related to studies in FcRn-expressing MDCK cell is available in Supplementary Information.

3. Results

3.1. Au–Fc retained pH-dependent binding to FcRn

To obtain a homogenous preparation of labeled Fc that retained binding to FcRn, we used a monomaleimido-derivatized 1.4 nm gold cluster to label reduced cysteines in the Fc hinge region, which can be selectively reduced without affecting intradomain disulfides (Williamson and Askonas, 1968). The hinge region is distant from the FcRn binding site, which is located at the interface between the Fc C_H2 and C_H3 domains (Martin et al., 2001) (Fig. 1a), thus increasing the likelihood that the labeled proteins will retain functional FcRn binding.

Our labeling protocol involved two sequential purification steps: first, size exclusion gel filtration to separate labeled Fc (Au–Fc) from unlabeled Fc and free Nanogold, and second, an FcRn affinity column (Huber et al., 1993) to ensure that the Au–Fc retained pH-dependent binding to FcRn. Results from size exclusion columns showed a shift in migration consistent with covalent attachment of Nanogold and no signs of Au–Fc aggregation (Fig. 1b). Nanogold/Fc ratios after FcRn affinity chromatography were typically 0.8–1.1, suggesting that most or all of the Fc molecules were labeled, consistent with SDS–PAGE analysis (Fig. 1c). Intact human IgG, however, demonstrated poor labeling efficiency when subjected to the same labeling protocol (data not shown). Since intact IgG and Fc bind with similar affinities and pH-dependent binding profiles to rat FcRn (Vaughn and Bjorkman, 1997), we used the more efficiently labeled Au–Fc, rather than Au–IgG, as a ligand for FcRn in subsequent experiments.

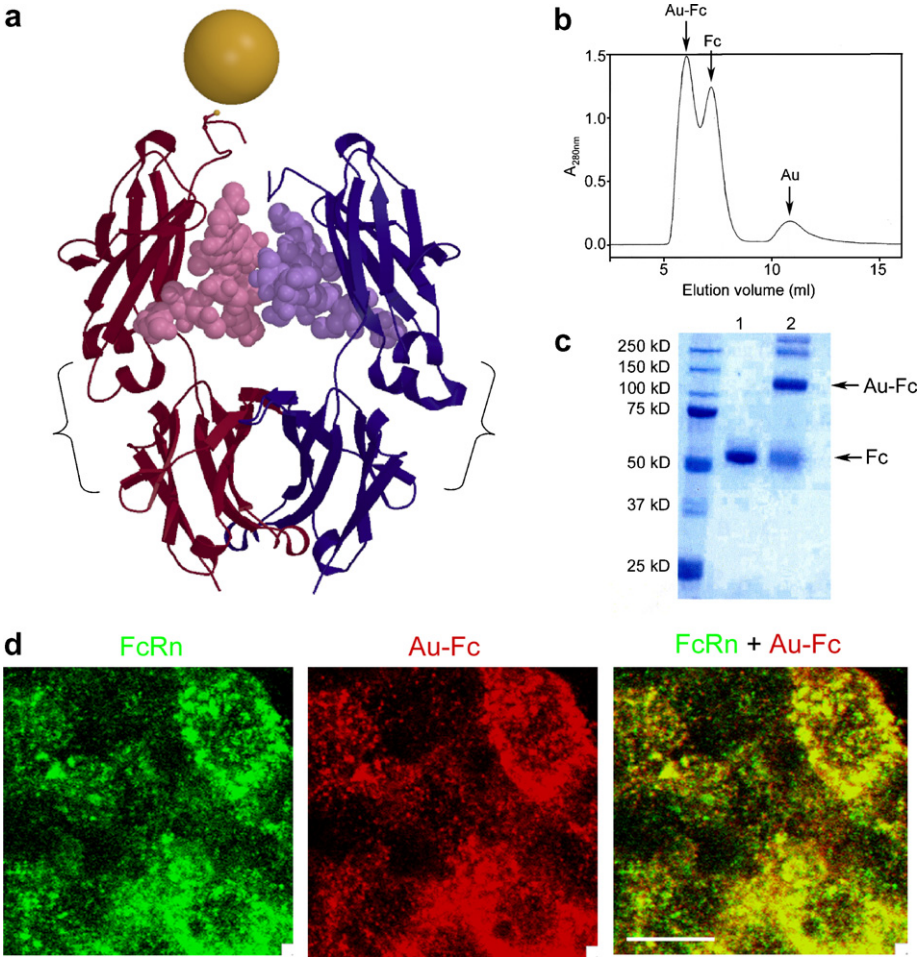

Fig. 1. Preparation of Au–Fc. (a) Ribbon diagram of the structure of Fc (pdb code 1I1c) with a gold sphere (drawn to scale) representing a 1.4 nm monomaleimido Nanogold covalently attached to a reduced cysteine in the Fc hinge region. One Nanogold is depicted, based on the calculated Nanogold/Fc ratios obtained in most labeling reactions (0.8–1.1). The Nanogold cluster bound in a region that is distant from the FcRn binding site (indicated on each Fc chain with a bracket). (b) S75 Superdex gel filtration profile following incubation of reduced Fc with 1.4 nm Nanogold. (c) SDS–PAGE analysis (10% acrylamide gel) of non-reduced and unboiled unlabeled Fc (lane 1) and Au–Fc (lane 2). The majority of Fc protein migrated at a higher apparent molecular weight in the Au–Fc sample, demonstrating covalent attachment of 1.4 nm Nanogold. (d) Confocal images (~5 μm below the apical surface) of FcRn-expressing MDCK cells after Au–Fc uptake (bar = 10 μm). Filter-grown monolayers were incubated with ~1 μM Au–Fc for 1 h at pH 6 and processed for immunofluorescence using antibodies against FcRn (green; left panel) and Fc (red; middle panel) as described in the Supplementary Methods. The merged image (right panel) shows regions of colocalization as yellow. The nearly equimolar ratio of gold to protein in our Au–Fc samples (see Section 2) suggested that most or all of the Fc detected by immunofluorescence contained gold. Untransfected MDCK cells showed only background levels of fluorescence when subjected to the same incubation and staining protocols (data not shown).

We used confocal microscopy to study an MDCK cell line that expresses rat FcRn and had previously been shown to bind, internalize, and bidirectionally transcytose rat IgG and Fc (Tesar et al., 2006). Our results showed that Au–Fc was bound by and endocytosed normally into these polarized cells by FcRn (Fig. 1d and Supplementary Methods). Examination of these cells by EM, however, showed that 1.4 nm Nanogold was too small to be routinely localized in cells with 2D projections or tomograms (Supplementary Figure 1 and Supplementary Information).

3.2. Specific enhancement of endocytosed 1.4 nm Au–Fc in chemically fixed intestinal cells

To facilitate locating 1.4 nm Au–Fc inside cells, we used gold enhancement to deposit gold atoms specifically on the 1.4 nm Nanogold, thereby enlarging the particles to 10–20 nm. These experiments were done using intestinal samples from neonatal rats that had been fed Au–Fc. The concentration of Au–Fc that was fed to neonatal rats was 2–3 μM, approximately equal to the IgG concentration in rat milk, because higher concentrations saturate FcRn, resulting in degradation of excess IgG (Benlounes et al., 1995). In this system for Au–Fc uptake, we had two controls for the specificity of uptake and gold enhancement: first, the presence or absence of ingested Au–Fc, and second, the requirement that enhanced gold particles should appear in physiologically relevant locations in cells; e.g., in locations corresponding to FcRn expression (apical cell surface, coated vesicles and tubulovesicular compartments) in samples from the proximal small intestine, and inside degradative compartments (e.g., giant lysosomes) in samples from the neonatal distal small intestine (ileum), which does not express FcRn (Rodewald, 1973).

Our original attempts to enhance chemically fixed tissues resulted in significant background color development, which came from auto-nucleation in both the Au–Fc-fed intestinal sample and the control sample (Fig. 2a and c). We therefore modified the enhancement protocol to slow the development speed and to increase the development time, resulting in specific enhancement such that the control intestinal sample did not show significant color development, and the Au–Fc-fed sample retained color development (Fig. 2b). EM images confirmed specific enhancement in that enhanced gold particles were found in giant lysosomes within samples derived from the neonatal ileum of Au–Fc-fed rats but not in neighboring goblet cells of the same sample (Fig. 3a). These results are consistent with the function of neonatal ileal cells in fluid phase uptake and degradation, and the secretory, rather than uptake, function of goblet cells (Rodewald, 1973). As another demonstration of specific enhancement, we found enhanced gold particles at the apical cell surface and inside tubular intracellular vesicles in the proximal small intestine (Fig. 3b), consistent with FcRn-mediated uptake in this region. In the distal small intestine, the majority of gold particles were in large lysosomes (Fig. 3a), consistent with fluid phase uptake in the distal small intestine, which does not express FcRn (Rodewald, 1973). In both proximal and distal intestinal samples, we did not see enhanced gold particles in organelles such as the mitochondria or the nucleus (data not shown), indicating that the enlarged gold particles corresponded to specifically enhanced Au–Fc that had been endocytosed into intracellular vesicles.

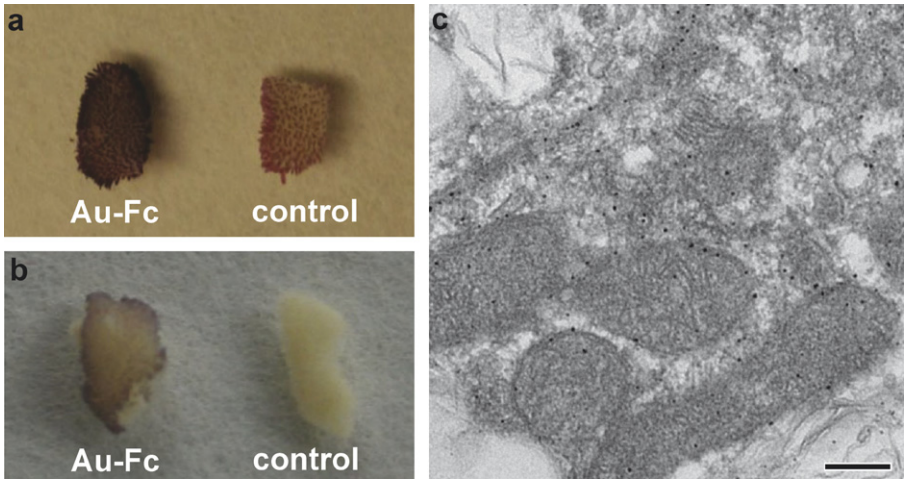

Fig. 2. Gold-enhanced, chemically fixed intestinal segments. Thirteen-day-old neonatal rats were fed ~2 μM Au–Fc or a control solution not containing Au–Fc prior to extraction, fixation and gold enhancement of duodenal samples. (a) Gold enhancement using GoldEnhance-EM 2113 (Nanoprobes, Inc.) following the manufacturer's protocol. (b) Gold enhancement using a modified protocol (Section 2; Methods). The control sample derived using the modified protocol showed a significant decrease of background color development, which resulted from auto-nucleation, compared with the control sample prepared using the original protocol. (c) Projection EM image derived from a 120 nm section of the control sample shown in Panel a (bar = 200 nm). Randomly distributed 5–10 nm background gold particles were found in mitochondria and regions of the cell that did not engage in FcRn-mediated endocytosis.

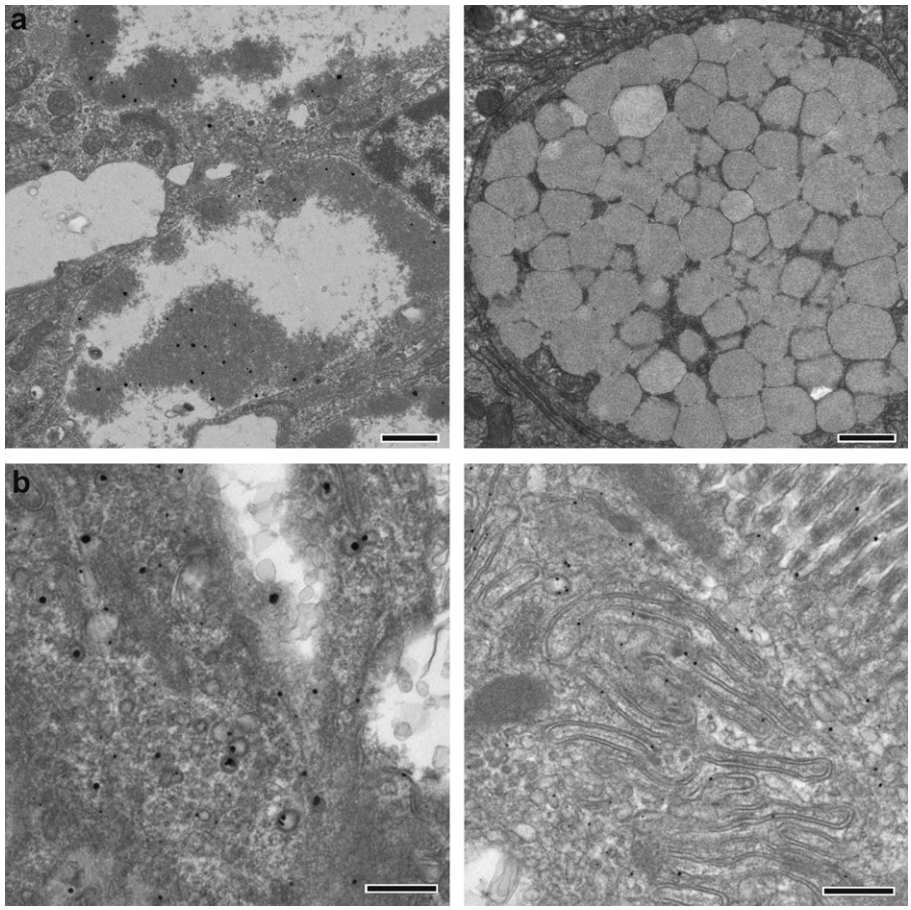

Fig. 3. Chemically fixed, gold-enhanced samples of intestinal segments prepared using the modified enhancing protocol. (a) Specificity of gold enhancement in 70 nm sections derived from the distal small intestine (bar = 1000 nm). A region of the ileum (left) showed enhanced gold particles in giant lysosomes, consistent with fluid phase uptake of Au–Fc. By contrast, gold particles were not found in secretion vesicles in an adjacent goblet cell (right), demonstrating a lack of background resulting from auto-nucleation events. (b) Specificity of Au–Fc uptake and gold enhancement in sections derived from the proximal small intestine (bar = 500 nm). The section on the right was derived from the enhanced segment shown in Fig. 2b. Gold particles were located in coated vesicles near the basolateral region of the cell (left; section thickness = 200 nm), on the surface of microvilli, in coated vesicles, and in the extracellular space near the apical surface of a cell (right; section thickness = 150 nm). The section on the left was gold-enhanced in the absence of added gum arabic, resulting in specific enhancement of 1.4 nm Au–Fc, but a non-uniform particle size. The addition of gum arabic to the section on the right resulted in a more uniform (~20 nm) size of enhanced gold particle.

3.3. A new method to enlarge 1.4 nm gold clusters in HPF/FSF samples

Having used chemically fixed neonatal intestinal samples to confirm that Au–Fc is taken up through fluid phase endocytosis in the distal small intestine and an FcRn-mediated pathway in the proximal small intestine, we next worked out a method to enlarge Au–Fc in HPF/FSF samples. Of critical importance for our efforts was the recent development of a silver enhancement method compatible with FSF, the first demonstration that enlargement of Nanogold is possible in organic solvents at low temperature (Morphew et al., in press). In this method, Nanogold particles were enlarged to 3–8 nm in tissue samples using a mixture of silver nitrate, hydroquinone, sodium citrate and sucrose in cold acetone. The resulting particles could be seen in tomograms, but were not large enough to be visualized in 2D projections (Morphew et al., in press). In addition, a general limitation of silver enhancement methods is that osmium compounds, which improve the preservation of membranes, cannot be added during fixation because they dissolve the layer of added silver (Hainfeld et al., 1999). To address both of these issues, we combined silver enhancement during FSF with gold-toning and gold enhancement to increase the size of the enlarged particles and render them impervious to osmium compounds used during fixation.

Silver-enhanced/gold-toned/gold-enhanced HPF/FSF duodenal samples showed that the Nanogold was enlarged to 10–16 nm and was easily visible in both projection images (Fig. 4) and tomograms (Fig. 5). The ability to directly visualize enlarged gold particles in projection images allows one to choose a region containing Au–Fc for subsequent tomography, and a tilt series can be recorded at a magnification (e.g., 6500×) that enables the reconstruction of a reasonably large portion of the cell.

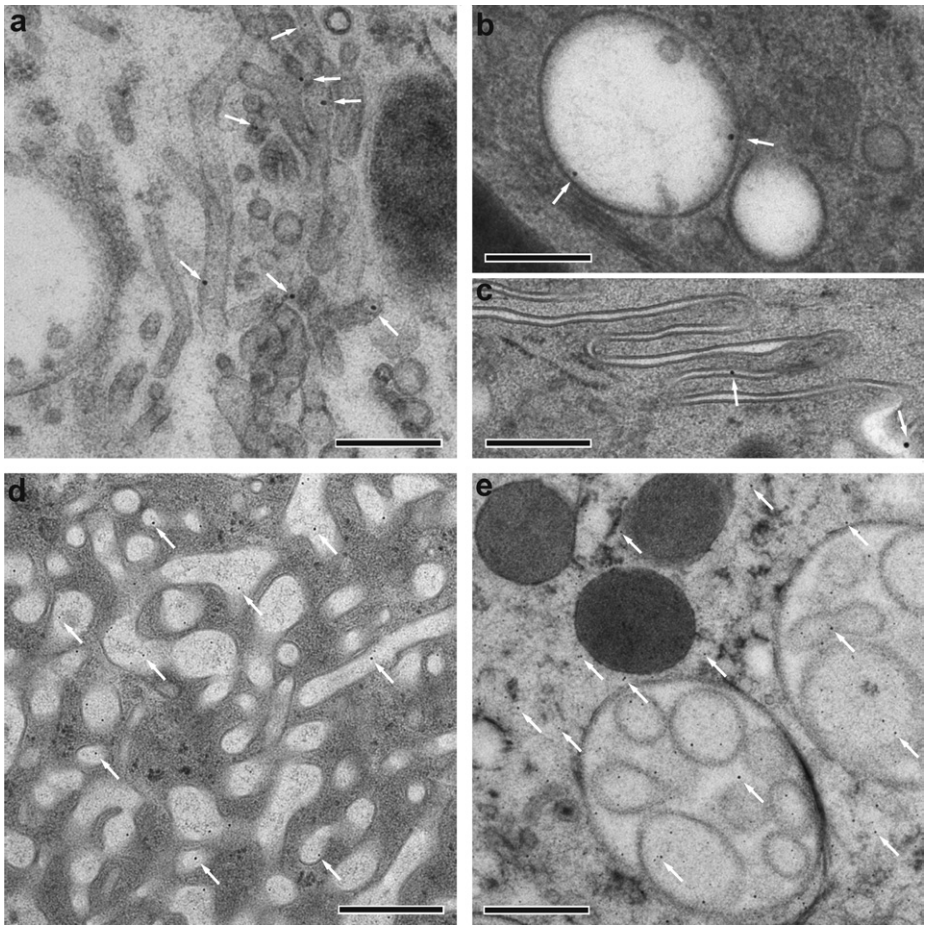

Fig. 4. Projection images of HPF/FSF samples of intestinal samples after silver enhancement/gold-toning/gold enhancement of 1.4 nm Au–Fc. (a) Section (150 nm) from the neonatal jejunum showing gold particles attached to inner surfaces of tubular vesicles, consistent with Au–Fc bound to FcRn (bar = 300 nm). (b) Section (150 nm) from the neonatal duodenum showing gold particles attached to the inner surface of a multivesicular body (bar = 300 nm). (c) Seventy nanometers section from the neonatal duodenum showing gold particles after release into the extracellular space from the basolateral membrane (bar = 500 nm). (d) Section (120 nm) from the neonatal ileum showing enlarged gold particles distributed only inside apical vesicles (bar = 500 nm). (e) Section (120 nm) from the neonatal jejunum showing auto-nucleation resulting in small (~5 nm) background gold particles distributed randomly inside and outside of vesicles (bar = 500 nm). Auto-nucleation in this case might have resulted from over-exposure to $NaBH_4$ and/or too long of a developing time.

Our enhancement protocol was compatible with the use of OsO_4 and uranyl acetate, thereby preserving contrast and details of the ultrastructure. Both projections (Fig. 4) and digital slices from tomograms (Fig. 5) showed high contrast and smooth membranes in both vesicles and cells, thus the gold enlarging procedure did not reduce the high-resolution possible with HPF/FSF. The enlarged gold particles were in locations suggesting they represented enhanced 1.4 nm Nanogold attached to Fc that was bound to FcRn: near the inner membrane leaflets of tubular vesicles (Figs. 4a and 5) and multivesicular bodies (Fig. 4b), and in the extracellular space near the basolateral surface (Figs. 4c and 5d). Notably, the majority of enhanced Au–Fc particles in duodenal samples were found within a 6–7 nm distance from a membrane, implying attachment to FcRn, which has a ~5 nm ectodomain (Burmeister et al., 1994). In the ileum, we again saw enhanced gold particles inside degradative vesicles (Fig. 4d), consistent with fluid phase uptake in this region of the neonatal intestine. The specificity of gold enlargement is demonstrated by comparing Fig. 4a–d with Fig. 4e, an example of non-specific enhancement in an HPF/FSF sample that was reduced too harshly and/or developed for too long. Such problems can usually be avoided by diluting the saturated reducing chemicals and/or reducing the developing times for the three steps in the enhancement procedure.

4. Discussion

Here we have demonstrated that a 1.4 nm gold-labeled Fc is a reliable tag for EM studies of receptor-mediated endocytosis and transport by FcRn. A monomaleimido-derivatized Nanogold was attached to Fc without affecting FcRn binding or uptake into cells. Although the small size of 1.4 nm Nanogold makes it ideal for preserving the proper binding and function of a labeled ligand, these clusters were not large enough to be located directly in EM projection images and in most tomograms derived from

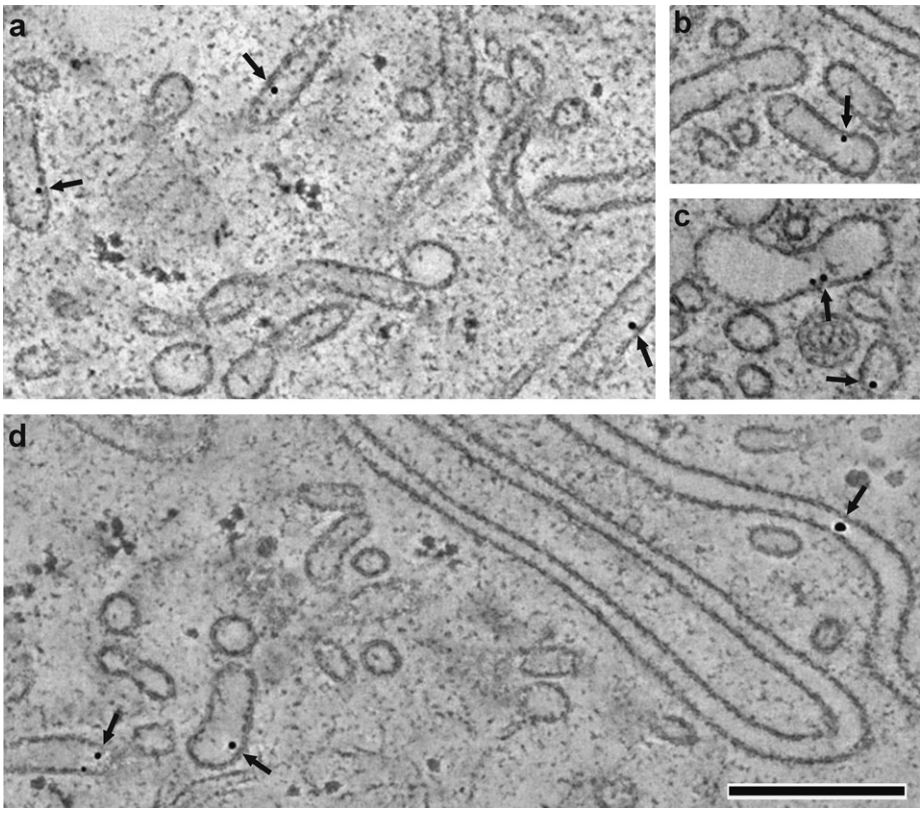

Fig. 5. Digital slices (1.6 nm) derived from tomograms of HPF/FSF samples of jejunal samples after silver enhancement/gold-toning/gold enhancement of 1.4 nm Au–Fc (bar = 300 nm). Dual axis tilt series were recorded at 6500× from 180 nm sections at 120 kV on a Tecnai T12 microscope. Panels (a–d) show enhanced gold particles near the membranes of tubular and spherical vesicles. Panel (d) shows enhanced Au–Fc that was released into the lateral intercellular space between adjacent intestinal cells.

stained cell sections. We therefore adapted auto-metallography and nanoparticle seeding techniques that are used to enlarge 1.4 nm Nanogold clusters by selectively depositing silver and/or gold atoms onto their surfaces (Busbee et al., 2003; Daniel and Astruc, 2004; Gole and Murphy, 2004; Hainfeld and Furuya, 1995; Hainfeld et al., 1999; Jana et al., 2001; Meltzer et al., 2001; Okitsu et al., 2005; Zou et al., 2006).

We initially concentrated on gold enhancement of neonatal rat intestinal samples that had been chemically fixed in order to quickly screen for specific Au–Fc uptake. Based on previous studies of IgG transport in the neonatal rat intestine (Rodewald, 1973), we expected to see FcRn-mediated uptake in the proximal small intestine and fluid phase uptake in the distal small intestine of a rat that has been fed Au–Fc. However, our first attempts using published gold enhancing protocols resulted in non-specific background deposition in both types of sample. The modifications described here reduced non-specific background in gold-enhanced chemically fixed samples, and showed images confirming specific enhancement in the different regions of the intestine. The reduction of auto-nucleation and improved control over development with our method should benefit other pre-embedding enhancement efforts involving chemically fixed tissue samples.

Having demonstrated that Au–Fc is a reliable marker for receptor-mediated and fluid phase endocytosis following chemically fixation, we next undertook to enlarge Nanogold in tissue samples prepared by HPF/FSF methods, which is preferable to chemical fixation for studies of dynamic events during intracellular trafficking (McIntosh et al., 2005). Expanding upon a previously described FSF-based method involving silver enhancement (Morphew et al., in press), we developed a new gold enlarging method for HPF/FSF samples that combines gold-toning and gold enhancement, following an initial silver enhancement step. Including gold enhancement in our method offers two potential advances: First, unlike silver, gold is not dissolved by osmium tetroxide (Hainfeld et al., 1999), a commonly used fixative in EM applications that results in optimal contrast of membrane structures. Second, by using gold enhancement following silver enhancement, we could enlarge the Nanogold clusters to 10–16 nm, which allows for direct visualization of particles in 2D projections prior to the selection of a region for tomography. By contrast, it was not possible to visualize enhanced particles in 2D projections using silver enhancement alone because the particles were enlarged to $\leqslant$8 nm (Morphew et al., in press). In principle, the gold-toning and gold enhancement steps could be used without a prior silver enhancement step in a HPF/FSF gold enlarging procedure. However, we

obtained optimal results (less auto-nucleation and a greater uniformity in particle size) by combining the silver enhancement step with gold-toning and gold enhancement. When auto-nucleation did occur, we could distinguish auto-nucleated particles from enhanced 1.4 nm Nanogold in EM images because the former were smaller and randomly distributed as compared with the latter.

We conclude that the combination of thiol-specific Nanogold labeling to obtain a minimally perturbed ligand with subsequent gold-enlargement allows the use of high-resolution electron tomography to accurately trace receptor–ligand complexes during endocytosis and intracellular trafficking.

Acknowledgments

We thank D.N. Mastronarde for advice on setting up SerialEM on the Caltech microscopes, E.T. O'Toole (University of Colorado) for help with IMOD, R.D. Powell (Nanoprobes, Inc.) for advice on gold enhancement, C.J. Ackerson and R.D. Kornberg (Stanford University) for preparing MPC gold bound to Fc for testing, and G.J. Jensen and W.F. Tivol (Caltech) for the use of the T12 microscope. This work was supported by the National Institutes of Health (2 R37 AI041239-06A1 to P.J.B.; RR000592 to J.R.M.) and gifts to Caltech to support electron microscopy from the Gordon and Betty Moore Foundation and the Agouron Institute.

Author contributions: W.H. designed and implemented the HPF/FSF and chemical fixation gold enlarging methods, administered Au–Fc to rats, prepared tissue samples and performed the corresponding EM experiments. M.K.M. and J.R.M. developed the original concepts for FSF-based silver enhancement. C.K., S.M., A.M.G., D.B.T. and N.E.T. prepared Au–Fc conjugates. D.B.T. and N.E.T. did the confocal microscopy in FcRn-MDCK cells. M.K.M. and P.J.B. did the EM studies in MDCK cells at the Boulder Laboratory for 3D EM of Cells. P.J.B. supervised and planned the project. P.J.B., W.H. and J.R.M. jointly wrote the manuscript.

Appendix A. Supplementary data

Supplementary data associated with this article can be found, in the online version, at doi:10.1016/j.jsb.2007.07.004.

References

Benlounes, N., Chedid, R., Thuillier, F., Desjeux, J.F., Rousselet, F., Heyman, M., 1995. Intestinal transport and processing of immunoglobulin G in the neonatal and adult rat. Biol. Neonate 67, 254–263.

Berryman, M.A., Rodewald, R.D., 1990. An enhanced method for post-embedding immunocytochemical staining which preserves cell membranes. J. Histochem. Cytochem. 38, 159–170.

Burmeister, W.P., Gastinel, L.N., Simister, N.E., Blum, M.L., Bjorkman, P.J., 1994. Crystal structure at 2.2 Å resolution of the MHC-related neonatal Fc receptor. Nature 372, 336–343.

Busbee, B.D., Obare, S.O., Murphy, C.J., 2003. An improved synthesis of high-aspect-ratio gold nanorods. Adv. Mater. 15, 414–416.

Daniel, M.C., Astruc, D., 2004. Gold nanoparticles: assembly, supramolecular chemistry, quantum-size-related properties, and applications toward biology, catalysis, and nanotechnology. Chem. Rev. 104, 293–346.

Danscher, G., 1981. Histochemical demonstration of heavy metals. A revised version of the sulphide silver method suitable for both light and electron microscopy. Histochemistry 71, 1–16.

Deerinck, T.J., Martone, M.E., Lev-Ram, V., Green, D.P.L., Tsien, R.Y., Spector, D.L., Huang, S., Ellisman, M.H., 1994. Fluorescence photooxidation with eosin: a method for high resolution immunolocalization and in situ hybridization detection for light and electron microscopy. J. Cell Biol. 126, 901–910.

Gaietta, G., Deerinck, T.J., Adams, S.R., Bouwer, J., Tour, O., Laird, D.W., Sosinsky, G.E., Tsien, R.Y., Ellisman, M.H., 2002. Multicolor and electron microscopic imaging of connexin trafficking. Science 296, 503–507.

Ghetie, V., Ward, E.S., 2000. Multiple roles for the major histocompatibility complex class I-related FcRn. Annu. Rev. Immunol. 18, 739–766.

Glepmans, B.N.G., Deerinck, T.J., Smarr, B.L., Jones, Y.Z., Ellisman, M.H., 2005. Correlated light and electron microscopic imaging of multiple endogenous proteins using Quantum dots. Nat. Methods 2, 743–749.

Gole, A., Murphy, C.J., 2004. Seed-mediated synthesis of gold nanorods: role of the size and nature of the seed. Chem. Mater. 16, 3633–3640.

Gounon, P., Rolland, J.P., 1998. Modification of unicryl composition for rapid polymerization at low temperature without alteration of immunocytochemical sensitivity. Micron 29, 293–296.

Griffiths, G., McDowall, A., Back, R., Dubochet, J., 1984. On the preparation of cryosections for immunocytochemistry. J. Ultrastruct. Res. 89, 65–78.

Hacker, G.W., Grimelius, L., Danscher, G., Bernatzky, G., Muss, W., Adam, H., Thurner, J., 1988. Silver acetate autometallography—an alternative enhancement technique for immunogold-silver staining (IGSS) and silver amplification of gold, silver, mercury and zinc in tissues. J. Histotechnol. 11, 213–221.

Hainfeld, J.F., Furuya, F.R., 1992. A 1.4-nm gold cluster covalently attached to antibodies improves immunolabeling. J. Histochem. Cytochem. 40, 177–184.

Hainfeld, J.F., Furuya, F.R., 1995. Silver-enhancement of Nanogold and undecagold. In: Hayat, M.A. (Ed.), Immunogold-silver Staining: Principles, Methods and Applications. CRC Press, Boca Raton, FL, pp. 71–96.

Hainfeld, J.F., Powell, R.D., 2000. New frontiers in gold labeling. J. Histochem. Cytochem. 48, 471–480.

Hainfeld, J.F., Powell, R.D., Stein, J.K., Hacker, G.W., Hauser-Kronberger, C., Cheung, A.L.M., Schofer, C., 1999. Gold-based autometallography. In: Bailey, G.W., Jerome, W.G., McKernan, S., Mansfield, J.F., Price, R.L. (Eds.), Proc. 57th Ann. Mtg, Micros. Soc., Amer., Springer-Verlag, New York, NY, pp. 486–487.

Handley, D.A., 1989. Methods for synthesis of colloidal gold. In: Hayat, M.A. (Ed.), Colloidal Gold: Principles, Methods, and Applications. Academic Press, San Diego, pp. 13–30.

Harding, C., Heuser, J., Stahl, P., 1983. Receptor-mediated endocytosis of transferrin and recycling of the transferrin receptor in rat reticulocytes. J. Cell Biol. 97, 329–339.

He, W., Cowin, P., Stokes, D.L., 2003. Untangling desmosomal knots with electron tomography. Science 302, 109–113.

He, W., Jensen, G.J., McIntosh, J.R., Bjorkman, P.J., submitted for publication. Three-dimensional itinerary of FcRn-mediated antibody transport across epithelial cells revealed by electron tomography.

Huber, A.H., Kelley, R.F., Gastinel, L.N., Bjorkman, P.J., 1993. Crystallization and stoichiometry of binding of a complex between a rat intestinal Fc receptor and Fc. J. Mol. Biol. 230, 1077–1083.

Jana, N.R., Gearheart, L., Murphy, C.J., 2001. Evidence for seed-mediated nucleation in the chemical reduction of gold salts to gold nanoparticles. Chem. Mater. 13, 2313–2322.

Kellenberger, E., 1991. The potential of cryofixation and freeze substitution: observations and theoretical considerations. J. Microsc. 161, 183–203.

Kremer, J.R., Mastronarde, D.N., McIntosh, J.R., 1996. Computer visualization of three-dimensional data using IMOD. J. Struct. Biol. 116, 71–76.

Ladinsky, M.S., Wu, C.C., McIntosh, S., McIntosh, J.R., Howell, K.E., 2002. Structure of the Golgi and distribution of reporter molecules at 20 degrees C reveals the complexity of the exit compartments. Mol. Biol. Cell 13, 2810–2825.

Martin, W.L., Bjorkman, P.J., 1999. Characterization of the 2:1 complex between the class I MHC-related Fc receptor and its Fc ligand in solution. Biochemistry 38, 12639–12647.

Martin, W.L., West, A.P., Gan, L., Bjorkman, P.J., 2001. Crystal structure at 2. 8 Å of an FcRn/heterodimeric Fc complex: mechanism of pH dependent binding. Mol. Cell 7, 867–877.

Mastronarde, D.N., 1997. Dual-axis tomography: an approach with alignment methods that preserve resolution. J. Struct. Biol. 120, 343–352.

Mastronarde, D.N., 2005. Automated electron microscope tomography using robust prediction of specimen movements. J. Struct. Biol. 152, 36–51.

McIntosh, J.R., Nicastro, D., Mastronarde, D.N., 2005. New views of cells in 3D: an introduction to electron tomography. Trends Cell Biol. 15, 43–51.

Meltzer, S., Resch, R., Koel, B.E., Thompson, M.E., Madhukar, A., Requicha, A.A.G., Will, P., 2001. Fabrication of nanostructures by hydroxylamine seeding of gold nanoparticle templates. Langmuir 17, 1713–1718.

Morphew, M., He, W., Bjorkman, P.J., McIntosh, J.R, in press. Silver enhancement of nanogold particles during freeze substitution fixation for electron microscopy. J. Microsc.

Murk, J.L.A.N., Humbel, B.M., Ziese, U., Griffith, J.M., Posthuma, G., Slot, J.W., Koster, A.J., Verkleij, A.J., Geuze, H.J., 2003. Endosomal compartmentalization in three dimensions: implications for membrane fusion. Proc. Natl. Acad. Sci. USA 100, 13332–13337.

Okitsu, K., Teo, B.M., Ashokkumar, M., Grieser, F., 2005. Controlled growth of sonochemically synthesized gold seed particles in aqueous solutions containing surfactants. Aust. J. Chem. 58, 667–670.

Rodewald, R., 1973. Intestinal transport of antibodies in the newborn rat. J. Cell Biol. 58, 189–211.

Rodewald, R., 1980. Distribution of immunoglobulin G receptors in the small intestine of the young rat. J. Cell Biol. 85, 18–32.

Sartori, N., Richter, K., Dubochet, J., 1993. Vitrification depth can be increased more than 10-fold by high-pressure freezing. J. Microsc. 172, 55–61.

Sawada, H., Esaki, M., 2000. A practical technique to postfix nanogold-immunolabeled specimens with osmium and to embed them in Epon for electron microscopy. J. Histochem. Cytochem. 48, 493–498.

Scopsi, L., 1989. Silver-enhanced colloidal gold method. In: Hayat, M.A. (Ed.), Colloidal Gold: Principles, Methods, and Applications. Academic Press, San Diego, pp. 252–288.

Slade, B.S., Wild, A.E., 1971. Transmission of human gamma-globulin to rabbit foetus and its inhibition by conjugation with ferritin. Immunology 20, 217–223.

Tesar, D.B., Tiangco, N.E., Bjorkman, P.J., 2006. Ligand valency affects FcRn-mediated transcytosis, recycling, and intracellular trafficking. Traffic 7, 1–16.

Vaughn, D.E., Bjorkman, P.J., 1997. High-affinity binding of the neonatal Fc receptor to its IgG ligand requires receptor immobilization. Biochemistry 36, 9374–9380.

Williamson, A.R., Askonas, B.A., 1968. Differential reduction of interchain disulphide bonds of mouse immunoglobulin G. Biochem. J. 107, 823–828.

Zou, X., Ying, E., Dong, S., 2006. Seed-mediated synthesis of branched gold nanoparticles with the assistance of citrate and their surface-enhanced Raman scattering properties. Nanotechnology 17, 4758–4764.

Chapter 5:

Investigation of FcRn Exocytosis by Total Internal Reflection Fluorescence Microscopy

This chapter describes work done as part of a collaboration with Sandy Simon's laboratory at The Rockefeller University in New York, New York. The goal of these studies was to visualize FcRn exocytosis at the plasma membrane and to determine if exocytosing FcRn-positive vesicles remain partially clathrin-coated during the process. I traveled to Dr. Simons laboratory and performed the experiments described here.

Introduction

The ability to sense and respond to environmental factors is one of the fundamental characteristics of living things. These external factors can be in the form of small molecules, macromolecules (proteins and nucleic acids), or even other cells or organisms. The important feature of such interactions between cells and their external environment is that they lead to chemical or structural changes through receptors or molecules at the cell surface that can in turn alter downstream molecules to give rise to larger-scale changes in protein and/or cellular structure and/or function. The events that comprise such a process are often spatially localized within a small region of the cell, such as the plasma membrane or within an individual trafficking endosome. Until recently, high-resolution techniques for the examination of cell-surface structures were limited to electron microscopy, which produces high resolution data but does not allow the visualization of dynamic processes in living cells, and confocal microscopy, which allows live cell visualization but lacks the resolution necessary to effectively study individual events occurring at the level of the plasma membrane.

Recent electron tomography studies of the transcytosis of gold-labeled Fc (Au-Fc) molecules by FcRn in the neonatal rat gut performed in our laboratory provided insights into the structure and distribution of trafficking endosomes and vesicles containing FcRn-ligand complexes (He, et al., 2008). One particularly surprising result was the presence of clathrin-coated vesicles that had fused with the lateral membrane and contained Au-Fc. Because the slightly basic pH and low concentration of Au-Fc in the lateral intracellular space (LIS)

should not be permissive for binding of Au-Fc to FcRn, it was hypothesized that these structures represented a glimpse of clathrin-mediated exocytosis. This hypothesis contradicts the conventional view of exocytosis, in which trafficking vesicles fully uncoat prior to fusing with the target membrane (Altstiel and Branton, 1983; Brodsky et al., 2001; Conner and Schmid, 2003). We wished to investigate this phenomenon in a system that was more amenable to experimental manipulation and that could be used to examine exocytotic events through time rather than at static moments, i.e., light microscopy of living cells.

Conventional confocal microscopy can obtain axial resolution of about 200 nm, which is substantially thicker than the plasma membrane (4-6 nm) (Gandhavadi et al., 2002; Ruta et al., 2005; White et al., 2001). Additionally, while the use of a pinhole to reject out-of-focus light has the advantage of increasing axial resolution, repeated excitation by the scanning beam results in slow image capture, which in turn increases photodamage and bleaching, making live-cell imaging application difficult to implement effectively. Many of these drawbacks are minimized by spinning disk confocal microscopy in which an array of pinholes in a disk is used to scan through the entire field of view, generating a confocal image (Graf et al., 2005; Nakano, 2002). This image can be captured by a charge-coupled device (CCD) camera rather than a photomultiplier tube (PMT), which greatly increases the speed of image acquisition. Because CCD cameras are highly sensitive, images can be acquired with lower excitation intensity, which in turn reduces photodamage (Graf et al., 2005; Nakano, 2002). These advantages make spinning disk the technique of choice for live-cell imaging. However, spinning disk confocal is still subject to the limited resolution of confocal microscopy, making visualization of highly localized events difficult.

Other attempts to improve the spatial resolution of conventional techniques have included image deconvolution, in which the point spread function is sharpened computationally, and two-photon microscopy, which improves resolution by varying the illumination non-linearly with position in the focal axis (for review see (Jaiswal and Simon, 2003)). Both of these approaches are subject to their own limitations. Image deconvolution, for example, is computationally intense and is prone to introducing artifacts (McNally et al., 1999). Two-photon microscopy allows for the collection of an optical slice with less noise from out-of-focus photons, but the axial resolution is still limited by the long wavelength of the infrared light used. Additionally, the high flux of photons necessary to achieve two-photon events on a reasonable timescale for imaging leads to heating and photodamage at rates that are often higher than conventional confocal microscopy (Jaiswal and Simon, 2003; So et al., 2000).

Total internal reflection fluorescence microscopy (TIRFM) allows for the visualization of event taking place within close proximity (~100 nm) of the plasma membrane in living cells. This offers the advantage of visualizing dynamic events taking place at the cell surface without interference from out of focus light, which is an inherent limitation with epifluorescence and even confocal microscopy (Figure 1) (Jaiswal and Simon, 2003; Nishikawa, 2007). TIRFM is able to simultaneously achieve the advantages of limiting out-of-focus illumination, fast image acquisition, and selective illumination of the portion of the cell that is within ~100 nm of the contact surface. These benefits have made TIRFM an ideal and preferred technique for investigating the dynamics of exocytosis and the roles played by

the various protein components of the exocytotic machinery (Holz, 2006; Jaiswal et al., 2004; Jaiswal et al., 2007; Oheim et al., 1998).

In order to investigate the question of whether clathrin is involved in the exocytosis of FcRn-Fc complexes I began a collaborative project with the laboratory of Dr. Sandy M. Simon at The Rockefeller University.

Materials and methods

Plasmids and construction of expression vectors

The vectors encoding the clathrin light-chain fused to EGFP or DsRed were provided by Sandy Simon (The Rockefeller University). The pCB6H mammalian expression vector containing rat FcRn and the pBJ1 vector containing rat β_2m have been described previously (Tesar et al., 2006). Superecliptic pHluorin-FcRn was generated by introducing a unique *AgeI* site after the nucleotides encoding the FcRn signal sequence in rFcRn-pCB6H. Superecliptic-pHluorin was amplified out of the pGEX-SE-pHluorin vector (a gift from Sandy Simon) by PCR using primers to add flanking *AgeI* sites. This product was inserted into the rFcRn-pCB6H vector immediately 3' of the signal sequence and 5' of the FcRn coding sequence resulting in an superecliptic pHluorin being fused to the N-terminus of FcRn in the expressed protein. The N-terminus of FcRn is located on the opposite side of the molecule as the ligand-binding site (Martin et al., 2001). Construction, expression, and purification of the tdTomato-Fc protein is described in Appendix II.

Cell culture and transfections

Madin-Darby Canine Kidney (MDCK) type II cells were trypsinized and transfected in solution using Lipofectamine 2000 (Invitrogen). Transfected cells were immediately plated onto poly-L-lysine-coated coverslips glued to the bottom of 60 mm plastic culture dishes (Matek). Transfected cells grown at confluent or sub-confluent density before experiments. For experiments involving the internalization of ligands, cells were first rinsed in Hank's Balanced salts with calcium and magnesium (HBSS+) supplemented with 1% ovalbumin and 20 mM MES pH 5.9 (HOM medium). tdTomato or Alexa633-Fc was added at a concentration of 100-1000 nM. Cells were incubated for 15-60 minutes, rinsed several times and then imaged in cell imaging media (CIM, HBSS+/1% fetal bovine serum (FBS)/20 mM HEPES pH 7.4).

Microscopy

Through-objective TIRFM and epifluorescence microscopy were performed with an inverted Olympus IX-70 microscope with an APO x60, N.A. 1.45 TIR objective (Olympus Scientific) equipped with a 12-bit cooled CCD camera (ORCA-ER; Hamamatsu Photonics). The camera, the Mutech MV1500 image acquisition card (Mutech), and the mechanical shutters (Uniblitz; Vincent Associates) were controlled by MetaMorph (Molecular Devices). The microscope was enclosed in a home-built chamber for temperature control, and all imaging was performed at 37°C. For TIRFM experiments, GFP, superecliptic pHluorin, tdTomato, and DsRed were excited with the 488-nm line of an air-cooled tunable argon laser (Omnichrome; model 543-AP A01; Melles Griot) reflected off a dichroic beam splitter

(z488rdc). For epifluorescence, the light of a xenon short-arc lamp [model UXL-150M0 (Ushio)] was passed through a 480/40 band pass excitation filter. The emitted fluorescence for both TIR-FM and epifluorescence microscopy was passed through appropriate emission filters (green channel, 515/30 or 525/50; red channel, 580lp or 600lp) as indicated for each experiment. Simultaneous dual-color TIRFM imaging of GFP, or pHluorin and tdTomato, or DsRed was achieved by exciting the sample with the 488 nm laser line. The emission was spectrally separated by means of an emission splitter (Dual-View; Optical Insights) equipped with a 515/30 band pass filter and a 580lp filter. All filters, dichroics, and polychroics were from Chroma Technologies. Images containing a region of interest were streamed to memory during data acquisition and saved to hard disk afterward. Data analysis was performed by using MetaMorph software (Molecular Devices).

Results and discussion

We wished to use TIRFM to investigate FcRn-mediated exocytosis at the plasma membrane and the possible involvement of clathrin therein. For my initial experiments we tried to visualize labeled ligand and fluorescent clathrin simultaneously with the hope that we would see "puffs" of exocytosing ligand colocalizing with clathrin. Glass-grown FcRn-MDCK cells were transfected with a construct encoding an EGFP-clathrin fusion protein. Cells were treated with tdTomato-Fc 24-48 hours post-transfection and imaged in TIRF mode on a home-built TIRF microscopy system (see Methods). For initial experiments, cells were treated with 500 nM ligand for 45 minutes. The cells were then fixed and imaged in TIRF

mode to examine the distribution of EGFP-clathrin and tdTomato-Fc (Figure 2). The principle limitation in these experiments was that the imaging set-up was not amenable to the clear visualization of tdTomato-Fc. First, the only available laser to excite tdTomato was a 1.5 mW 543 nm laser. This laser is simply not strong enough to give good excitation, especially when one considers that the excitation maximum of tdTomato falls at 554 nm. Second, to avoid bleed-through of EGFP into the tdTomato channel it was necessary to use at least a 580 long-pass emission filter when imaging tdTomato, which cut off a significant portion of the emission spectrum. Thus, long exposures were required to see tdTomato-Fc in the fixed specimen (~500 ms, Figure 2). Exposure times of this length would not allow one to discern the individual movements of puncta in a living specimen simply because many such movements are likely too fast to be captured clearly under such conditions. Additionally, it was clear that much of the tdTomato-Fc had already been exocytosed into the intracellular space in the fixed sample. This result indicated that shorter ligand incubation times followed by rapid washes would be necessary to visualize ligand in living cells.

My next experiments attempted to use Alexa633-labeled Fc as a ligand. This seemed like a good choice of ligand (given the constraints of the imaging setup) due to its being spectrally well-separated from EGFP, thus allowing me to collect the full emission spectrum without fear of bleed through. After ligand treatment (500 nM ALexa633-Fc), EGFP-clathrin/FcRn-MDCK cells were quickly washed in cold buffer and placed on the microscope stage. Movies were collected with 200-300 ms exposure time over 200-400 frames. A representative frame from one of these movies is shown in Figure 3. The puncta of ligand fluorescence in these movies could be classified into two categories; fast-moving puncta that

move within and out of the plane of focus, and static puncta that move little or not at all. We did not observe events that clearly resembled exocytosis – one would expect exocytosis to appear as a brief "puff" of fluorescence as the molecules are released into the extracellular environment and rapidly diffuses. No such puffs were seen in any of the collected data.

Despite the fact that a similar segregation into a fast- and slow- or non-moving populations was previously observed for clathrin (Rappoport et al., 2003a; Rappoport et al., 2003b), two-color analysis of simultaneously imaged EGFP-clathrin and tdTomato-Fc or Alexa633-Fc failed to show any significant degree of colocalization. It was later determined that the morphology of the non-moving spots was consistent with membrane-proximal lysosomes as seen in a previous study (Jaiswal et al., 2002). Thus, I performed experiments varying the concentration of Fc during loading to see if we could preferentially load trafficking compartments and avoid overloading of lysosomes. It was determined that with as little as 10 nM Alexa633-Fc or tdTomato-Fc, moving spots could be visualized in TIRFM mode while accumulation of ligand in large, static structures was avoided. Thus, in future experiments I used significantly lower ligand concentrations.

At this point the principle constraint was being able to identify exocytosing Fc. This proved to be very difficult, as with the limited signal we were unable to identify an unambiguous case of exocytosis based on morphology alone. It became clear that direct visualization of FcRn-mediated exocytosis would require the use of pH-sensitive probes, such as superecliptic pHluorin, to unambiguously identify sites of receptor and/or ligand exit from the plasma membrane. pHluorin is a mutagenized EGFP with high pH sensitivity. When

excited at 488 nm it is brightly fluorescent at neutral pH (>7.0) but exhibits no fluorescence at acidic pH (<6.0) (Miesenbock et al., 1998). It has been used as pH sensor for intracellular compartments in a variety of studies (Jankowski et al., 2001; Kuhn et al., 2007; Ohara-Imaizumi et al., 2002; Schuster et al., 2005). Superecliptic pHluorin is a brighter and slightly more pH-sensitive version of the pHluorin molecule (pKa = 7.18 versus 7.07 for regular pHluorin) (Sankaranarayanan et al., 2000). To allow for visualization of receptor exocytosis directly, I generated a recombinant FcRn that has superecliptic pHluorin appended to its N-terminus (Figure 4). The N-terminus of FcRn is located on the opposite face of the molecule as the ligand binding site and should not interfere with ligand internalization (Martin et al., 2001).

MDCK cells transfected with pHluorin-FcRn and DsRed clathrin were imaged in TIRFM mode. A plane from a movie showing pHluorin-FcRn and DsRed-clathrin expression in shown in Figure 5. Many of these pHluorin-FcRn puncta can be seen that “puff” in the movie. This is consistent with a labeled membrane protein within a vesicle fusing with the plasma membrane and diffusing radially within it (Jaiswal et al., 2007). The DsRed-clathrin puncta are less mobile and do not “puff”, consistent with previous observations of labeled clathrin being imaged in TIRFM mode (Rappoport et al., 2003a; Rappoport et al., 2003b). Two classes of pHluorin-FcRn spots could be identified. The first were spots that appear at the plasma membrane and immediately “puff”. The average lifetime of the fluorescence form one of these “completely fusing” pHluorin-FcRn spots is 1-2 seconds. Examining 29 events such as this failed to find even one FcRn “puff” that colocalized with clathrin. A representative puncta from this class is shown in Figure 6. A second class of pHluorin-FcRn

spots are those that approach the membrane and partially fuse (as demonstrated by the evolution of bright pHluorin-FcRn fluorescence) but do not show the "puff" characteristic of complete fusion. Analysis of 13 of these "incompletely fusing" spots revealed that they have an average lifetime of ~4-6 seconds and are less abundant than the "completely fusing" spots. None of the spots examined showed any colocalization with clathrin. A representative example of this class is shown in Figure 7.

Having failed to find difference in the presence or absence of clathrin in the two classes of pHluorin-FcRn spots, I sought to determine if pHluorin-FcRn and DsRed-clathrin colocalize to any degree by looking at the merged images throughout the recording. This revealed that some spots of pHluorin-FcRn/DsRed-clathrin fluorescence were indeed present (Figure 8). The small panels in Figure 8A show a close-up of a single such event. It is readily apparent that the pHluorin-FcRn fluorescence is much less bright than DsRed clathrin. However, quantitative analysis of the fluorescence intensity values of both channels within the region of interest (Figure 8B) clearly shows that pHluorin-FcRn and DsRed-clathrin both appear and disappear at the same time. The difficulty in interpreting these data is that we cannot be certain that this vesicle is not a newly-endocytosed CCV containing pHluorin-FcRn that happened to pass close to the membrane on its way to join the endosomal network and has yet to be acidified. A similar problem prevents meaningful analysis of colocalizing spots that are present at the beginning of the recording and subsequently disappear; these very likely represent endocytotic events rather than exocytosis. However, it is clear, at the very least, that FcRn and clathrin do colocalize in membrane proximal vesicles that can be imaged using TIRFM. Future experiments will focus on identifying the origin and fate of these vesicles,

which will yield insight into the involvement of clathrin in the intracellular trafficking of receptors and their ligands.

Conclusions and future directions

While it is encouraging that we are now able to unambiguously identify sites at which FcRn-positive vesicles are fusing with the plasma membrane, the lack of an efficacious labeled ligand for these studies continues to provide difficulties. Because we are able to image only the receptor at this time it is impossible to conclusively say which types of events (completely fusing, incompletely fusing, those colocalized with clathrin, or some subset of the three) would actually be correlated with ligand release in a physiological setting. To help resolve this issue for future TIRFM studies I am developing an additional reagent; an Fc molecule with a superecliptic pHluorin appended to both C- and N-termini of each chain. The pHluorin-Fc-pHluorin homodimer will have four pHluorins contributing to its fluorescence instead of the single pHluorin present in superecliptic pHluorin-FcRn. This reagent will be used in concert with fluorescent clathrin expression to correlate the presence of clathrin-positive spots at the plasma membrane with exocytosis, visualized by the evolution of pHluorin fluorescence when pHluorin-Fc-pHluorin molecules are released into the extracellular environment. This reagent will overcome the difficulty of interpreting a pHluorin-FcRn/clathrin spot such as that shown in Figure 8. Because the extracellular pH is not permissive for the binding of Fc to FcRn and because no exogenous ligand will be present, any colocalizing pHluorin-Fc-pHluorin and DsRed clathrin, fluorescence must

represent an intracellular vesicle that has partially fused with the plasma membrane, eliminating the possibility that the vesicle represents newly endocytosed receptor-ligand complexes. Furthermore, the Simon lab will soon have its TIRFM microscope outfitted with a three-way splitter, which will allow me to perform experiments in which three proteins are visualized; clathrin, FcRn, and a labeled ligand. Also, the lab is in the process of installing a 568 nm laser line with more power than the 546 nm 1.5 mW laser that was previously being used to excite tdTomato. The use of a stronger 568 nm line may allow tdTomato-Fc to be visualized clearly, which has not yet been possible. The combination of these improvements will allow a much more powerful analysis of Fc trafficking and the identification of sites of exocytosis without having to rely on changes in vesicle morphology alone, which are intrinsically more difficult to resolve in an unambiguous fashion.

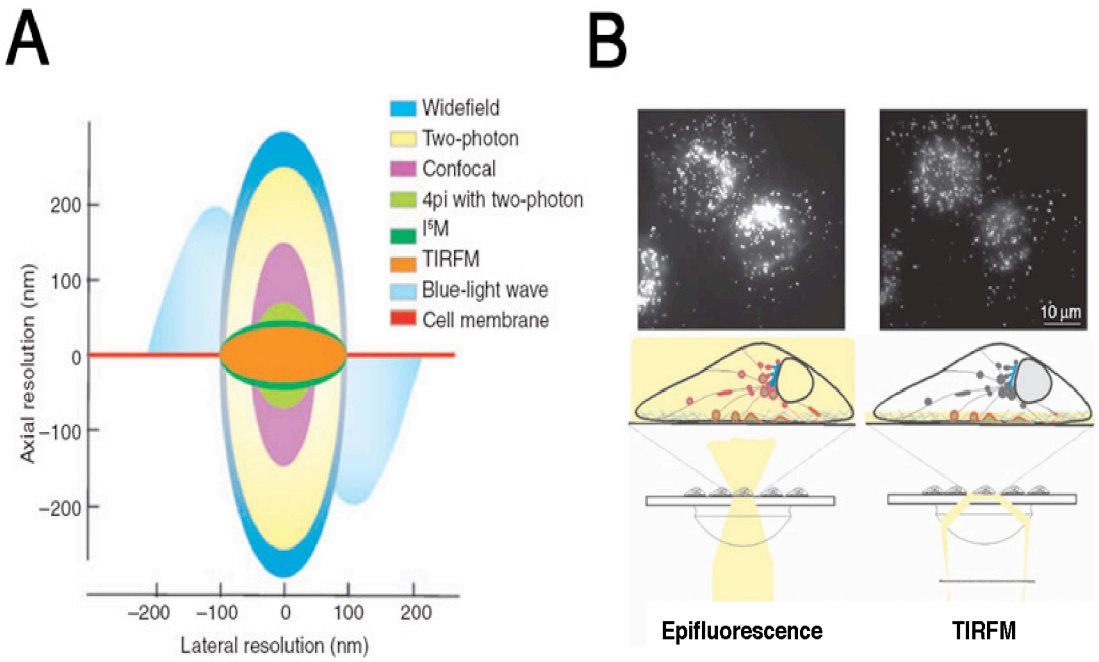

Figure 1. TIRF Microscopy. (A) Relative degrees of axial resolution attainable by different microscopy techniques. (B) Comparison of the illumination properties of epifluorescence and confocal imaging with TIRF imaging. (Adapted from (Jaiswal and Simon, 2007))

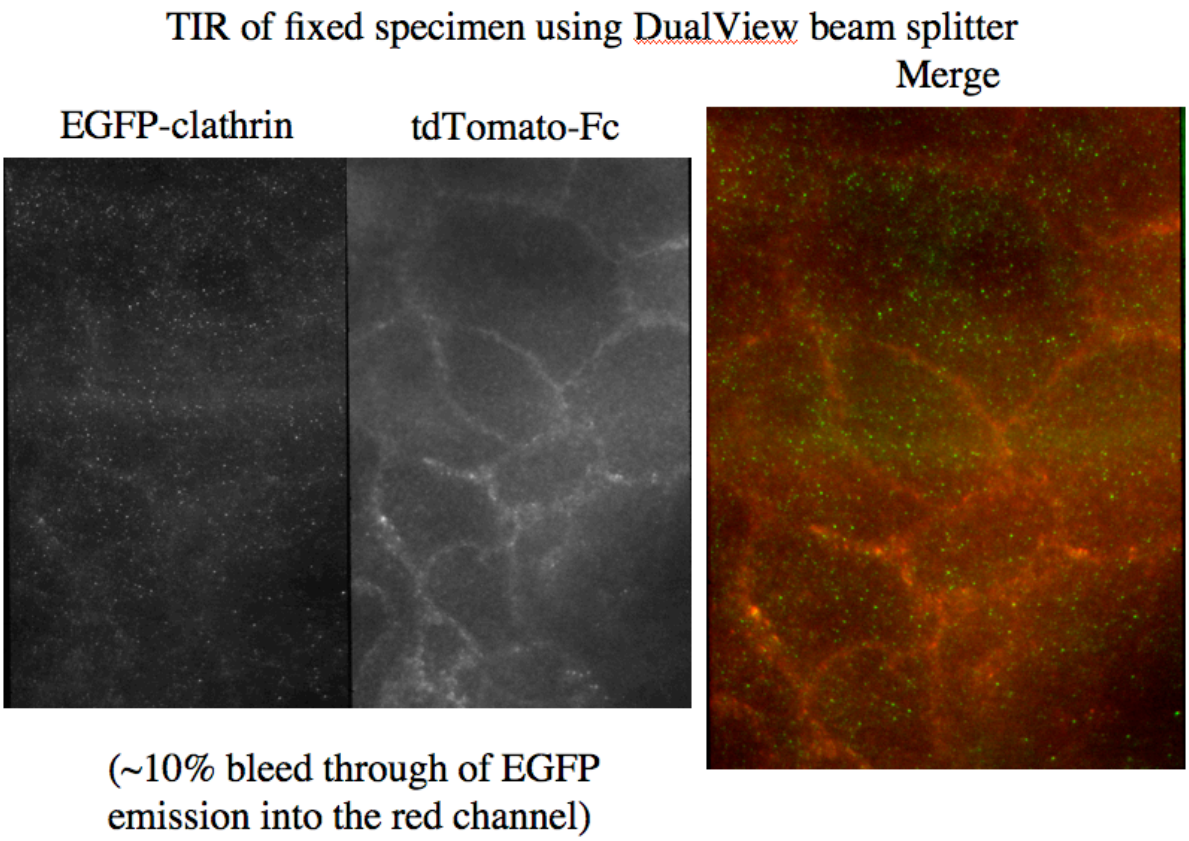

Figure 2. TIRFM of a fixed sample of FcRn-MDCK cells. The transfected EGFP-clathrin is shown in green in the merged image. tdTomato-Fc is shown in red. Despite using a 580 long-pass emission filter for tdTomato-Fc there is still a small amount of bleed-though of EGFP fluorescence into the red channel.

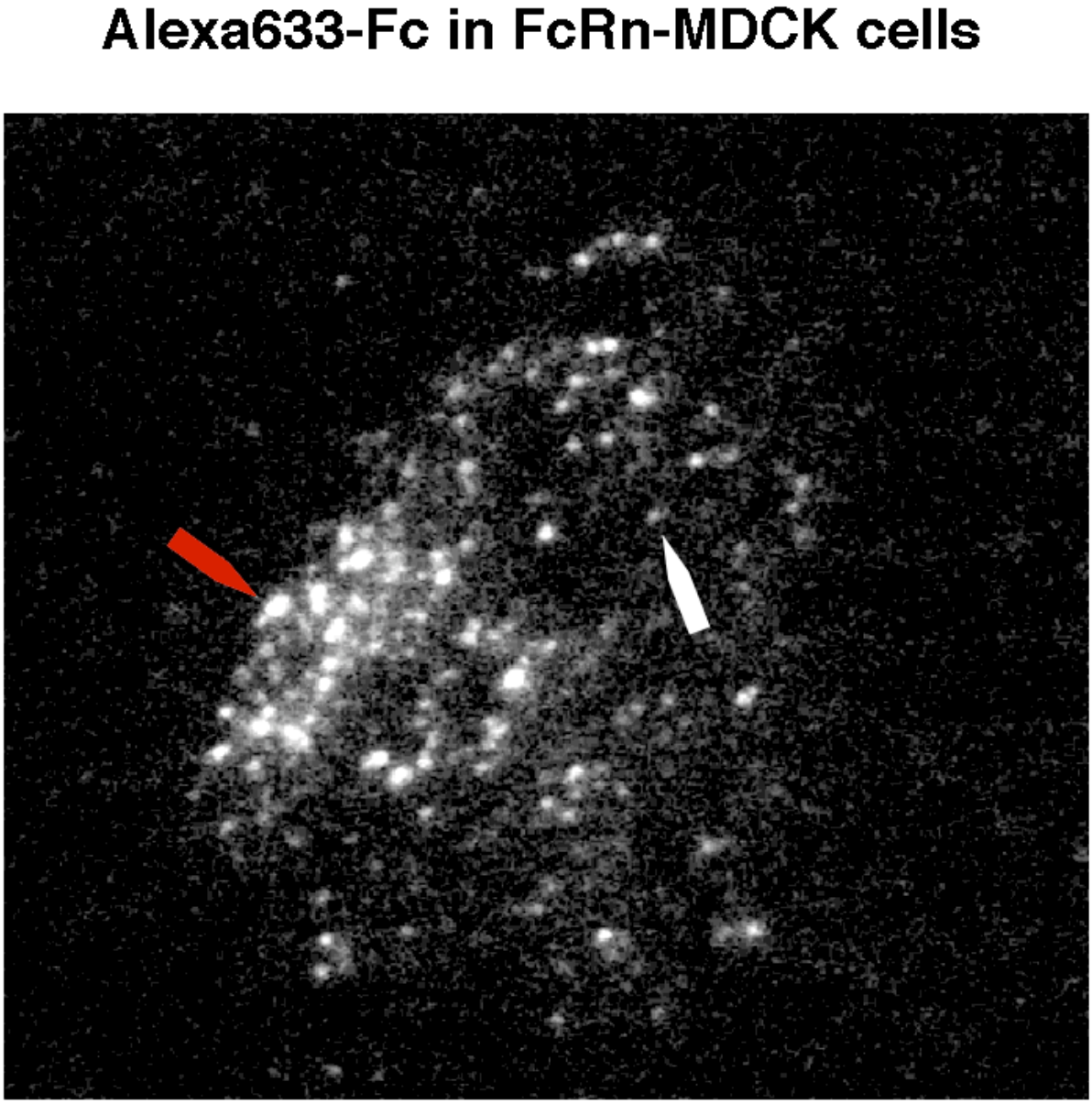

Figure 3. Alexa633-Fc in FcRn-MDCK cells. Cells were incubated with 500 nM Alexa633-Fc for 25 minutes and then visualized in TIRFM mode. Some puncta (white arrowhead) move fairly rapidly while other (red arrowhead) do not move at all.

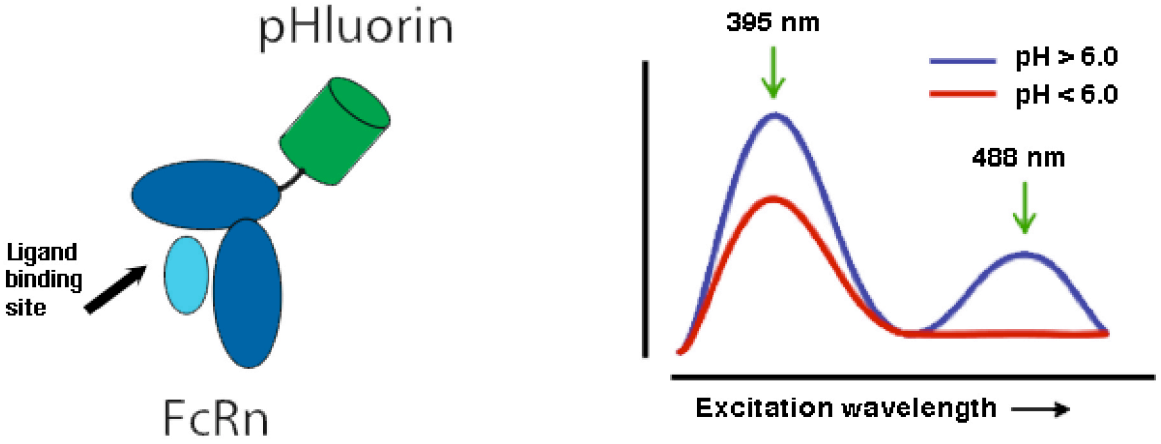

Figure 4. Superecliptic pHluorin-FcRn. The superecliptic pHluorin was appended to the N-terminus of FcRn, away from the ligand binding site. pHluorins are excited by 488 nm light at neutral pH, but show no fluorescence at acidic pH. (Spectra image adapted from http://www.bristol.ac.uk/synaptic/research/projects/mechanisms/phluorins.htm)

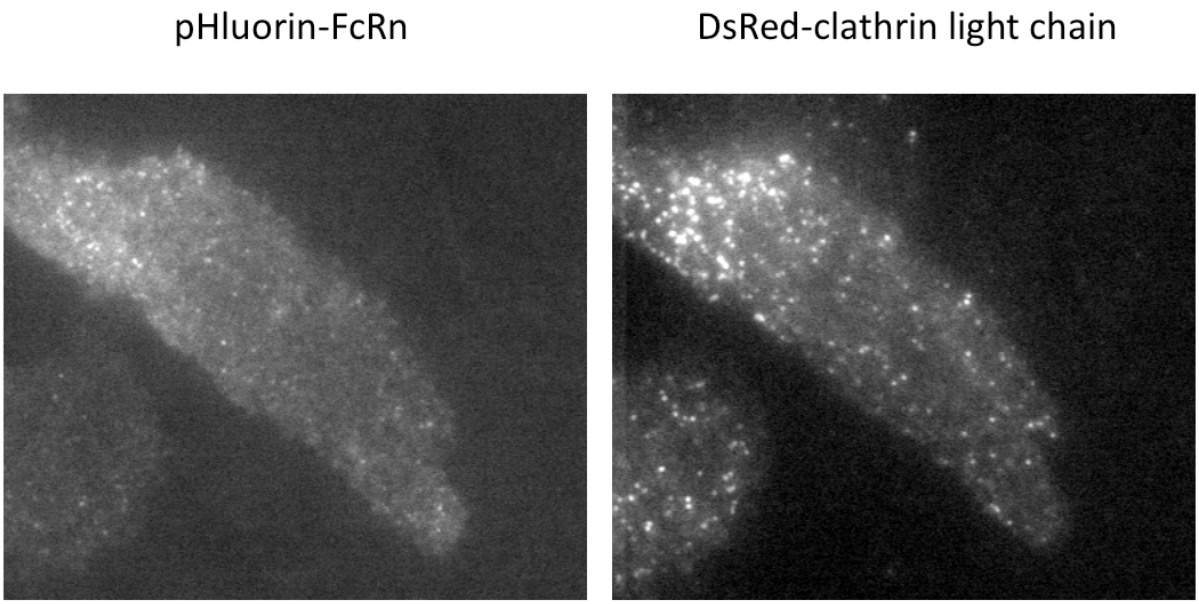

Figure 5. Supereclipticpt pHluorin-FcRn and DsRed-clathrin expressed in MDCK cells. Individual puncta represent pHluorin-FcRn-positive or DsRed-clathrin-positive vesicles within the imaging plane. pHluorin-FcRn spots should represent vesicles that are either fused with the plasma membrane or are recently internalized that have yet to be acidified.

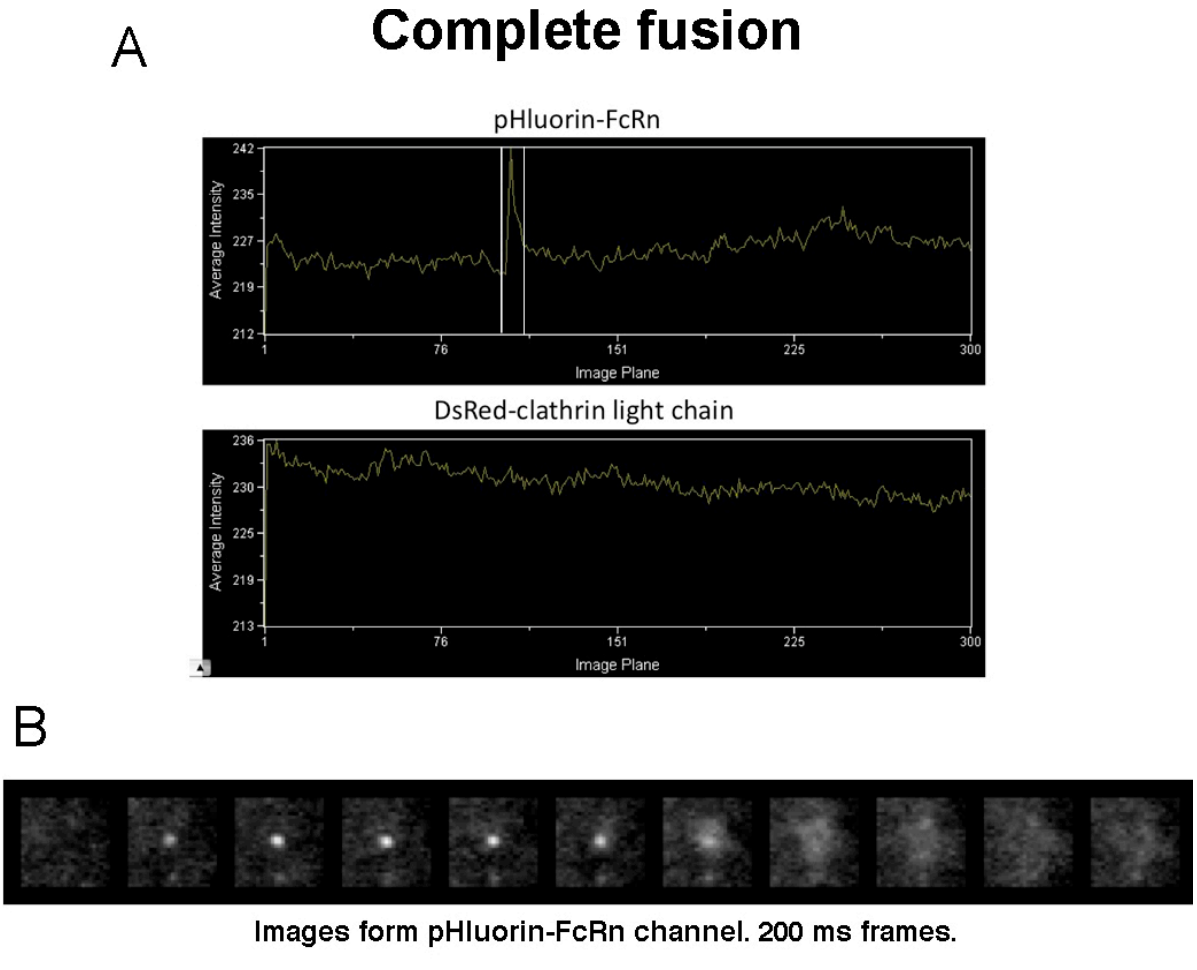

Figure 6. A completely fusing pHluorin-FcRn spot. (A) Average intensity graphs of pHluorin-FcRn and DsRed-clathrin fluorescence over time in the region of interest surrounding a completely fusing spot that shows the characteristic "puff" associated with complete fusion of a tagged receptor with the plasma membrane. The white lines in the pHluorin intensity graph denote the position of the first and last frames from the region shown in (B). The exposure time was 200 ms.

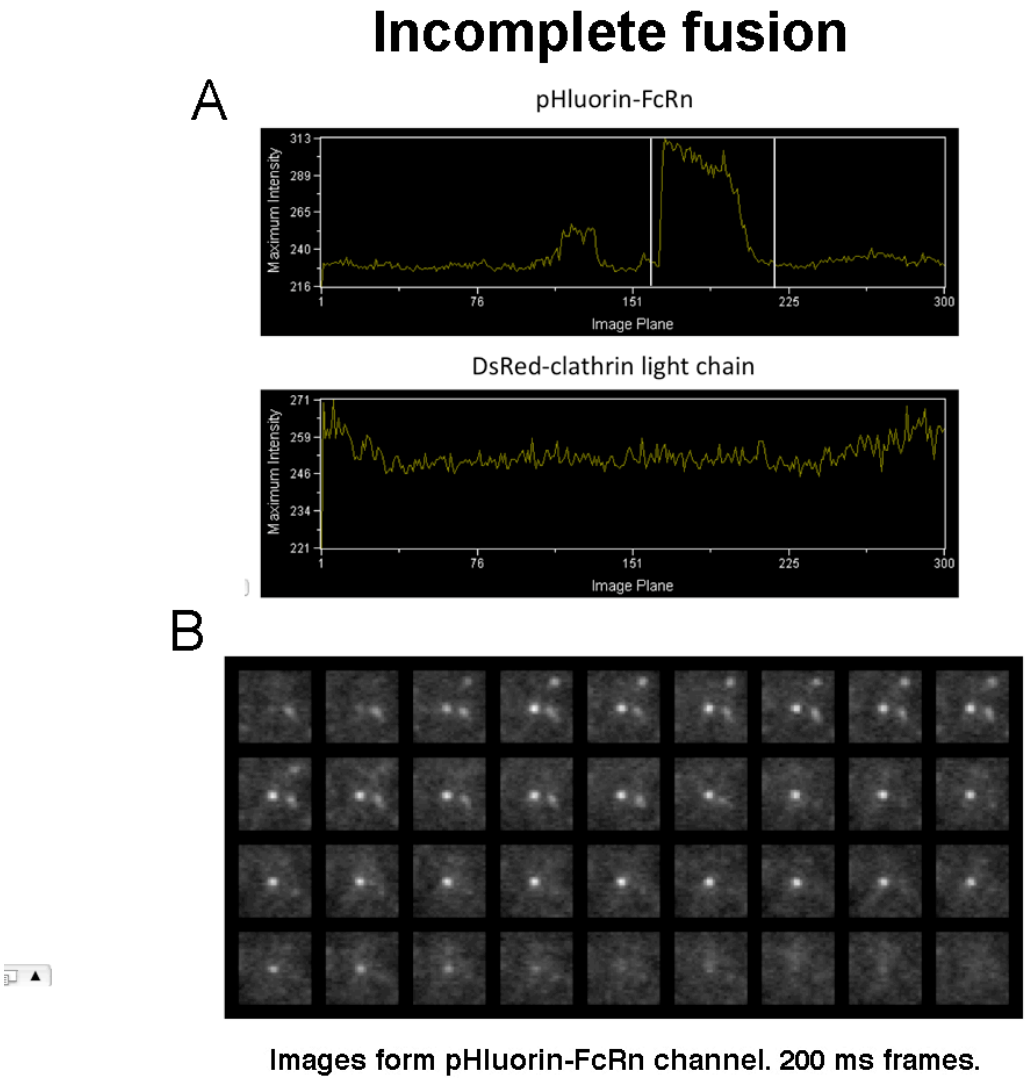

Figure 7. An incompletely fusing pHluorin-FcRn spot. (A) Average intensity graphs of pHluorin-FcRn and DsRed-clathrin fluorescence over time in the region of interest surrounding an incompletely fusing spot that enters the plane of focus and leaves without "puffing". The white lines in the pHluorin intensity graph denote the position of the first and last frames from the region shown in (B). The exposure time was 200 ms.

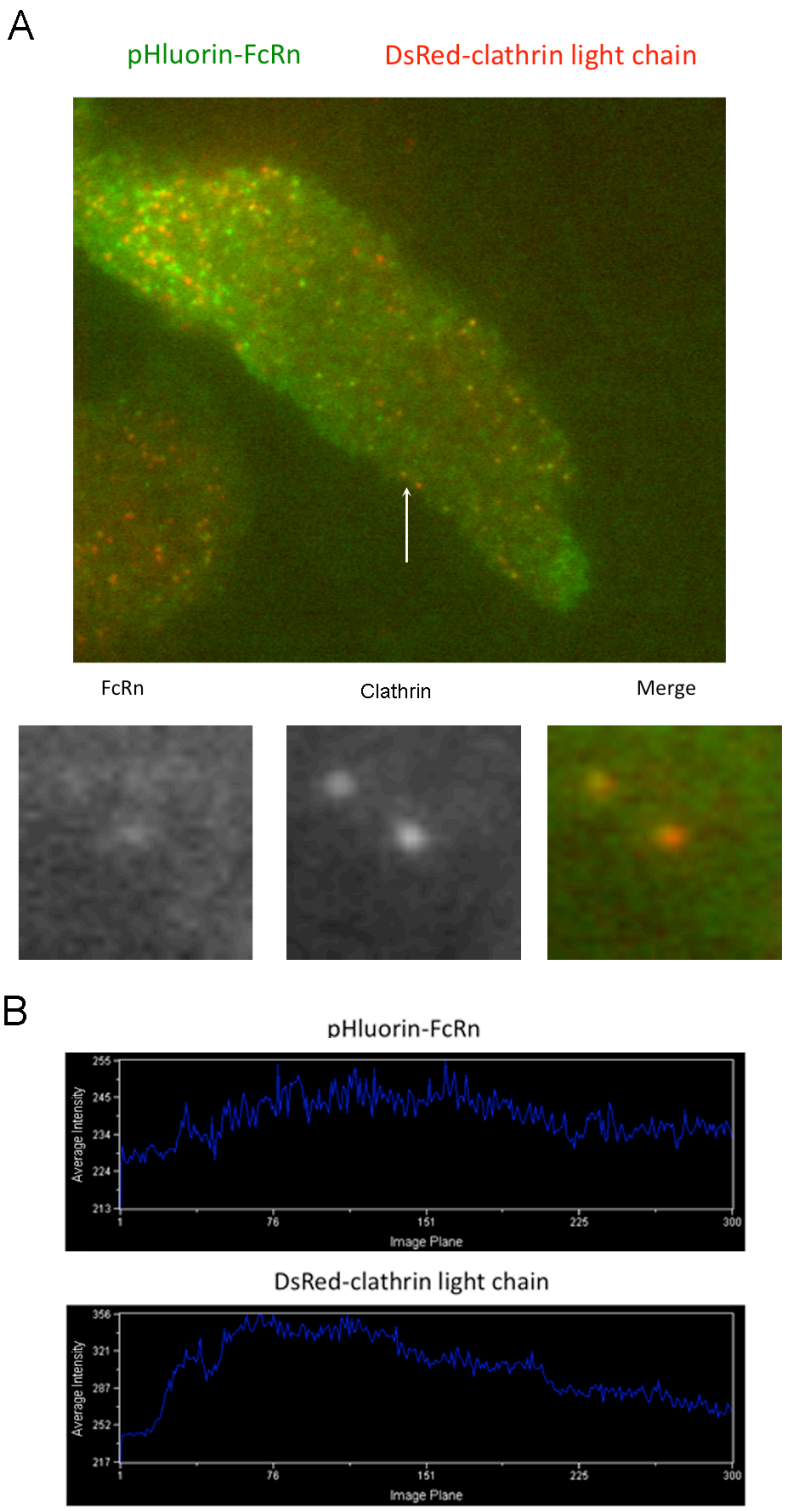

Figure 8. A colocalizing pHluorin-FcRn/DsRed-clathrin spot. (A) Merged image of the pHluorin-FcRn and DsRed-clathrin channels. Several spots with both FcRn and clathrin present are visible. Panels are close-up images of the spot indicated by the white arrow. (B) Average intensity graphs of the pHluorin and DsRed channels for the region of interest shown in the small panels of (A).

References

Altstiel, L., and Branton, D. (1983). Fusion of coated vesicles with lysosomes: measurement with a fluorescence assay. Cell *32*, 921-929.

Brodsky, F.M., Chen, C.Y., Knuehl, C., Towler, M.C., and Wakeham, D.E. (2001). Biological basket weaving: formation and function of clathrin-coated vesicles. Annual review of cell and developmental biology *17*, 517-568.

Conner, S.D., and Schmid, S.L. (2003). Regulated portals of entry into the cell. Nature *422*, 37-44.

Gandhavadi, M., Allende, D., Vidal, A., Simon, S.A., and McIntosh, T.J. (2002). Structure, composition, and peptide binding properties of detergent soluble bilayers and detergent resistant rafts. Biophysical journal *82*, 1469-1482.

Graf, R., Rietdorf, J., and Zimmermann, T. (2005). Live cell spinning disk microscopy. Advances in biochemical engineering/biotechnology *95*, 57-75.

Holz, R.W. (2006). Analysis of the late steps of exocytosis: biochemical and total internal reflection fluorescence microscopy (TIRFM) studies. Cellular and molecular neurobiology *26*, 439-447.

Jaiswal, J.K., Andrews, N.W., and Simon, S.M. (2002). Membrane proximal lysosomes are the major vesicles responsible for calcium-dependent exocytosis in nonsecretory cells. The Journal of cell biology *159*, 625-635.

Jaiswal, J.K., Chakrabarti, S., Andrews, N.W., and Simon, S.M. (2004). Synaptotagmin VII restricts fusion pore expansion during lysosomal exocytosis. PLoS biology *2*, E233.

Jaiswal, J.K., Fix, M., Takano, T., Nedergaard, M., and Simon, S.M. (2007). Resolving vesicle fusion from lysis to monitor calcium-triggered lysosomal exocytosis in astrocytes. Proceedings of the National Academy of Sciences of the United States of America *104*, 14151-14156.

Jaiswal, J.K., and Simon, S.M. (2003). Total internal reflection fluorescence microscopy for high-resolution imaging of cell-surface events. Current protocols in cell biology / editorial board, Juan S Bonifacino [et al *Chapter 4*, Unit 4 12.

Jaiswal, J.K., and Simon, S.M. (2007). Imaging single events at the cell membrane. Nature chemical biology *3*, 92-98.

Jankowski, A., Kim, J.H., Collins, R.F., Daneman, R., Walton, P., and Grinstein, S. (2001). In situ measurements of the pH of mammalian peroxisomes using the fluorescent protein pHluorin. The Journal of biological chemistry *276*, 48748-48753.

Kuhn, Y., Rohrbach, P., and Lanzer, M. (2007). Quantitative pH measurements in Plasmodium falciparum-infected erythrocytes using pHluorin. Cellular microbiology *9*, 1004-1013.

Martin, W.L., West, A.P., Jr., Gan, L., and Bjorkman, P.J. (2001). Crystal structure at 2.8 A of an FcRn/heterodimeric Fc complex: mechanism of pH-dependent binding. Mol Cell *7*, 867-877.

McNally, J.G., Karpova, T., Cooper, J., and Conchello, J.A. (1999). Three-dimensional imaging by deconvolution microscopy. Methods (San Diego, Calif *19*, 373-385.

Miesenbock, G., De Angelis, D.A., and Rothman, J.E. (1998). Visualizing secretion and synaptic transmission with pH-sensitive green fluorescent proteins. Nature *394*, 192-195.

Nakano, A. (2002). Spinning-disk confocal microscopy -- a cutting-edge tool for imaging of membrane traffic. Cell structure and function *27*, 349-355.

Nishikawa, S. (2007). [Basics of TIRFM]. Nippon rinsho *65*, 263-269.

Ohara-Imaizumi, M., Nakamichi, Y., Tanaka, T., Katsuta, H., Ishida, H., and Nagamatsu, S. (2002). Monitoring of exocytosis and endocytosis of insulin secretory granules in the pancreatic beta-cell line MIN6 using pH-sensitive green fluorescent protein (pHluorin) and confocal laser microscopy. The Biochemical journal *363*, 73-80.

Oheim, M., Loerke, D., Stuhmer, W., and Chow, R.H. (1998). The last few milliseconds in the life of a secretory granule. Docking, dynamics and fusion visualized by total internal reflection fluorescence microscopy (TIRFM). Eur Biophys J *27*, 83-98.

Rappoport, J.Z., Taha, B.W., Lemeer, S., Benmerah, A., and Simon, S.M. (2003a). The AP-2 complex is excluded from the dynamic population of plasma membrane-associated clathrin. The Journal of biological chemistry *278*, 47357-47360.

Rappoport, J.Z., Taha, B.W., and Simon, S.M. (2003b). Movement of plasma-membrane-associated clathrin spots along the microtubule cytoskeleton. Traffic (Copenhagen, Denmark) *4*, 460-467.

Ruta, V., Chen, J., and MacKinnon, R. (2005). Calibrated measurement of gating-charge arginine displacement in the KvAP voltage-dependent K+ channel. Cell *123*, 463-475.

Sankaranarayanan, S., De Angelis, D., Rothman, J.E., and Ryan, T.A. (2000). The use of pHluorins for optical measurements of presynaptic activity. Biophysical journal *79*, 2199-2208.

Schuster, S., Enzelberger, M., Trauthwein, H., Schmid, R.D., and Urlacher, V.B. (2005). pHluorin-based in vivo assay for hydrolase screening. Analytical chemistry *77*, 2727-2732.

So, P.T., Dong, C.Y., Masters, B.R., and Berland, K.M. (2000). Two-photon excitation fluorescence microscopy. Annual review of biomedical engineering *2*, 399-429.

Tesar, D.B., Tiangco, N.E., and Bjorkman, P.J. (2006). Ligand valency affects transcytosis, recycling and intracellular trafficking mediated by the neonatal Fc receptor. Traffic (Copenhagen, Denmark) *7*, 1127-1142.

White, S.H., Ladokhin, A.S., Jayasinghe, S., and Hristova, K. (2001). How membranes shape protein structure. The Journal of biological chemistry *276*, 32395-32398.

Appendix I:

Generation of a Recombinant Fluorescent Ligand for Live-Cell Imaging of FcRn Trafficking

This chapter describes the construction, expression, and purification of a recombinant Fc molecule with a tandem dimer of fluorescent proteins attached to the N-terminus of each chain. The purpose of this reagent was to allow for faster and more prolonged acquisition of spinning disk confocal images for live-cell imaging experiments.

Introduction

Spinning disk technology is specifically suited for the fast acquisition of events in living cells that happen beyond the temporal resolution of conventional confocal microscopes. The use of highly sensitive charge-coupled device (CCD) detectors allows for image acquisition under conditions of limited laser exposure, which greatly increases fluorophore lifetime over the course of an experiment (Graf et al., 2005; Nakano, 2002). We are currently using spinning disk technology to visualize rapid events during FcRn trafficking in living cells. The principle limitations of live-cell imaging techniques are that the fluorophore of choice must be bright and photostable in order to minimize exposure time required and thus maximize the temporal resolution achieved, and furthermore must be stable at the low pH (~ 5.5) of endosomes. As chemically labeled Fc proteins do not provide sufficiently bright labels I attempted to generate recombinant Fc ligands that are tagged with fluorescent proteins.

Materials and methods

Ligands

Recombinant wild-type rat Fc (wtFc) was expressed and purified as described previously (Martin and Bjorkman, 1999). wtFc was labeled directly with AlexaFluor 488 succinimidyl ester (Invitrogen) to obtain a dye:protein ratio of 1.5–2.0:1. Labeled ligands were desalted on Zeba spin columns (Pierce) and stored in phosphate buffered saline (PBS) or

HEPES/NaCl with 0.001% azide at 4 degrees. Proteins were used within one month of labeling.

Construction of tdTomato-Fc expression vector

The pTT5 mammalian expression vector encoding the Fc fragment of human IgG_1 was kindly provided by Anthony West (Bjorkman Lab, Caltech). The tandem dimeric Tomato (tdTomato) construct described previously (Shaner et al., 2004) was kindly provided by Dr. Robert Campbell from the University of Alberta, Canada. The tdTomato gene was amplified out of this vector by PCR using primers which added a 5' *PacI* site and a 3' *FseI* site. The amplified product was inserted in-frame to the 5' end of the human Fc gene in pTT5 by *Paci/FseI* double-digest and ligation. The entire open reading frame was verified by DNA sequencing.

Expression and purification of tdTomato-Fc

tdTomato-Fc in the pTT5 expression vector was used to transfect 293EBNA cells in suspension culture with Lipofectamine 2000. The supernatant from 500 mL of culture was acidified to pH 5.9 using MES (100 mM final concentration) and passed over an FcRn-column overnight in the cold room. After washing exhaustively with buffer (25 mM MES/150 mM NaCl/0.002% sodium azide) the column was eluted with 25 mM HEPES pH 8/150 mM NaCl/0.002% azide. The eluate was concentrated and ~ 2 mg of protein was passed over an SD200 gel filtration column into 20 mM HEPES pH 7.4/150 mM NaCl/ 0.002% sodium azide. The concentration of tdTomato-Fc in the final sample was determined using the extinction coefficient of tdTomato at 554 nm (ε = 138,000 $M^{-1}cm^{-1}$), correcting for

the fact that there are two tdTomato chains in each intact tdTomato-Fc dimer. Both the aggregate and monomer peak from the SD200 elution were analyzed by SDS-PAGE on a 10% acrylamide gel. Two microliters of each concentrated peak were run under both reducing and no-reducing conditions.

Cell culture and ligand treatments

The FcRn-MDCK cell line has been described previously (Tesar et al., 2006). Cells were grown at confluent or sub-confluent density on poly-L-lysine-coated coverslips glued to the bottom of 60 mm plastic culture dishes (Matek). For internalization of ligands, cells were first rinsed in Hank's Balanced Salts with calcium and magnesium (HBSS+) supplemented with 1% ovalbumin and 20 mM MES pH 5.9 (HOM medium). tdTomato or Alexa488-Fc were added at a concentration of 100–500 nM. For experiments directly comparing fluorphore lifetimes, the fluorophores were both added at a concentration of 100 nM. Cells were incubated for 15–60 minutes, rinsed several times and then imaged in HOM or HBSS+/1% fetal bovine serum (FBS)/20 mM HEPES pH 7.4.

Spinning disk confocal microscopy

FcRn-MDCK cells treated with tdTomato-Fc or Alexa488-Fc at pH 5.9 were imaged in a 37 °C chamber enclosing a Zeiss AxioObserver equipped with an UltraVIEW spinning disk confocal system. A PlanApo 100x 1.46 NA oil immersion objective was used. The center quarter of a 1Kx1K CCD camera chip was used for data collection with no binning. tdTomato-Fc was excited with the 568 nm laser line. Laser power was set to 18% with 75% output. Frames were collected continuously over 180–300 sec with exposure times varying

from 50–400 msec.

Results and discussion

My previous efforts to visualize trafficking events in living cells have been limited to the use of primary amine-reactive fluorescent dyes to label Fc proteins. While these reagents offer the ability to visualize a recombinantly expressed ligand that lacks an endogenous tag, they have thus far not provided the brightness or photostability required to visualize trafficking events with high spatial and temporal resolution. Indeed, getting a "good" image using Alexa-labeled Fc proteins often requires exposure times of 400 milliseconds or more. As such, exposure times must be decreased (and image quality thereby sacrificed) in order to image fast events within the cell. In order to obtain an FcRn ligand that has better fluorescent properties than the Alexa dyes, I decided to create a recombinant Fc fusion protein in which a fluorescent protein was fused to the N-terminus (in the position where the Fab would normally reside). After a failed attempt to do this with regular EGFP due to the fact that EGFP is virtually non-fluorescent at the acidic pH of endosomes (Scharnagl et al., 1999), I identified tdTomato as a good candidate due to its brightness and superior pH stability (pKa = 4.7) (Figure 1A and B) (Shaner et al., 2004). tdTomato is a tandem dimer of a variant of the DsRed fluorescent protein. Whereas DsRed is normally a tetramer, tdTomato contains a series of mutations that disrupt one of the two dimer interfaces within the tetramer. The resulting molecule will homodimerize, allowing the expression of two fluorophores in a single compact structure (Shaner et al., 2004).

Purification of tdTomato-Fc

The tdTomato gene was fused such that the protein was attached to the N-terminus of human Fc in the pTT5 mammalian expression vector (Figure 1C). Rat FcRn binds and internalized human Fc as efficiently as it does rat Fc (Tesar et al., 2006). tdTomato-Fc was purified out of 293EBNA supernatants by FcRn affinity chromatography and gel filtration chromatography on an SD200 column. The elution from a single passage of the tdTomato-Fc supernatant over the FcRn column contained approximately 7 mg of protein. About 1.5 mg of this was run over the SD200 column. Two peaks, one corresponding to the void volume and likely representing aggregates (Peak 1) and the other running just behind where intact IgG elutes (Peak 2) were collected and analyzed by 10% SDS-PAGE (Figure 2A and B). It is apparent from PAGE analysis that although both Peaks 1 and 2 contain tdTomato-Fc (Figure 2B), Peak 1 contains less tdTomato-Fc, despite having a higher absorbance at 280 nm (Figure 3A and C). Whether the presence of tdTomato-Fc in the aggregate peak simply represents normally aggregated protein or whether there is some propensity of tdTomato-Fc to aggregate via *trans* associations of the dimeric Tomato fluorescent protein modules with other tdTomato-Fc molecules is unclear. Regardless, it seems that approximately two-thirds of the expressed tdTomato-Fc remains in the stable dimeric form.

Imaging of tdTomato-Fc and AlexaFluor 488-Fc in FcRn-MDCK cells

To evaluate the utility of tdTomato-Fc as a ligand for live cell imaging in FcRn-MDCK cells, cells were grown on lysine-coated coverslips and allowed to internalize tdTomato-Fc or Alexa488-Fc (100 nM) at 37 degrees prior to being mounted in a heated chamber for imaging on the UltraVIEW spinning disk confocal system. Images were collected from either single

planes or multiple planes spaced 0.5 μm apart. Using a 150 ms exposure time, tdTomato-Fc is readily visible with relatively low laser power (18%) (Figure 3). Samples were imaged for 180–300 seconds of continuous exposure (~ 700–2000 images) and, although the fluorescence does significantly decrease over time, small structures are still clearly visible and the background remains low. This was compared to imaging data in which Alexa488-labeled Fc was visualized using 400 ms exposure times (required to get appreciable signal) (Figure 3). After 137 exposures the sample has been significantly bleached with a 24% reduction in average pixel intensity (Figure 3, left panels), whereas tdTomato-Fc is still very bright after 137 scans (8% average pixel intensity reduction, Figure 3, right panels). Only after 784 scans does the tdTomato-Fc sample exhibit a reduction in average intensity (27%) comparable to that seen in the Alexa488-Fc samples after 137 scans. Thus, these data suggest that, under exposure conditions that provide roughly equal amounts of emission signal, tdTomato-Fc can be imaged six times as long as the corresponding Alexa-labeled ligand or, conversely, can be imaged equally as long with six times the temporal resolution as the Alexa-labeled Fc. Additionally, being a recombinantly expressed molecule, the tdTomato-Fc should offer the advantage of eliminating sample-to-sample variability that is inherent to chemically labeling protein molecules with fluorescent dyes.

Future directions

The usefulness of tdTomato-Fc for live cell imaging will be further tested by varying parameters such as exposure time and imaging interval to determine what conditions provide the optimum combination of good signal and good temporal resolution. Data from these experiments will be analyzed using the Imaris image analysis package with the end goal

being to achieve automated tracking of tdTomato-Fc-positive vesicles during intracellular trafficking.

A

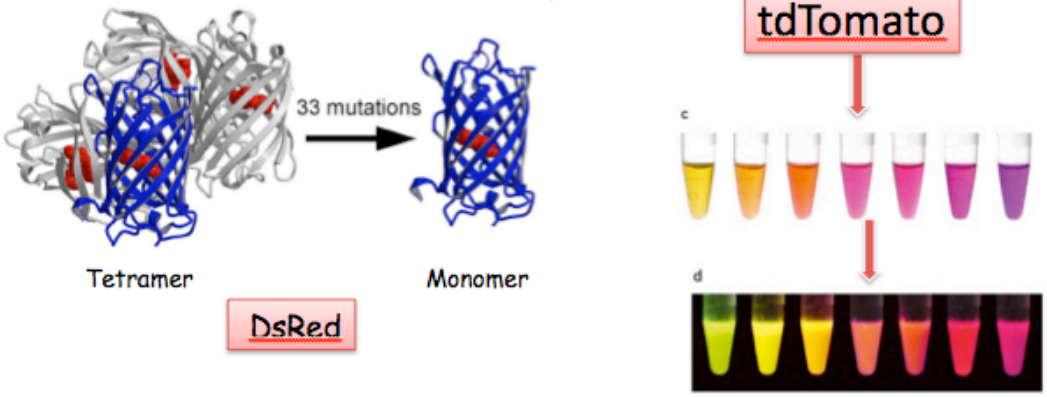

B

	Ex (nm)	Em (nm)	E (M-1cm-1)	QY	pKa
tdTomato	554	581	138,000	0.69	4.7

C

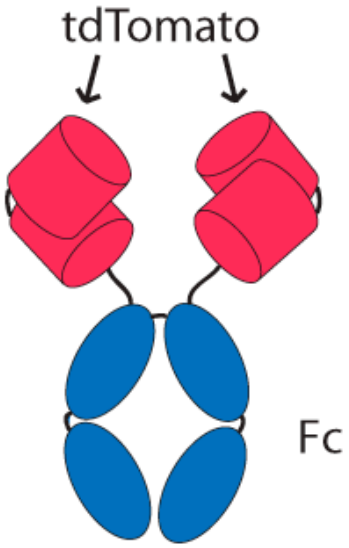

Figure 1. tdTomato. (A) A series of mutations at the dimer interfaces of the natively tertrameric DsRed can be used to generate dimeric or monomeric DsRed. Mutagenesis of wild-type DsRed was used to create a library of variants with different fluorescent properties, including tdTomato (red arrow). (B) Fluorescent properties of tdTomato. Ex: excitation maximum, Em: emission maximum, E: extinction coefficient, QY: quantum yield. (C) Schematic representation of the tdTomato-Fc homodimer. Panel A adapted from Shaner et al., 2004.

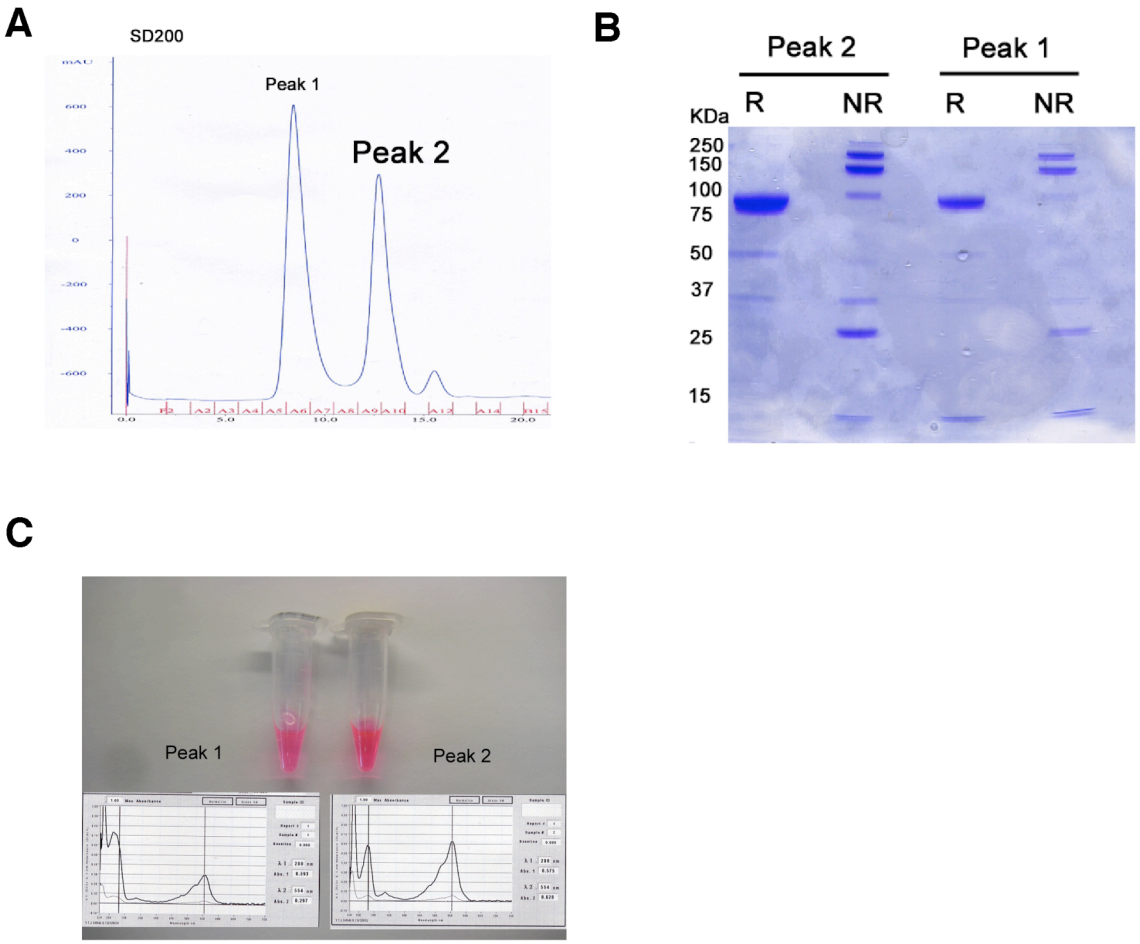

Figure 2 Purification of tdTomato-Fc. (A) After purification on an FcRn-affinity column tdTomato-Fc was subjected to gel filtration chromatography on an SD200 column. The elution profile is shown. Two peaks, one running with the void volume (Peak 1) and the other running slightly slower compared with IgG (Peak 2) were collected. (B) SDS-PAGE analysis of both peaks from the SD200 column elution. (C) Concentrated protein from peak 1 and peak 2. Absorbance curves for each sample show an absorbance maximum at 554 nm, the excitation maximum of tdTomato. More tdTomato-Fc is present in peak 2 despite an overall lower absorbance at 280 nm compared to peak 1.

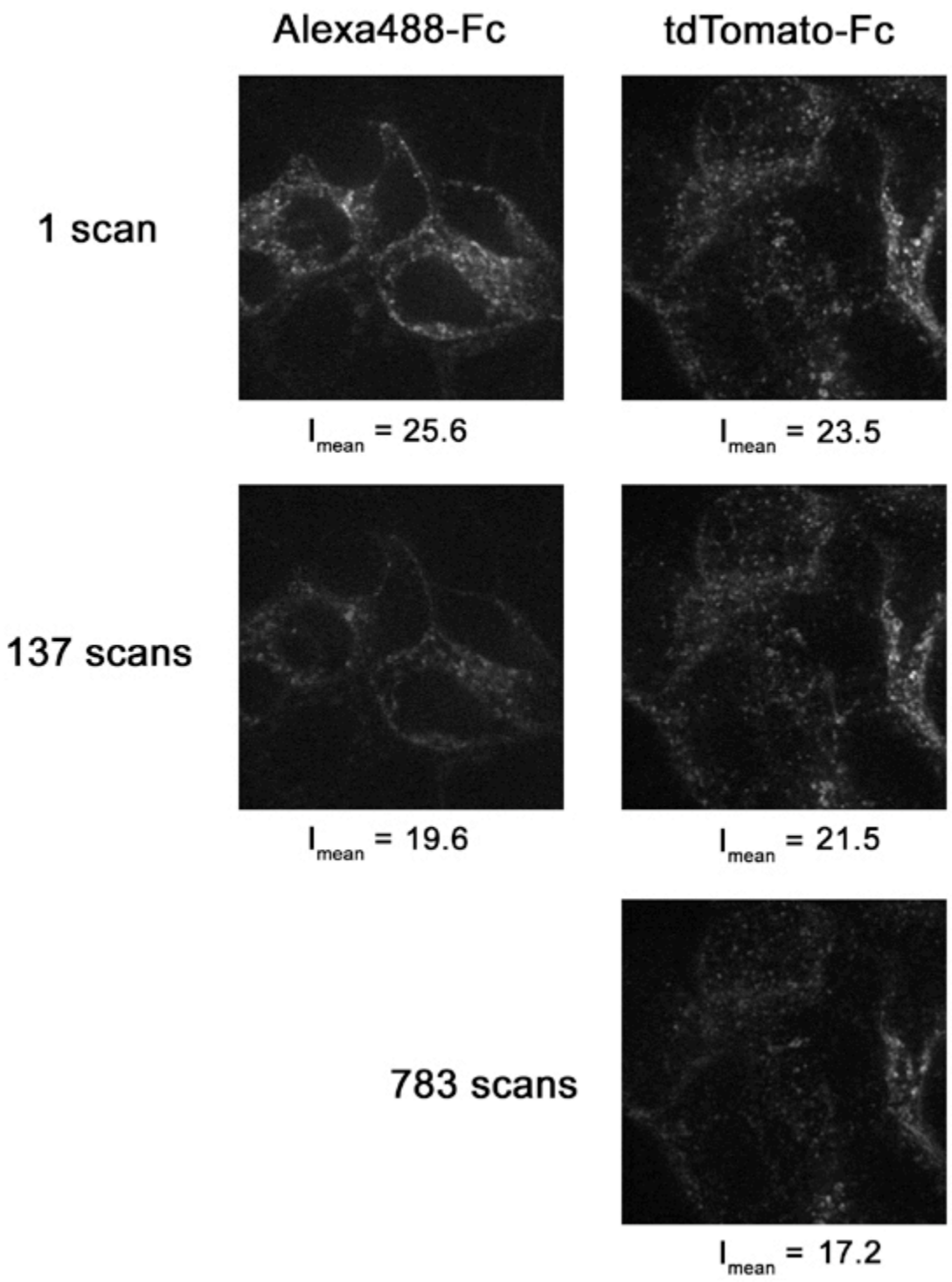

Figure 3 Relative bleaching rates of Alexa-labeled Fc and tdTomato-Fc. FcRn-MDCK cells were incubated with either Alexa488-Fc or tdTomato-Fc for 45 minutes prior to imaging on a spinning disk confocal system. Scans were taken continuously with 400 ms and 150 ms exposure times for Alexa488-Fc and tdTomato-Fc, respectively. The mean intensity of each image is indicated below the panels.

References

Graf, R., Rietdorf, J., and Zimmermann, T. (2005). Live cell spinning disk microscopy. Advances in biochemical engineering/biotechnology *95*, 57-75.

Martin, W.L., and Bjorkman, P.J. (1999). Characterization of the 2:1 complex between the class I MHC-related Fc receptor and its Fc ligand in solution. Biochemistry *38*, 12639-12647.

Nakano, A. (2002). Spinning-disk confocal microscopy -- a cutting-edge tool for imaging of membrane traffic. Cell structure and function *27*, 349-355.

Scharnagl, C., Raupp-Kossmann, R., and Fischer, S.F. (1999). Molecular basis for pH sensitivity and proton transfer in green fluorescent protein: protonation and conformational substates from electrostatic calculations. Biophysical journal *77*, 1839-1857.

Shaner, N.C., Campbell, R.E., Steinbach, P.A., Giepmans, B.N., Palmer, A.E., and Tsien, R.Y. (2004). Improved monomeric red, orange and yellow fluorescent proteins derived from Discosoma sp. red fluorescent protein. Nature biotechnology *22*, 1567-1572.

Tesar, D.B., Tiangco, N.E., and Bjorkman, P.J. (2006). Ligand valency affects transcytosis, recycling and intracellular trafficking mediated by the neonatal Fc receptor. Traffic *7*, 1127-1142.

Appendix II:

Attempts to Detect FcRn Homodimers Using Förster Resonance Energy Transfer and Bimolecular Fluorescence Complementation

This chapter describes my work to determine if FcRn can dimerize at the cell membrane. Two different biophysical assays, FRET and BiFC, were chosen for these studies because both are well-established methods for the detection of protein-protein interactions.

Introduction

A structure-based hypothesis was previously proposed to account for the ability of cells to distinguish endosomes containing FcRn-IgG complexes destined for recycling or transcytosis from endosomes destined for a degradative pathway (Raghavan and Bjorkman, 1996). The hypothesis suggests that an oligomeric ribbon of FcRn dimers bridged by the homodimeric Fc regions of IgG molecules, as seen in the crystal structure of an rFcRn/Fc complex (Burmeister et al., 1994b), forms inside acidic trafficking vesicles. Formation of the oligomeric ribbon between the adjacent membranes of a tubular endosome could act as an intracellular trafficking signal, designating vesicles containing such complexes for entry into the transcytotic or recycling pathways. A requirement for formation of the oligomeric ribbon is a homodimeric Fc or IgG molecule capable of bridging between FcRn proteins on opposing membrane faces. Consistent with this hypothesis, previous studies have demonstrated that a heterodimeric Fc molecule (hdFc), consisting of one FcRn-binding chain and one non-FcRn-binding chain, is less efficiently transcytosed across neonatal mouse intestine (Kim et al., 1994) and exhibits a shorter serum half-life (Popov et al., 1996) than a wild-type homodimeric Fc molecule (wtFc). These results could indicate that both FcRn binding sites are required for the purposeful movement of vesicles containing FcRn-Fc complexes through the transcytotic pathway of the polarized gut epithelium. However, it is not possible to ascertain whether the decreased trans-intestinal transfer of the hdFc results from the disruption of a trafficking signal that requires a homodimeric ligand capable of bridging between two FcRn molecules, or from the fact the monovalent hdFc cannot form

high avidity 2:1 FcRn/Fc complexes, thereby reducing the amount of hdFc that is bound and internalized by FcRn.

We previously used *in vitro* experiments involving rFcRn-transfected MDCK cells to demonstrate that hdFc is transcytosed across monolayer in significant quantities, but that the transport is rendered less efficient by virtue of increased degradation of hdFc in lysosomes (Tesar et al., 2006). This suggests that avidity plays a key role in FcRn-mediated transport by keeping the ligand bound to the receptor throughout the entire transport process rather than allowing it to dissociate within the endosome and be transported to the lysosome with other fluid-phase components. While these results make it clear that the formation of an oligomeric ribbon is not strictly required for transport of Fc by FcRn, it does not completely rule out ribbon formation or receptor dimerization as important parts of the transport process. Previous studies using co-immunoprecipitations have suggested that FcRn molecules form dimers in cells co-transfected with two different epitope-tagged forms of FcRn (Praetor et al., 2002). However, these studies are less than convincing due to the fact that the dimers appeared to be covalent, and covalent dimers of FcRn are known to form when the co-expression of the β_2m light chain is not in balance with expression of the heavy chain (Claypool et al., 2002; Praetor and Hunziker, 2002). Furthermore, disulfide-linked FcRn dimers are known to be retained in the endoplasmic reticulum (Claypool et al., 2002; Praetor and Hunziker, 2002), making it highly unlikely that they hold any functional relevance for the receptor *in vivo*. However, it has been reported that phosphorylation of serine-313 in the FcRn cytoplasmic tail is required for efficient apical to basolateral transcytosis (McCarthy et al., 2001), consistent with a physiologically relevant role for dimerization of FcRn *in vivo*.

We wanted to test for the presence of FcRn dimers on the surface of transfected cells. We performed experiments using two biophysical assays; Förster Resonance Energy Transfer (FRET) and Bimolecular Fluorescence Complementation (BiFC).

FRET has long been used as an effective tool for detecting protein-protein interactions (Jares-Erijman and Jovin, 2003). A typical FRET experiment involves generating fusion proteins in which donor and acceptor molecules (often cyan fluorescent protein [CFP] and yellow fluorescent protein [YFP], respectively) are attached to two potentially interacting partners. Excitation of the donor molecule results in non-radiant energy transfer to the acceptor, which in turn will fluoresce if the donor and acceptor are in close (~ 5 nm) proximity with their dipole moments aligned parallel to one another (Dale et al., 1979). (Figure 1) While FRET can theoretically be detected directly by observing the presence of acceptor fluorescence upon donor excitation, this approach is potentially confounded by bleed-though excitation of the acceptor at the donor excitation wavelength. To circumvent this problem, an acceptor bleaching protocol can be used. In this approach, the donor molecule is visualized to assess a baseline intensity. In the presence of FRET some of the donor emission is lost to the acceptor and is thus not observed. After heavily bleaching the acceptor molecule the intensity of the donor is re-evaluated. An increase in donor fluorescence after bleaching of the acceptor is an indication that FRET was occurring and that the two molecules of interest interact.

We employed an acceptor bleaching approach to use FRET to evaluate potential interactions between FcRn proteins that had CFP or YFP recombinantly fused to their C-termini. The

cytoplasmic tail of these constructs was removed in order to promote the accumulation of FcRn at the cell surface and increase the readout signal. CFP and YFP fusions of the α- and β-chains of HLA-DR, a class II MHC protein that is an obligate heterodimer, served as a positive control (Figure 2).

BiFC is another assay for protein-protein interactions that has gained popularity in recent years. In this assay proteins of interest are fused to one of two recombinant halves of YFP (designated YN for the N-terminal half and YC for the C-terminal half). When these halves are brought into close proximity they combine to form the active YFP fluorophore, providing positive readout for the association of their fusion partners (Figure 5A). This technique has been used to probe the interaction of several proteins including various transcription factors and G-protein subunits (for review see (Kerppola, 2008)). I generated FcRn fusion proteins of the YN and YC halves (Figure 5B). YN and YC were fused to the C-terminus of the FcRn cytoplasmic tail separated by the RSIAT linker (Hu et al., 2002; Hu and Kerppola, 2003). The bJunYN and bFosYC constructs consisting of the bZip family members Fos and Jun attached to the BiFC proteins were kindly provided to me by Dr. Chang-Deng Hu of Purdue University for use as positive controls.

Materials and methods

Generation of expression vectors

The plasmids encoding the full-length rat FcRn heavy chain with GFP fused to the C-terminus and the rat β_2-microglobulin light chain in the pCB6H and pBJ1 mammalian expression vectors, respectively, have been described previously (Tesar et al., 2006).

The cytoplasmic tail-less mutant of FcRn was made by using site-directed mutagenesis (SDM) to introduce an *XhoI* site after Arg304 of the coding sequence of FcRn-GFP (Arg304 is the last residue of the stop-transfer motif in FcRn). This allowed the cytoplasmic tail to be removed by *XhoI* digest to remove the coding bases between the first residue of the cytoplasmic tail and the first residue of the GFP cassette. In the absence of endocytotic motifs encoded within the cytoplasmic tail, FcRn is endocytosed much less efficiently than full-length FcRn, causing the tail-less form to accumulate at the cell surface (Dickinson et al., 2008).

The FcRn-YFP and FcRn-CFP constructs, along with their respective cytoplasmic tailless variants were constructed by subcloning the EYFP or ECFP genes from the pEYFP-1 and pECFP-1 vectors (Clontech) into the FcRn-GFP or FcRn-tail-less-GFP vectors by a *Xho*I/*Hind*III double digest and ligation. FcRn-tail-less-YFP DNA was cotransfected into MDCK cells along with an expression vector for rat β_2m, and cells stably expressing both chains were isolated via FACS. The vectors encoding CFP fusions were amended by the addition of an N-terminal FLAG epitope tag to allow FACS of cells expressing both CFP and YFP FcRn variants. The YFP and CFP portions of the fusion proteins included the A206K substitution, which prevents the potentially confounding homodimerization of GFP and its variants (Zacharias et al., 2002).

For the generation of the bimolecular fluorescence complementation (BiFC) constructs, the FcRn-YFP construct was modified by PCR to introduce either a *Hind*III or *Xho*I site between residues 172 and 173 of EYFP. Digestion with *Hind*III (removing the C-terminal 66 residues of EYFP) or with *Xho*I (removing the N-terminal 172 residues of EYFP) followed by re-ligation yields the FcRn-YN (EYFP residues 1–172) and FcRn-YC (EYFP residues 172–238) expression constructs, respectively.

Antibodies

The mouse monoclonal antibodies 1G3 (anti-rFcRn heavy chain) and 4C9 (anti-rat b2m) were generated in our laboratory (Raghavan et al., 1994) and can be purchased from the American Tissue Culture Collection. 2B10C11, a mouse monoclonal antibody against rat ß2m, was the kind gift of Lennart Lögdberg. A polyclonal rabbit anti-serum used for Western blotting was raised against purified rFcRn/$ß_2$m heterodimers. AC17 mouse mAb against the canine lysosomal-associated membrane protein-2 (LAMP-2) was a gift from Dr. Enrique Rodriguez-Boulan of Cornell University. Rabbit polyclonal antisera against the tight junction-associated protein ZO-1 was obtained from Zymed. A mouse monoclonal antibody against EEA1 was from BD Transduction. AlexaFluor 488-, 546-, and 633-labeled secondary antibodies (goat anti-mouse, goat anti-rabbit, and goat anti-rat) were purchased from Molecular Probes.

Endocytosis of fluorescently - labeled ligands

For fluorescent ligand uptake, cells were pre-incubated in HBSS+/MES pH 5.9 as described above, and fluorescently - labeled ligand (500 nM) was added to the input surface. After incubating for 30 minutes at 37°C, cells were placed on ice, briefly rinsed with ice-cold MBS (10 mM MES pH 5.9, 150 mM NaCl), and then washed twice with HBS (10 mM HEPES pH 8.0, 150 mM NaCl) to remove surface-bound ligand prior to being fixed and processed for immunofluorescence.

Immunofluorescence

Cells were washed briefly with ice-cold PBS+ (PBS supplemented with 1 mM $CaCl_2$, 0.5 mM $MgCl_2$, and 0.25 mM $MgSO_4$) and fixed using a pH-shift protocol (Apodaca et al., 1994). Briefly, cells were incubated for 5 min at room temperature in 4% paraformaldehyde (PFA) in 80 mM PIPES pH 6.5, 5 mM EGTA, 2.0 mM $MgCl_2$, and then transferred to 4% PFA, 100 mM sodium borate pH 11.0 for 10 minutes. After quenching excess aldehyde with freshly - prepared 75 mM NH_4Cl, 20 mM glycine in PBS for 10 min, the cells were washed twice with PBS and blocked for 30 minutes at room temperature in PBS containing 8% normal goat serum and 0.025% saponin. Cells were then incubated overnight at 4°C in blocking buffer containing primary antibodies diluted in block buffer. Cells were washed and then incubated with the appropriate AlexaFluor-conjugated secondary antibodies diluted 1:500 in blocking buffer for 1 hour at room temperature. For experiments involving localization of internalized Fc proteins, unlabeled ligands were detected after internalization using AlexaFluor-conjugated goat anti-rat IgG antibodies. After extensive washing with PBS, cells were treated with 0.1% Triton X-100 for 5 minutes, washed once with PBS, and then

post-fixed with 4% PFA in 100 mM sodium cacodylate pH 7.4 for 30 minutes at room temperature. The cells were washed twice more with PBS and the filters were cut out of their holders using a scalpel and a fine-tipped pair of forceps. Excised filters were mounted on glass slides using ProLong Gold antifade medium (Molecular Probes), sealed with beeswax, and stored at -20°C until viewing on a confocal microscope.

Confocal Microscopy

All experiments were conducted using an inverted Zeiss LSM META confocal microscope equipped with a Zeiss Plan-Apochromat 100× oil objective (NA 1.4). Green fluorophores were excited with the 488 nm line of an argon ion laser. Orange and far-red dyes were excited with the 543 nm and 633 nm lines of a He-Ne laser, respectively. Fluorescence was detected through a variable confocal pinhole set to 1.0 Airy units for the longest wavelength used within a given experiment, and the pinholes of other channels were adjusted to maintain a constant optical section thickness across all channels. The gain and offset of the photomultipliers was adjusted for each channel individually so that the observed fluorescence signal filled the linear range of the detectors, with the background being slightly positive and saturation being minimized

Bimolecular fluorescence complementation

Untransfected MDCK II cells were seeded on poly-L-lysine-coated glass coverslips and grown for 24 hours until ~ 70% confluent. Cells were transfected with FcRn-YN and FcRn-YC BiFC constructs along with the rβ_2m expression vector using Lipofectamine 2000 reagent (Invitrogen) in serum-free medium. Cells singly transfected with either FcRn-YN or

FcRn-YC along with rβ_2m served as negative controls. Transfection complexes were removed after 8 hours and replaced with complete growth medium. Cells were fixed and processed for immunofluorescence ~ 48 hours post-transfection. Separate coverslips of parallel transfections were stained with antibodies against rFcRn (1G3 mAb), rβ_2m (2B10C11 mAb), and GFP (anti-GFP polyclonal antibody from BD Transduction Labs). Another set of coverslips were treated with 500 nM wtFc at pH 6 for 30 minutes to allow internalization by FcRn-YN or FcRn-YC, and stained with Alexa-546-conjugated goat anti-rat antibody to visualized endocytosed wtFc. BiFC was examined using setting appropriate for visualization of EYFP (Hu et al., 2002).

Results and discussion

The requirement of receptor dimerization to initiate intracellular responses has been extensively documented both for receptors that mediate endo-/transcytotic processes (e.g., the polymeric Ig receptor, pIgR) (Luton and Mostov, 1999), and those that do not (e.g., the EphRTKs) (Himanen et al., 2001; Stapleton et al., 1999), and often involves dimerization followed by phosphorylation of serines, threonines, or tyrosines in the cytoplasmic tail domain of the participating receptors upon binding of their cognate ligands (Heldin, 1995; Kalo and Pasquale, 1999; Okamoto et al., 1994). Dimers of FcRn were observed in the crystals of the rat receptor alone and in complex with Fc (Burmeister et al., 1994a; Burmeister et al., 1994b). At least one study has reported the presence of FcRn dimers in transfected cells (Praetor et al., 2002). However, subsequent studies demonstrated that the

findings in this study were likely an artifact due to the lack of balanced co-expression of β_2m (Claypool et al., 2002; Praetor and Hunziker, 2002). In order to clarify these results we sought to use two biophysical assays to detect dimerization of FcRn in living cells.

FRET experiments using live FcRn-CFP/YFP co-transfected and HLA-DR-αCFP/βYFP MDCK cells were performed using the acceptor photobleaching method, in which the emission intensity of the donor (CFP) is evaluated before and after bleaching the acceptor (YFP) with multiple scans of intense 514 nm laser light. After bleaching of the acceptor, the intensity of the donor should increase if FRET occurs between the non-bleached donor/acceptor pair, as the acceptor is rendered unable to capture energy from the donor fluorescence. Photobleaching experiments were carried out both in the presence and absence of IgG to determine if FcRn may form a constitutive or an induced dimer. In some experiments, I used the Zeiss LSM 510 Meta to obtain complete fluorescence spectra from the cells during 458 nm excitation of CFP. My initial experiments attempted to detect FRET in cells expressing the tail-less forms of FcRn-CFP/YFP. Because the FcRn FRET constructs lacked cytoplasmic tails, these molecules should be restricted to the cell surface, thus allowing FRET data to be collected from a relatively constant population of molecules, rather than a labile population that is constantly entering and leaving the confocal imaging plane. As shown in Figure 3, several regions of interest (ROIs) were evaluated for the CFP donor intensity before and after the photobleaching of the YFP acceptor. It is apparent from visual examination of the CFP panels in Figure 3A that there is not a significant, if any, increase in the intensity of CFP after the acceptor has been substantially bleached (Figure 3A, YFP panels), indicating that FRET was not occurring. This was confirmed by calculating the

FRET efficiency for several ROIs in the image. FRET efficiency by the acceptor photobleaching method is given by the equation

$$\text{FRET efficiency} = \left[1 - \left(\frac{CFP\ emission\ pre-bleach}{CFP\ emission\ post-bleach}\right)\right] \times 100\%$$

with values for this quantity varying from ~ 15–50% for real FRET depending on the starting intensities of the donor and acceptor molecules (Jares-Erijman and Jovin, 2006; Piston and Kremers, 2007; Van Munster et al., 2005; Vogel et al., 2006). The FRET efficiencies of ROIs in the FcRn experiment varied between -19.3% and 7.2%. Negative FRET efficiencies are not possible for real interactions. Additionally, 7.2% is much lower than published values for protein-protein interactions detected in this way (Van Munster et al., 2005).

In order to determine if the negative result obtained in the FcRn FRET assay could be considered true evidence that FcRn does not dimerize at the cell surface, we conducted positive control experiments using MDCK cells cotransfected with CFP and YFP fusions of the α and β chains, respectively, of the MHC class II molecule HLA-DR, an obligate heterodimer. The results of a representative experiment are shown in Figure 4. The FRET efficiency for the cells shown was 7.7%, which is fairly low for what should be a positive control. FRET efficiency values for other experiments using the HLA-DR system ranged from ~ 0.5%–7.7% (not shown). Thus, it is difficult to conclude on the basis of these experiments alone that FcRn does not dimerize. Possible reasons for the lack of observed FRET include the orientation of the fluorophores relative to one another in both the potential FcRn dimer and the HLA-DR positive control—efficient FRET requires that the dipole of the

donor and acceptor not be oriented orthogonally to one another, with optimum FRET occurring when they are aligned parallel to one another (Dale et al., 1979).

After obtaining the inconclusive results from the FRET-based FcRn dimerization assay I attempted to examine the capacity of FcRn to form dimers by utilizing a different assay, so-called Bimolecular Fluorescence Complementation (BiFC). This assay exploits the fact that two recombinantly split halves of YFP (an N-terminal half, and a C-terminal half, referred to as YN and YC, respectively) which are non-fluorescent on their own, can combine and mature into the active YFP fluorophore when brought into close spatial proximity with the appropriate geometry (Hu et al., 2002). This approach has been used to examine the dimerization of the bZIP transcription factors Fos and Jun in living and fixed cells (Hu et al., 2002; Hu and Kerppola, 2003), as well as interactions between members of the Myc/Mad/Max family of transcription factors (Grinberg et al., 2004).

Wild-type MDCK cells grown on poly-L-lysine-coated glass slides were transfected with FcRn-YN and FcRn-YC constructs along with the β_2m light chain, and visualized for YFP fluorescence ~ 48 hours post-transfection. Cells singly transfected with either FcRn-YN/β_2m or FcRn-YC/β_2m served as negative controls. As shown in Figure 6, YFP fluorescence resulting from BiFC is observed in neither the FcRn-YN/YC/β_2m transfection nor the control transfections. Since this negative result could be due to improper expression and/or folding of the mutant constructs, immunofluorescence was used to assess the expression of the mutant proteins. As seen in Figure 6, both the singly and doubly - transfected cells are positive for staining with the anti-FcRn antibody 1G3. FcRn positive compartments are seen

throughout the cells, indicating that the expressed protein is not misfolded in the ER. Similar results were also seen in stainings performed with a mAb against β_2m, and a polyclonal anti-GFP antibody. Lastly, to confirm that the expressed mutant receptors are able to traffic to the cell surface and functionally internalize ligand, a third set of transfected cells was incubated at pH 6 with 500 nM wtFc. Staining of these cells with an anti-rat IgG antibody confirmed that the FcRn-YN and FcRn-YC fusions were able to reach the cell surface and endocytose ligand, further suggesting that the absence of BiFC signal was not due to a defect in the expression or folding of these proteins. These controls were also performed on MDCK cells singly transfected with either the FcRn-YN or FcRn-YC construct (along with β_2m) to confirm that each construct expressed properly (data not shown). Whether the absence of BiFC is due to the absence of FcRn dimerization or due to an experimental flaw is unclear. The failure to detect BiFC was not due to the imaging conditions, as BiFC is seen in a non-homologous positive control system using bFos-YN and bJun-YC (data not shown). A more ideal positive control not used here would have been an HLA-DR α-YN/β-YC system. However, the failure to detect the association of these two chains in the FRET-based assay makes it seem less promising. Furthermore, while the results of the FcRn BiFC experiment do seem unintepretable without a solid positive control, it would still be difficult to prove the relevance of a negative result from this assay. Factors such as linker length and the relative placement of the YN and YC halves in the putative FcRn dimer could cause a negative result in the presence of a true dimer. Thus, it seems reasonable to argue that only a well-controlled positive result can be interpreted for these types of experiments.

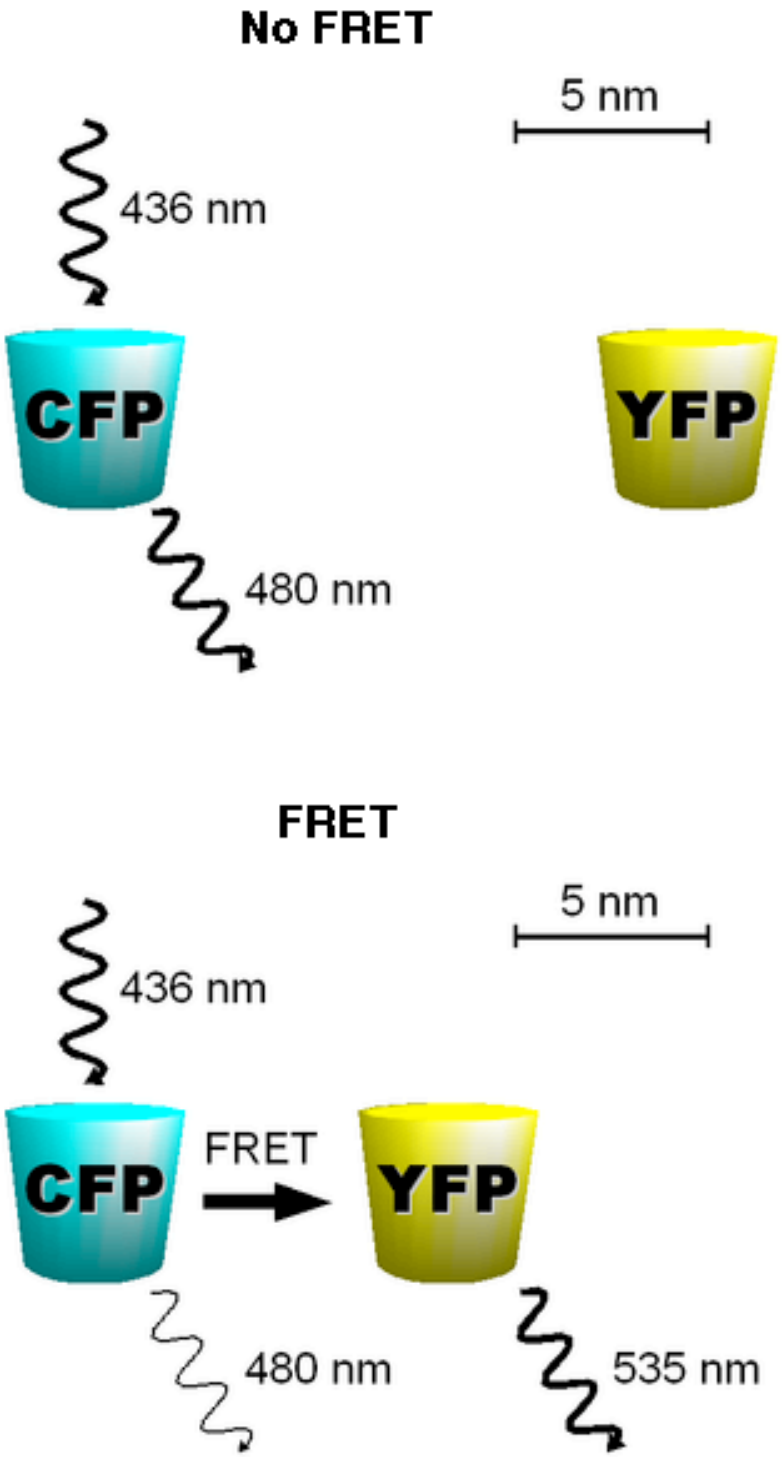

Figure 1. Schematic representation of the FRET assay. When a donor molecule (CFP) and acceptor molecule (YFP) are brought into close (~ 5 nm) spatial proximity, excitation of the donor results in non-radiative transfer to the acceptor. This can also be read out as an increase in donor intensity after bleaching of the acceptor molecule.

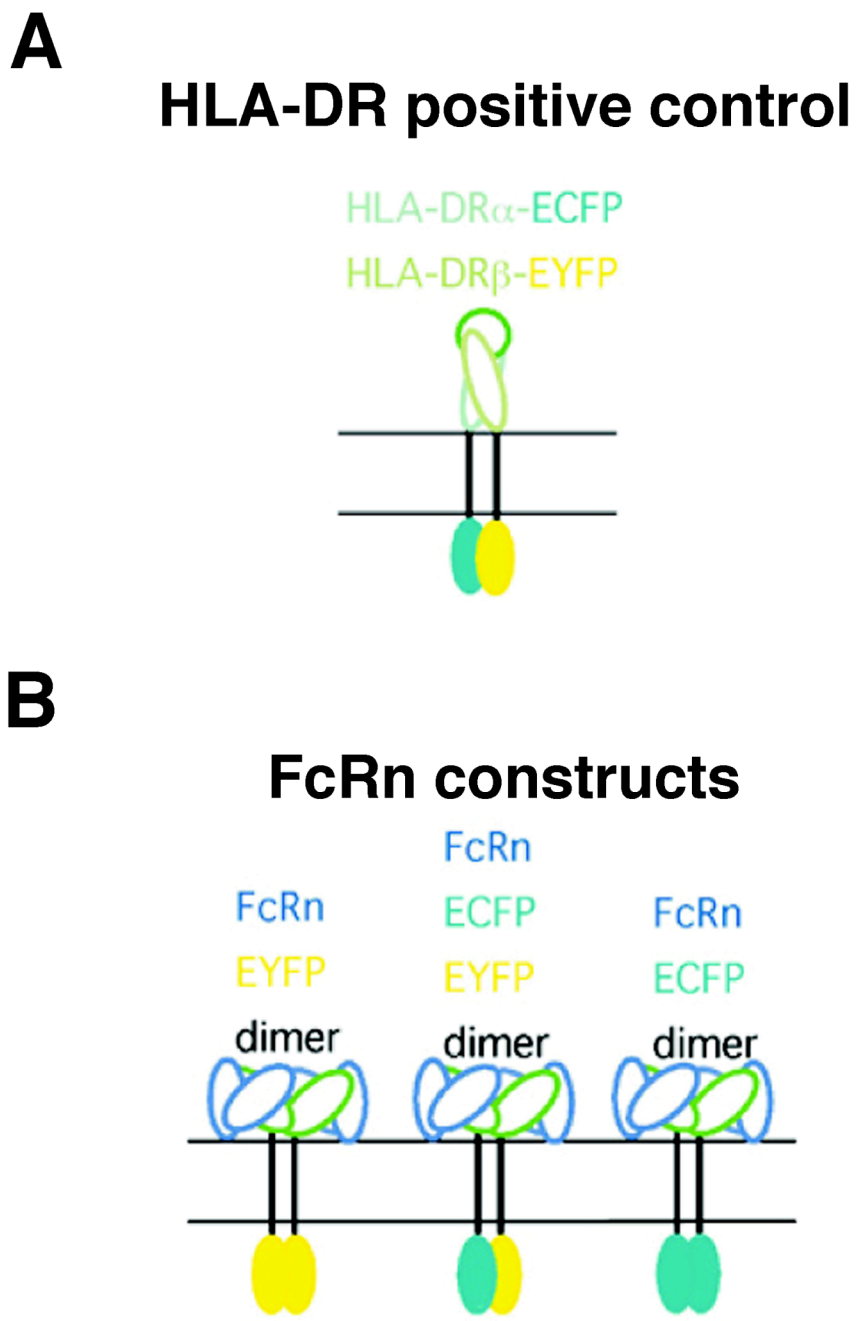

Figure 2. Schematic representation of FRET-based FcRn dimerization assay. (A) CFP and YFP fusions of the α- and β-chains of HLA-DR, an obligate heterodimer, serves as a positive control for FRET readout. (B) CFP and YFP fusion of a cytoplasmic tail-less form of FcRn will be tested for dimerization-induced FRET. Three types of dimers may form. Only the heterodimeric FcRn-CFP/FcRn-YFP dimer should exhibit FRET.

A

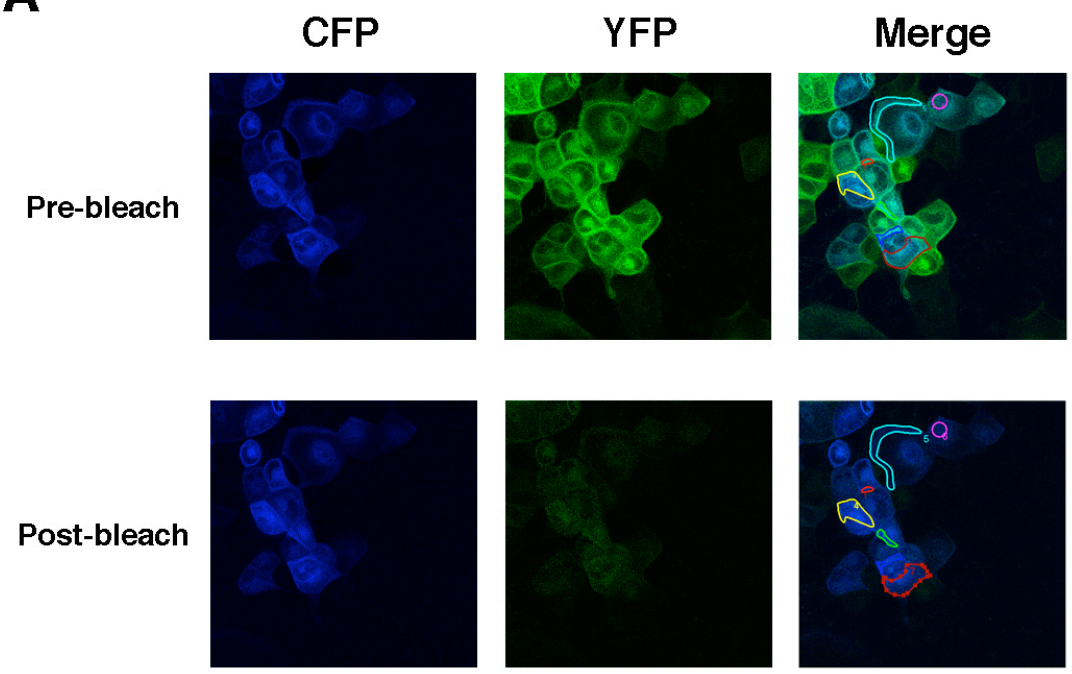

B

	YFP		CFP		
ROI	Pre-bleach	Post-bleach	Pre-bleach	Post-bleach	**FRET efficiency (%)**
1	1619	1744	2546	420	7.2
2	2298	2449	2997	635	6.2
3	2552	2400	2751	616	-6.3
4	2468	2580	1825	567	4.3
5	980	834	1267	280	-17.5
6	1389	1270	1195	326	-9.4
7	1873	1570	1818	436	-19.3

Figure 3. FRET measurement of tail-less FcRn-YFP/FcRn-CFP co-expressing MDCK cells. (A) A representative field of cells is shown before and after bleaching of the YFP acceptor. (B) Seven regions of interest (ROIs) were defined and the FRET efficiencies of those regions was determined by the change in donor intensity after acceptor bleaching.

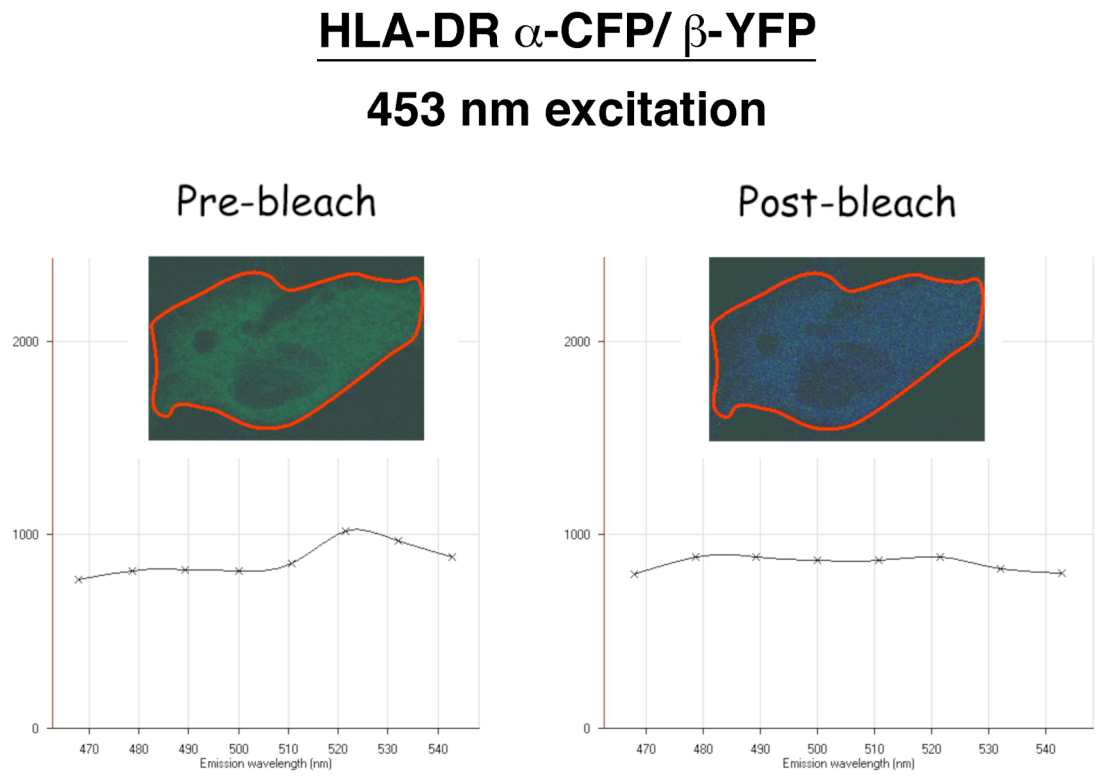

$$\text{FRET efficiency} = \left[1 - \left(\frac{CFP\ emission\ pre-bleach}{CFP\ emission\ post-bleach}\right)\right] \times 100\%$$

$$= \left[1 - \left(\frac{814.3}{882.4}\right)\right] \times 100\% = \underline{\mathbf{7.7\%}}$$

Figure 4. FRET measurements of an HLA-DR α-CFP/B-YFP heterodimer expressed in MDCK cells. The α-CFP and β-YFP chains were co-transfected into MDCK cells and imaged after 48 hours. One representative cell is shown before and after bleaching of the YFP acceptor. Emission spectra before and after bleaching using 453 nm excitation are shown. FRET should be detected by recovery of the CFP donor after bleaching. The ratio of donor fluorescence before and after acceptor bleaching gives a FRET efficiency of 7.7 %.

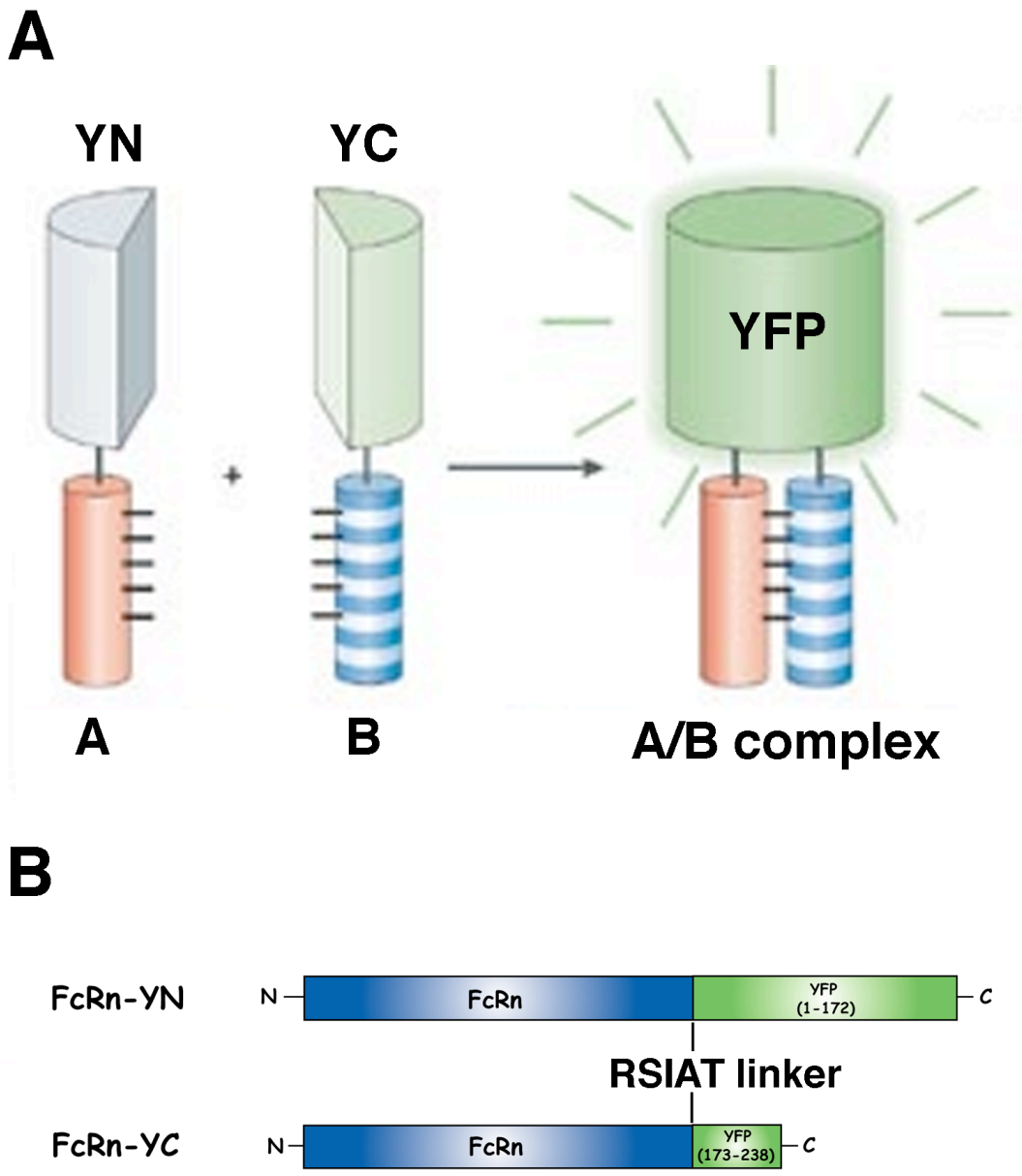

Figure 5. The principle of Bimolecular Fluorescence Complementation (BiFC) for the detection of protein-protein interactions. (A) Yellow fluoresent protein (YFP) is recombinantly split into two non-fluorescent halves. The N-terminal and C-terminal halves (YN and YC, respectively) are fused to proteins of interest (A and B). When the proteins interact, the YN and YC halves are brought into close spatial proximity, where they combine to form an active YFP fluorophore, providing readout for the interaction of their fusion partners. (B) FcRn fusions of the YN and YC truncations used for BiFC experiments. (Figure 3A adapted from Kerppola, *Nat Rev Mol Cell Bio,* 2006.)

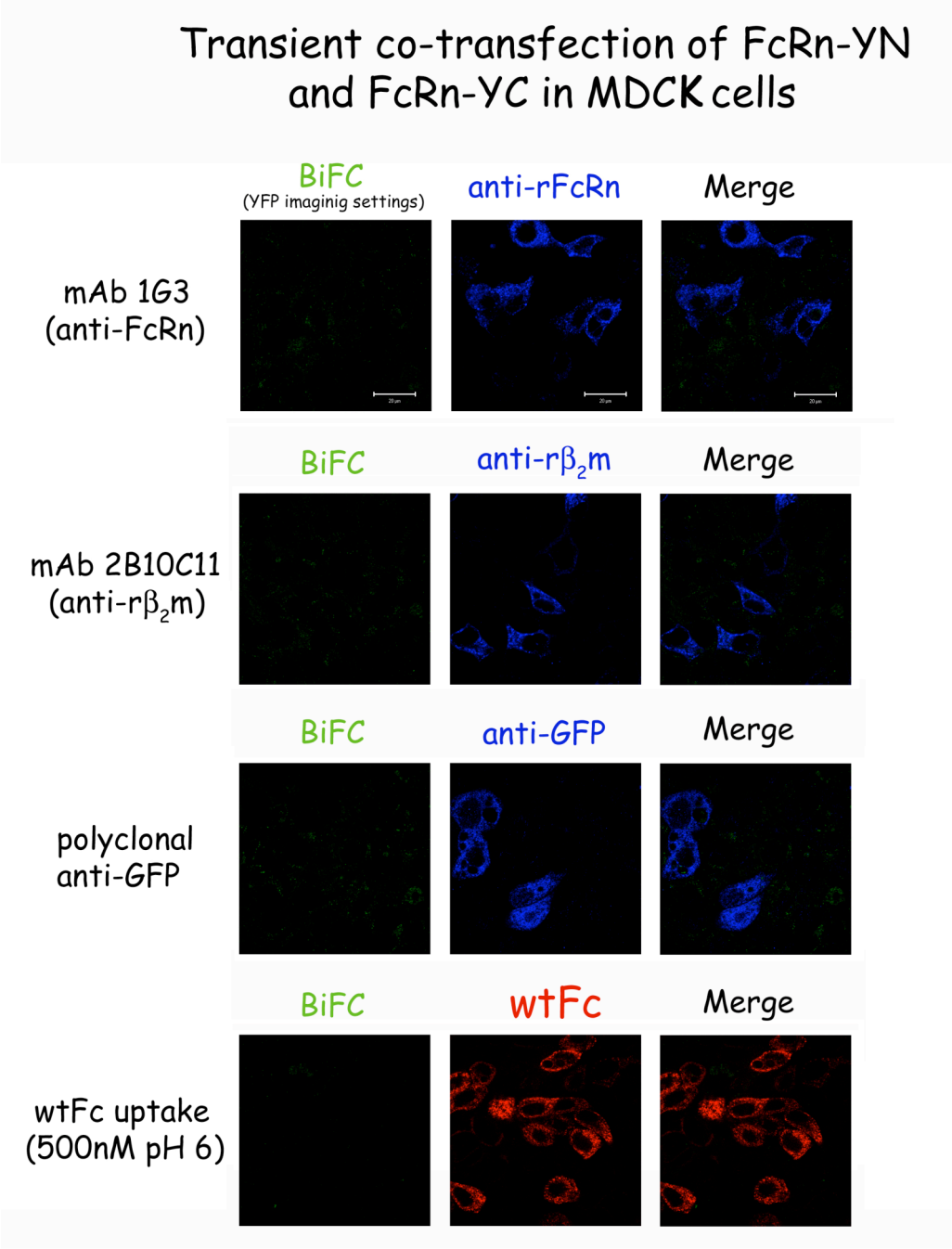

Figure 6. BiFC experiments using FcRn-YN/FcRn-YC co-transfected MDCK cells. Cells transiently transfected with the BiFC constructs were stained with antibodies against the FcRn heavy chain, β_2m light chain, and GFP to verify full-length expression of the constructs. Cells were treated 500 nM at pH 6 and stained with AlexaFluor 568 goat anti-rat IgG to verify functional internalization of ligand by the FcRn constructs.

References

Apodaca, G., Katz, L.A., and Mostov, K.E. (1994). Receptor-mediated transcytosis of IgA in MDCK cells is via apical recycling endosomes. J Cell Biol *125*, 67-86.

Burmeister, W.P., Gastinel, L.N., Simister, N.E., Blum, M.L., and Bjorkman, P.J. (1994a). Crystal structure at 2.2 A resolution of the MHC-related neonatal Fc receptor. Nature *372*, 336-343.

Burmeister, W.P., Huber, A.H., and Bjorkman, P.J. (1994b). Crystal structure of the complex of rat neonatal Fc receptor with Fc. Nature *372*, 379-383.

Claypool, S.M., Dickinson, B.L., Yoshida, M., Lencer, W.I., and Blumberg, R.S. (2002). Functional reconstitution of human FcRn in Madin-Darby canine kidney cells requires co-expressed human beta 2-microglobulin. J Biol Chem *277*, 28038-28050.

Dale, R.E., Eisinger, J., and Blumberg, W.E. (1979). The orientational freedom of molecular probes. The orientation factor in intramolecular energy transfer. Biophysical journal *26*, 161-193.

Dickinson, B.L., Claypool, S.M., D'Angelo, J.A., Aiken, M.L., Venu, N., Yen, E.H., Wagner, J.S., Borawski, J.A., Pierce, A.T., Hershberg, R.*, et al.* (2008). Ca2+-dependent Calmodulin Binding to FcRn Affects Immunoglobulin G Transport in the Transcytotic Pathway. Molecular biology of the cell *19*, 414-423.

Grinberg, A.V., Hu, C.D., and Kerppola, T.K. (2004). Visualization of Myc/Max/Mad family dimers and the competition for dimerization in living cells. Mol Cell Biol *24*, 4294-4308.

Heldin, C.H. (1995). Dimerization of cell surface receptors in signal transduction. Cell *80*, 213-223.

Himanen, J.P., Rajashankar, K.R., Lackmann, M., Cowan, C.A., Henkemeyer, M., and Nikolov, D.B. (2001). Crystal structure of an Eph receptor-ephrin complex. Nature *414*, 933-938.

Hu, C.D., Chinenov, Y., and Kerppola, T.K. (2002). Visualization of interactions among bZIP and Rel family proteins in living cells using bimolecular fluorescence complementation. Mol Cell *9*, 789-798.

Hu, C.D., and Kerppola, T.K. (2003). Simultaneous visualization of multiple protein interactions in living cells using multicolor fluorescence complementation analysis. Nature biotechnology *21*, 539-545.

Jares-Erijman, E.A., and Jovin, T.M. (2003). FRET imaging. Nature biotechnology *21*, 1387-1395.

Jares-Erijman, E.A., and Jovin, T.M. (2006). Imaging molecular interactions in living cells by FRET microscopy. Current opinion in chemical biology *10*, 409-416.

Kalo, M.S., and Pasquale, E.B. (1999). Signal transfer by Eph receptors. Cell Tissue Res *298*, 1-9.

Kerppola, T.K. (2008). Bimolecular Fluorescence Complementation (BiFC) Analysis as a Probe of Protein Interactions in Living Cells. Annual review of biophysics *37*, 465-487.

Kim, J.K., Tsen, M.F., Ghetie, V., and Ward, E.S. (1994). Localization of the site of the murine IgG1 molecule that is involved in binding to the murine intestinal Fc receptor. Eur J Immunol *24*, 2429-2434.

Luton, F., and Mostov, K.E. (1999). Transduction of basolateral-to-apical signals across epithelial cells: ligand-stimulated transcytosis of the polymeric immunoglobulin receptor requires two signals. Mol Biol Cell *10*, 1409-1427.

McCarthy, K.M., Lam, M., Subramanian, L., Shakya, R., Wu, Z., Newton, E.E., and Simister, N.E. (2001). Effects of mutations in potential phosphorylation sites on transcytosis of FcRn. J Cell Sci *114*, 1591-1598.

Okamoto, C.T., Song, W., Bomsel, M., and Mostov, K.E. (1994). Rapid internalization of the polymeric immunoglobulin receptor requires phosphorylated serine 726. J Biol Chem *269*, 15676-15682.

Piston, D.W., and Kremers, G.J. (2007). Fluorescent protein FRET: the good, the bad and the ugly. Trends in biochemical sciences *32*, 407-414.

Popov, S., Hubbard, J.G., Kim, J., Ober, B., Ghetie, V., and Ward, E.S. (1996). The stoichiometry and affinity of the interaction of murine Fc fragments with the MHC class I-related receptor, FcRn. Mol Immunol *33*, 521-530.

Praetor, A., and Hunziker, W. (2002). beta(2)-Microglobulin is important for cell surface expression and pH-dependent IgG binding of human FcRn. J Cell Sci *115*, 2389-2397.

Praetor, A., Jones, R.M., Wong, W.L., and Hunziker, W. (2002). Membrane-anchored human FcRn can oligomerize in the absence of IgG. J Mol Biol *321*, 277-284.

Raghavan, M., and Bjorkman, P.J. (1996). Fc receptors and their interactions with immunoglobulins. Annu Rev Cell Dev Biol *12*, 181-220.

Raghavan, M., Chen, M.Y., Gastinel, L.N., and Bjorkman, P.J. (1994). Investigation of the interaction between the class I MHC-related Fc receptor and its immunoglobulin G ligand. Immunity *1*, 303-315.

Stapleton, D., Balan, I., Pawson, T., and Sicheri, F. (1999). The crystal structure of an Eph receptor SAM domain reveals a mechanism for modular dimerization. Nat Struct Biol *6*, 44-49.

Tesar, D.B., Tiangco, N.E., and Bjorkman, P.J. (2006). Ligand valency affects transcytosis, recycling and intracellular trafficking mediated by the neonatal Fc receptor. Traffic (Copenhagen, Denmark) *7*, 1127-1142.

Van Munster, E.B., Kremers, G.J., Adjobo-Hermans, M.J., and Gadella, T.W., Jr. (2005). Fluorescence resonance energy transfer (FRET) measurement by gradual acceptor photobleaching. Journal of microscopy *218*, 253-262.

Vogel, S.S., Thaler, C., and Koushik, S.V. (2006). Fanciful FRET. Sci STKE *2006*, re2.

Zacharias, D.A., Violin, J.D., Newton, A.C., and Tsien, R.Y. (2002). Partitioning of lipid-modified monomeric GFPs into membrane microdomains of live cells. Science *296*, 913-916.